UCLouvain

AGRO LOUVAIN

Faculty of Bioscience Engineering

Building and quantification of a bioactive coating containing LL37-Alginate complexes

Master Thesis

Autor: Antoine Matheys

Supervisors: Prof. Christine Dupont

Ir. Cédric Vranckx

Readers: Prof. Sophie Demoustier

PhD. Aurélien Vander Straeten

Academic Year: 2020-2021

Master thesis presented in view of obtaining the degree of Master in bioengineering: Chemistry and Bioindustries.

Acknowledgements

All along this year, I received the help and support of many people, and I would like to thank all of them for allowing me to complete this master thesis.

Firstly, I want to thank Prof. Christine Dupont for letting me conduct my master thesis in her laboratory. Her numerous advice and positive comments were of great help in the realization of this master thesis.

I also want to thank Cédric Vranckx who supervised me daily during my work. His supervision was really didactic and he showed me around the laboratory and equipment, so getting through this master thesis would not have been possible without his great help. His continuous availability in addition of his advice and feedbacks, allowed me to push myself and to carry out this work in the best way.

I would also like to thank Prof. Sophie Demoustier and PhD. Aurélien vander Straeten for agreeing to be part of my master thesis jury and for taking the time to evaluate my work.

I want to thank Pierre Eloy for conducting the XPS experiment with me and for showing to me how to treat the data.

Finally, I want to thank all the people in the C2 laboratory for the great ambiance they made daily in the lab. I really enjoyed working with them and I wish them all the best of luck in their work and future.

Table of contents

List of abbreviations

ALG	Alginate
AMP(s)	Antimicrobial peptide(s)
BCA	Bicinchoninic acid
BCA(SDS)	BCA test using SDS as detergent
BCA(NO)	BCA test using the diluent of the NO test as detergent
CHI	Chitosan
FITC	Fluorescein isothiocyanate
HDP(s)	Host defense peptide(s)
LbL	Layer-by-layer
LOD	Limit of detection
LoF	Lack of fit
LOQ	Limit of quantification
Lys	Lysozyme
MIC	Minimal inhibitory concentration
NO	NanoOrange
O-Ph	O-phthalaldehyde
PAA	Poly(acrylic acid)
PAH	Poly(allylamine hydrochloride)
PE(s)	Polyelectrolyte(s)
PEM	Polyelectrolyte multilayer
PPC(s)	Protein-polyelectrolyte complex(s)
PSS	Poly(stryrenesulfonate)
QCM	Quartz crystal microbalance
QCM-D	Quartz crystal microbalance with dissipation
SAM(s)	Self-assembled monolayer(s)
SDS	Sodium dodecyl sulfate
TOC	Total organic carbon
XPS	X-ray photoelectron spectroscopy

Context of the study

The use of a dressing is now a daily treatment for open wounds. Our knowledge on the subject comes from the fact that we were already using dressings back to 2000 before Christ. Of course, the aims at the time were only to provide protection to the wound and absorb the potential exudate. Driven by the necessity to ensure a sterile environment, the rustic methods moved on to more scientific techniques. A lot of different dressings started to come out and were divided in multiple subgroups, one for each type of wound, always more sophisticated to improve its function. [1] Passive, interactive and bioactive dressings emerged.

Nowadays, the interest of developing effective dressings is still the goal of multiple studies, including this one. In particular, this master thesis aims to study a specific bioactive coating that can be applied on a dressing. Indeed, the idea is to immobilize a sufficient amount of LL37, a particular peptide, onto the dressing. This peptide possesses a great wound healing capability thanks to its angiogenesis, neovascularization and antibacterial properties which can thus improve the healing capacity of a dressing.

The research for this master thesis takes place in the context of the PhD thesis of C. Vranckx in the laboratory of Prof. Christine Dupont (BSMA). His thesis aims to develop a similarly constructed coating onto the surface of a hip prosthesis in order to decrease the prosthetic joint infection after surgery and to promote osseointegration. This is once again possible thanks to the properties of the LL37.

This work will be divided in the following parts: first, a section will present the state of the art to give the theoretical information around the problematic. Then, the objectives of this master thesis and the strategy chosen to reach them will be expressed. A “materials and methods” section will follow, presenting the technical information. After that, the obtained results will be exposed, firstly discussed individually and then more globally. The main conclusions will finally be drawn, alongside the future work that can be realized.

State of the art

1. Context

Healing sciences are more and more efficient each year thanks to the continuous development of numerous advanced techniques. To illustrate the knowledge evolution and the greatness of the wound healing field, a brief history of wound care will be presented. A more biologic approach will then be exposed, followed by explaining more precisely the scientific concepts encountered during this master thesis.

1.1 A brief history of wound care

The oldest record of wound healing technique is traced back to 2200 BC and a time line of its evolution since then is presented in Figure 1. [2] At that time, they applied the "three healing gestures" that consist of: firstly, wash the wound with beer and hot water, then apply a plaster, and finally cover the wound with a bandage. [3] The plasters were made of oil, mud, and a mixture of herbs. Their function was to provide protection and absorb exudate. At that time, they did not have the scientific knowledge to understand what was happening during the healing. The medicine was thus coming from trial and error and was passed on to the next generation. [4] However, the concepts of washing and covering the wound were already present at the time but the techniques needed to be improved.

Then step by step, the healers passed from casting spells to more down-to-earth methods. The major issue that they faced was to stop the bleeding by using all kind of material or by burning the wound. [4] The use of honey and grease emerged at that time. The Egyptian probably have played an important role in the banding technique evolution due to their culture of the embalming dead bodies. [1] Even without understanding the principle of contagion, they regularly changed the dressing to maintain it clean. [5]

The concept of cleanliness really comes with the Greeks. They washed the wound with boiled water, vinegar, and wine. Then, they applied a dressing composed of wool or silk, also soaked in wine or boiled water. [4] The first classification of the different types of wounds emerged. The four signs of inflammation, that are still used today, come from the Romans and are redness, swelling, heat and pain. [1] The Greco-Roman medicine remained the most popular practice during all the Middle Ages. [5] Among the other techniques, they tended to let the wound rot a bit to see if it was infected by a curable bacteria and produced some pus, or by gangrene which generally leads to the patient death. [3]

Wound care was well improved during the numerous wars. Indeed, wars brought a lot of wounds to heal and allowed an improvement of the healing techniques. [3] As the surgeons began to understand the concept of homeostasis, they started to use instruments to stop the bleeding, like a sort of tourniquet. The use of guns became more common and the injuries they caused were a real challenge to heal. This new type of wound drove the surgeons to try treatments that differed from their textbooks. The concept of innovation towards new therapies spread quickly and led to an empiricism period. [5] The number of injured soldiers pushed the surgeons to quickly heal the wound and frequently led to numerous amputations of any limb that could not be saved. [5]

From the 19th century, amputation leaves place to some more conservative interventions. The observation of post-surgery gangrene infection led to the understanding of the germ theory. [5] The understanding that microorganisms responsible for wound infection exist everywhere led to the development of antiseptic techniques, like treating the wound with a dressing soaked in carbolic acid (=phenol). In 1891, the Johnson & Johnson company was the first to start the mass production of sterile surgical dressings. They sterilized cotton and gauze with dry heat and then by steam and pressure. [3] The first nonadherent dressing also emerged, allowing no trauma upon removal, compared to adherent one. [2], [3] The use of this dressing with some chemicals was the classical way to heal wound until the discovery of antibiotics such as penicillin. [5]

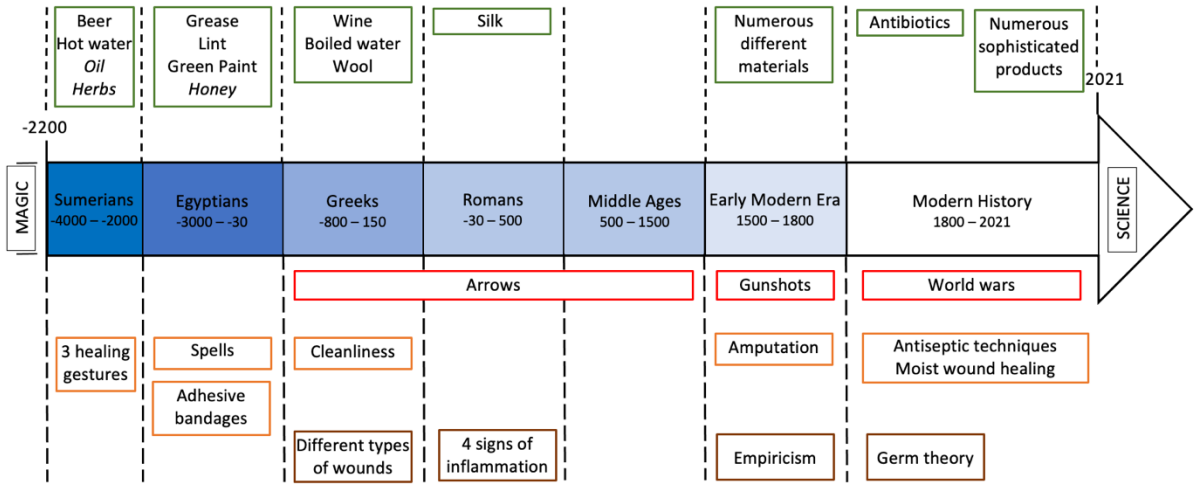

Figure 1 : Timeline of the wound healing evolution. The used materials are in green, the civilizations in blue, the types of wounds in red, the healing techniques in orange and the important theories in brown. This timeline is non-exhaustive and is here to illustrate the great evolution of wound care.

In the 1980s, the current moist wound healing was introduced. Indeed, it was shown that by creating a moist environment, healing was improved, and pain reduced, when compared with dried dressings. [6] This fundamental change was due to the understanding of the concept of occlusion that allows the wound area to be kept moist. [2]

The late 20th and early 21st century have seen the beginning of the modern wound care revolution. [6] A lot of different dressings that we still use today were developed, always more sophisticated and specific to the type of wound to heal.

This completes the short time travel from healing spells to smart dressings development. It is interesting to point out here that the research on wound healing led to the development of many different techniques that fall under a broader discipline: tissue engineering. Just by searching "dressing tissue engineering" on Google Scholar, there already are distinct approaches appearing on the first page: electrospinning, aerogel, or scaffold to cite some of them. The numerous possible approaches confirm that wound treatment represents a large part of healthcare issues in the world and the smart dressing is one of the promising approaches and will be thus detailed in the next section. [4], [7]

1.2 Diversification of dressings

Since the last three decades, the evolution of dressings has led to a remarkable multiplication of different products, responding to the numerous public inquiries. [6] To illustrate this, one can make the metaphor that, every wound can find the right dressing: breathable, comfort, waterproof, pretty, small, large, specialized, etc. This considerable expansion is driven by the changes in public demands but also by the increasing number of non-healing and infected wounds that need to be cured. [8] In face of that vast pool of dressings, the appropriate choice can be tricky and will differ in function of the type of wounds, patient health, evolution of the healing process, etc. [6]

It is possible to classify the dressings in four global categories: absorptive, nonadherent, occlusive and others with biological activity. [2] This last type of dressing is the one that can be constructed with the bioactive coating studied in this master thesis, and will be a little bit more detailed here. All the healing products that rely on biological activities are gathered in the same category including creams, ointments, solutions, and antimicrobial dressings. Biologically-active dressings can be made of collagen, chitosan, hyaluronic acid, or peptides, to name a few materials. That is probably the cause of their significant unit cost. [6] The biologically-active dressing is at the cutting edge of dressing's technology and this is where the work of this master thesis takes place, by studying a coating containing peptides showing some interesting healing properties that will be explored in the following section.

2. A more biologic approach

Coatings can be designed that present healing capacities susceptible to improve the dressing properties. The coating studied here is made of chitosan (CHI), alginate (ALG), and LL37, a host defense peptide (HDP). Before describing each of these elements in more detail, it is important to have a quick understanding of how the healing process works, in order to discuss its possible improvement.

2.1 The healing process

The healing process is quite complex and is divided in four different overlapping steps: hemostasis, inflammation, proliferation, and remolding. [7] Just after an injury, the hemostasis will start to restore or repair the damaged tissues to maintain the balance between proliferation and cell death constant. The inflammation phase will also directly begin, and some inflammatory cells are sent to the wound site to fight the infection. Then, the proliferative phase starts with the formation of granulation tissue, epithelialization, and angiogenesis. And finally, the remolding phase allows the new collagen matrix to be cross-linked and organized. [9] HDPs can affect these four global steps, particularly by promoting angiogenesis and the inflammatory process for example. It is thus important to keep these four steps in mind while describing the influence of HDPs on them.

2.2 Host defense peptides

Host defense peptides, also called antimicrobial peptides (AMPs), are part of the innate immune system and represent the first line of defense against many invading pathogens. [9]

2.2.1 General structure

HDPs have a cationic nature. They are relatively short amphiphilic peptides with less than 50 amino acids. They have been detected in several species like plants, insects, and animals including humans. [8] In mammals, HDPs are divided in two groups: defensins which are the most representative, and cathelicidins. Defensins have a β-sheet structure stabilized by two or four disulfide bridges whereas cathelicidins have an α-helical structure. [10] Cathelicidin peptides present a variety of structures but share a highly conserved N-terminal domain and a variable AMP domain on the C-terminus as illustrated in Figure 2. [9], [11]

2.2.2 Expression

The expression of HDPs is upregulated when an injury or an infection occurs. [8] Figure 2 gives an illustration of the gene product cathelicidin for a sequence of an AMP composed of 37 amino acids, which is in fact LL37. This product can be cleaved by proteinase-3 which is part of the serine protease family. This leads to the release of the AMP that can perform multiple actions on the site of the wound. This AMP can also be cleaved again by other serine proteases and can generate four different sizes of secondary peptides which will present different profiles of biological actions. [12] Following a skin injury, the HDPs level in the skin area increases rapidly, due to an increase of the synthesis by keratinocytes and by a release coming from the degranulation of recruited neutrophils. [8] This high concentration compensates the relatively short half-life of HDPs due to a rapid protease digestion or to peptide aggregation but is sometime responsible for toxicity towards blood cells or skin fibroblasts. However, the cytotoxic concentrations are generally way higher than the minimum inhibitory concentration (MIC) allowing the use of these peptides over a certain concentration range. [13]

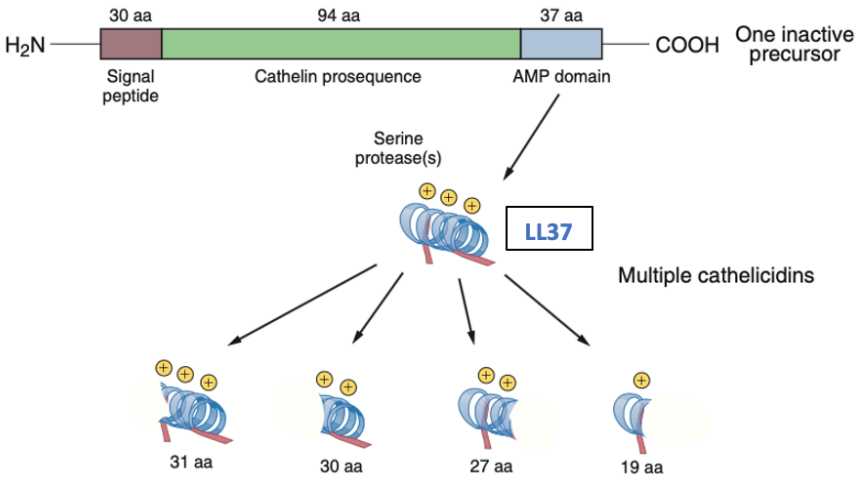

Figure 2 : Illustration of the inactive cathelicidin precursor that can be cleaved by proteinase to release the LL37. This peptide can be cleaved again and generates four peptides of 31, 30, 27, and 19 amino acids respectively. [12]

2.2.2 Multiple capacities of HDPs for wound healing

In addition to their antimicrobial properties, the importance of HDPs is that they can link the innate and adaptive immune systems. [11] They play a key role in the activation and the modulation of the two system responses following an infection or inflammation. [8] As they can participate in numerous healing functions, the following point will firstly present the antimicrobial properties and the second one, their role as immunomodulator, as illustrated in Figure 3.

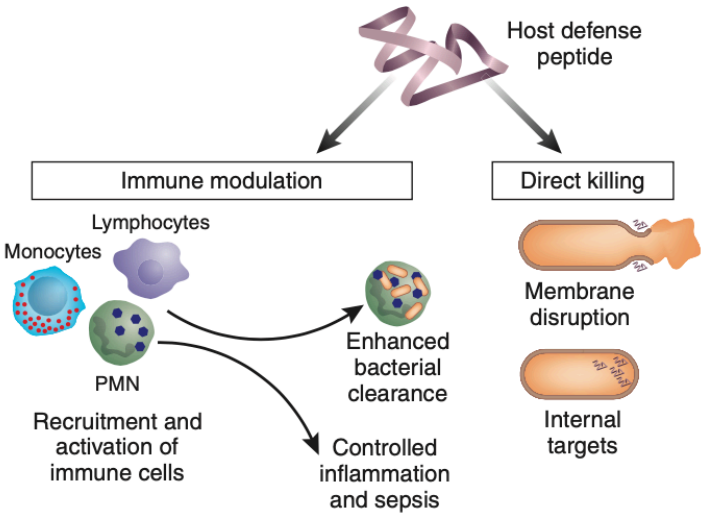

Figure 3 : The two global functions of the host defense peptide: the direct killing of microbes and the immune modulation. [10]

a) Antibacterial properties

The antibacterial activity of AMPs is possible thanks to their cationic and amphiphilic nature. [10] As the microbial cell surfaces are polyanionic, the AMPs will attach and accumulate on their surface. The insertion of the AMPs into the bacterial cell membrane leads to a physical disruption of the membrane and thus to a lysis of the cell. They also can cross the membrane and act on internal targets. This technique allows them to have a broad antimicrobial spectrum against gram-positive and gram-negative bacteria, fungi, and viruses. [9]–[11] Their use may thus reinforce the numerous therapeutic techniques developed to fight bacteria that become resistant to conventional antibiotics. [8]

When present at the wound site, such HDPs provide a soluble antimicrobial barrier that permits to a superficial epidermal wound to heal without major complications in vertebrates. [8] The non-healing and infected wounds are the challenging ones and require more assistance in order to heal completely, like the mobilization of additional HDPs for example.

b) An immunomodulator agent

In addition to their antimicrobial properties, HDPs also show some immunomodulatory activities like the recruitment and activation of inflammatory cells, the stimulation of epithelial proinflammatory factors, the stimulation or inhibition of apoptosis, and anti-endotoxin activity for example. [10], [11] So, HDPs play a role in the second and the third phase of the wound healing process which are respectively the inflammation and the proliferation phase, as described above. As HDPs can be combined with other techniques, their use really represents a promising approach for wound healing improvement. [8]

The importation of additional HDPs on the wound site could thus possibly improve the wound healing process, and that will be the goal of the bioactive coating present on the dressing. It should indeed release, in the wound area, external LL37 whose properties are described in the next section.

2.3 The LL37 peptide

hCAP-18/LL37 is the only human cathelicidin antimicrobial peptide. hCAP-18 is the precursor that can be cleaved to generate the LL37 peptide. It can be detected in cells, tissues, and body fluids. It is upregulated in response to cutaneous infection or injury and is lacking in chronic wounds. [8], [9]

2.3.1 LL37 structure

LL37 is composed of 37 amino acids, starting by two leucines, which led to the name of LL37. Its molecular mass is around 4.5 kDa. It has two aspartates and three glutamates as negative amino acid residues, and as positive ones: five arginines and six lysines. That gives a global charge of +6 to LL37 at pH 6.5. As a member of the cathelicidin family, it is amphiphilic and has an α-helical structure. [9] This peptide is expressed and stored in specific granules of neutrophils, natural killer cells, and mast cells, in its inactive preform: the hCAP-18 which has an approximate mass of 18 kDa. After the degranulation of these cells, the hCAP-18 is released and cleaved extracellularly into its active form (LL37) thanks to the proteinase 3. [11], [14]

LL37 possesses one hydrophobic surface thanks to the four phenylalanine residues present on the external surface of the α-helix, all pointing to the same direction as illustrated in Figure 4. The same orientation of these phenylalanines will allow LL37 to kill microbes as explained below. The LL37 sequence can be divided in three regions which will bring different properties to LL37: the N-terminal, the C-terminal, and the C-terminal tail regions. [14]

2.3.2 LL37 properties

Its cationic and hydrophobic nature will allow the LL37 to have many antibacterial actions presented first below, as well as host defense effects, like its improvement of angiogenesis, that will be explained in a second time. [14]

a) Antimicrobial activities

As part of the cathelicidin family, LL37 has a broad spectrum of antimicrobial, antifungal, and antiviral activities. [7] These numerous activities are possible thanks to the C-terminal helix of the peptide that possesses several hydrophobic clusters. [15] The killing mechanism relies on the membrane-disrupting properties of LL37 that occurs after its fixation on the microbe membrane, thanks to the difference of the surface charge between LL37 and microbe cells. [11], [14]

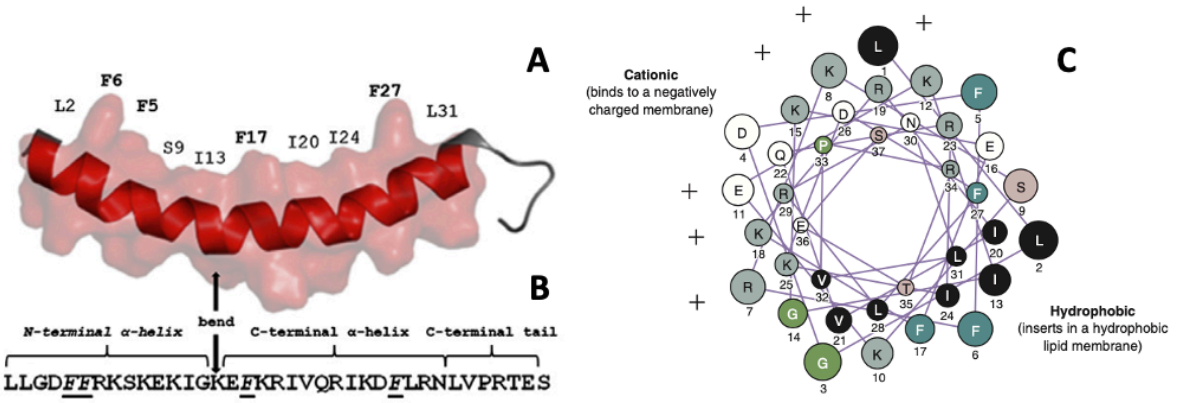

Figure 4 : Structure of the LL37 peptide. A) Three-dimensional structure of LL37 showing the alpha-helix conformation. B) Sequence of LL37 peptide divided in 3 regions. C) A schematic wheel plot of the 37 amino acids that compose LL37 showing the distribution of the positive charges and the hydrophobic residues in black. [12], [14]

The α-helix conformation is the active form of the peptide as it is responsible for the insertion of the peptide in the targeted cell membranes. This allows a cell-selective killing of both gram-negative and gram-positive bacteria. Indeed, the acidic polymers in gram-negative and the teichoic acids in gram-positive permit the accumulation of LL37 on the bacteria cell walls. [10] The LL37 mechanism of action is a toroidal pore or carpet-like mechanism that is commonly used by other HDPs. Figure 4C illustrates the fact that LL37 has a hydrophobic surface on one side and a hydrophilic positively-charged surface on the opposite side, which allows their antimicrobial mechanism of action. [16], [17] The ability of LL37 to prevent biofilm formation of certain bacteria, like *Pseudomonas aeruginosa*, has also be shown and LL37 appears to be the only cathelicidin capable of this anti-biofilm action. This peptide is also able to inhibit several viruses as the HIV-1 virus for example, by interacting with the membrane envelope and the protein capsid. [14] Of course, LL37 does not act alone but in concert with other antimicrobial components to exert an optimal killing capacity. [11]

b) Immunomodulating activities

Beside its broad antimicrobial function, the LL37 peptide possesses several additional functions that can be divided in three categories: the ability to signal tissue and cell damages, to stimulate and modulate the immune system, and to improve wound healing. This time it is the N-terminal part of the α-helix, common to all the cathelicidin peptides, that is involved in several of these actions. [14]

A main function of LL37 is its chemotactic effect: it can attract cells that can fight the microbes (mast cells, lymphocytes, neutrophils, etc.) to the infection site. Once those cells are on site, LL37 can stimulate and modulate their actions, resulting in a balance between the production and the release of pro and anti-inflammatory cytokines. LL37 can also regulate the apoptosis of cells present on the infection site: by suppressing the apoptosis of the epithelial cells and neutrophils to extend the period where those cells can respectively produce chemokines and cytokines, and clear microbes from the infection site. After the clearance of the wound, the tissues need to be repaired and LL37 also plays an important role here. LL37 has been reported to activate some receptors on epithelial cells and fibroblasts resulting respectively in the proliferation and migration of the epithelial cells, and in the inhibition of the collagen production to avoid too much scar tissue. Finally, the peptide also plays an important role in the creation of new blood vessels thanks to its angiogenic and neovascularization properties. [8], [9], [11], [14]

c) LL37 cytotoxicity

This promising peptide still present certain drawbacks. At a concentration superior to 13 µM or 58 µg/mL, studies have shown that LL37 can be cytotoxic against several eukaryote cells like leucocytes. However, this concentration is higher than the MIC values (1-10 µM) for bacteria and than the concentration needed to promote wound healing which is reported to be between 1 and 5 µg/mL. [11] This reinforces the idea that LL37 acts following a cell-selective killing mechanism. The cytotoxicity also seems to be attenuated by some components of human plasma such as some lipoproteins (apolipoprotein B and A-I for example) that show a high binding with LL37. [11], [18], [19]

LL37 can be degraded by proteolytic enzymes in the wound environment and a higher and more frequent dose can thus be required to produce therapeutic effect. However, the wound fluid seems to slow down the degradation, allowing to increase the time of action of the peptide. [9], [11] LL37 can also be used to achieve specific delivery inside the cell. However, when the LL37 concentration inside the cell is too high, it can lead to the formation of pores in the cell membrane, that can cause the lysis of the cell. [14]

To conclude this biologic approach, it is important to keep in mind that despite the minor drawbacks described, the LL37 peptide is involved from the start of an injury by its microbe obstruction activities, to the recovery of the tissues damaged during the infection by its modulation of the innate and adaptive immune response, permitting a complete wound healing. This validates the utilization of LL37 in the coating studied in this master thesis. The fact that the number of articles concerning LL37 reported in Google Scholar has doubled in the last decade, as plotted in Figure 5, really shows the interest in the LL37 peptide as a promising therapeutic agent. However, its utilization in this work raises new challenges like its immobilization in the coating, that will be discussed in the next section.

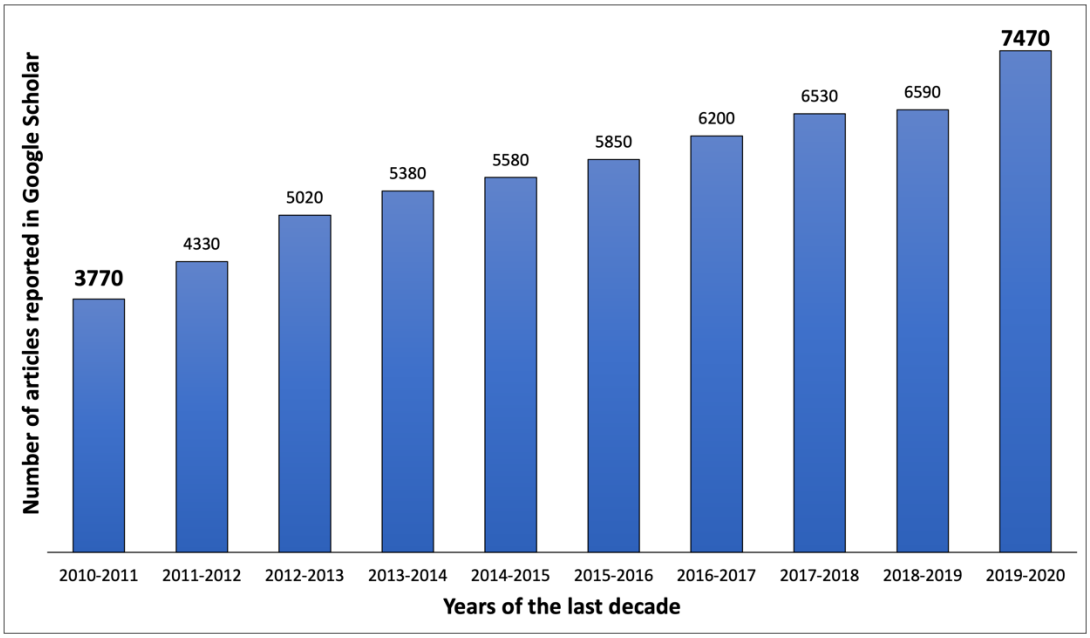

Figure 5 : Evolution of the number of articles concerning LL37 reported in Google Scholar per year over the last decade.

3. Surface modifications to form the bioactive coating

Now that the multifunctional host defense peptide LL37 is well known, the appropriate technique for its integration into the bioactive coating can be studied. When talking about surface modifications, it is either possible to directly alter the surface or to add a coating on it, which will be the case in this work. [20] Firstly, a quick review of protein/peptide immobilization methods will lead to the choice of the most adapted method for the coating construction. Then, the chosen technique will be explained alongside the properties it confers to the coating. Finally, the coating formation will be studied and some results from the literature will be exposed.

3.1 Protein immobilization methods

Proteins, by their large size and their amphiphilic nature, are surface active and thus adsorb easily on a surface. [20] The interest in fixing some functional proteins on a surface has led to the development of numerous immobilization techniques that can be classified in function of their bonding particularities. The review of the different bonding possibilities will lead to the choice of the most adapted immobilization method for the coating construction.

3.1.1 Chemical and physical protein immobilization methods

a) Non-specific immobilization methods

The non-specific immobilization methods can be divided in non-covalent methods (including passive adsorption and electrostatic interactions with the surface) and covalent methods. They represent the classical methods that rely on physicochemical adsorption phenomena or on functional groups naturally present in proteins. They are widely used due to their large flexibility and their ease of use which allow their straightforward application to all proteins. [21]

Firstly, the easier way to immobilize proteins is by passive adsorption onto a hydrophobic surface thanks to spontaneous adsorption. Another simple way is by creating electrostatic interactions between the proteins and a charged surface. Those immobilizations are based on weak interactions which means that the proteins can easily be desorbed from the coating. The major advantage of those methods is that the protein does not need to be modified for its immobilization. Also, there is no additional coupling agent or surface modification required. [21]

Secondly, the covalent immobilization is based on a covalent link between the protein and the surface. Different binding possibilities exist either based on a function present directly on the proteins which can thus be used directly in its natural form, or by incorporating a specific building block in the protein that will interact with the surface and allows covalent binding. The covalent immobilization is a more chemoselective approach that permits to integrate the protein with a certain orientation that may enhance its activity. For HDPs, a covalent immobilization could increase their long-term stability and their resistance to environmental conditions while decreasing their toxicity, when compared with a non-covalent method. However, it is important to point out here that those last property improvements are function of the HDPs, their length, flexibility, kind, the presence of a spacer, the HDPs surface density and their orientation after immobilization. In addition, as the protein is modified, a denaturation of the protein could occur after its modification. Those property improvements are thus not guaranteed in all situations. [13], [21]

b) Site-specific immobilization methods

It is also possible to immobilize a protein by using its ability to recognize and connect to a specific site of the surface. Both proteins and surface thus need to be modified before the immobilization occurs. This method allows to have a uniform orientation and avoid the steric hindrance of available bioactive sites that occurs for non-specific immobilization methods. It usually relies on the labeling of the protein with an azide group (RN_3) and permits to be sure that each site possesses a protein in its active form. This is particularly useful in nanotechnologies where a relatively small number of proteins are present at each location and thus need to have their maximal biological activity. [21]

3.1.2 Biologically-mediated immobilization method

To complete the different immobilization methods, it is possible to use some methods based on biological reactions to immobilize a modified protein on a functionalized surface. It can be highly selective and done under mild conditions that will reduce the risk of protein degradation. The attachment sequence can be added genetically to the protein, then expressed with the protein and will after detect the specific site on the surface. It is possible, for example, to use a his_6 tag to build a covalent bond or to link an additional enzymatic protein to the protein of interest, that will covalently bind with a specific ligand present on the surface. [21]

3.1.3 Choice of the immobilization method

a) Choice of the interaction type

For the LL37 used in this work, it is less interesting to use methods that require modification of either the surface or the peptide because the LL37 is already in its active form (α-helix) in solutions mimicking plasma, intracellular and interstitial fluid. [11] So, the LL37 does not really need to be immobilized in a certain orientation because it can take its conformation for optimal activity in the physiological medium. [11] Also, every additional step made to specialize the peptide or the surface represents an additional cost for the bioactive coating. In addition, as explained above, both the N-terminal and the C-terminal sequences of the peptide present interesting properties for wound healing and antimicrobial effects. Thus, if it is immobilized by altering one of the peptide ends, it could impact its properties. Hence, a non-specific immobilization method was chosen for the building of the coating.

The type of binding (covalent or not) of non-specific immobilization methods will in fact reflect two different possible strategies: a substance-releasing or a substance covalent immobilization. Both strategies have their advantages and drawbacks: the substance-releasing coating has the potential to extend its activities further than the surface but needs a sustained dosage, delivered over a prolonged period. The covalent immobilization on the other hand has an activity that lasts longer, decreases the possible toxicity, and does not accumulate in tissues, but its action is limited to the surface and there is a risk of denaturation of the proteins. [13] To maintain the activity of LL37 all over the wound and as it is a soluble HDP, it is more interesting if the LL37 is released out of the coating. [7] The immobilization method of LL37 for this work will be thus a non-specific, non-covalent method to bind the HDP only weakly to the coating.

b) Choice of the technique

Several bottom-up approaches were developed over the years to effectively shape the properties of a surface, relying on the spontaneous self-assembly of small molecules into more complex ones. Those bottom-up fabrication methods include Langmuir-Blodgett and self-assembled monolayers (SAMs). These methods both present some drawbacks, especially the limitation of the film stability and robustness under ambient and physiological conditions that makes difficult the transfer of molecules on the solid surface. In addition, SAMs present a limited loading capacity due to their monolayer nature. However, other surface engineering methods like polymer grafting or plasma treatment have being developed but all the methods cited above present limitations regarding their cost of instrumentation and production and the restriction in the number of usable materials and surfaces. [20], [22]

To overcome these limitations, another bottom-up approach can be used: the layer-by-layer method (LbL) which allows a stable multilayer construction and will be explained in the next section.

3.2 Layer-by-layer method

The LbL assembly is a widely used method, probably due to its capability to construct a multilayer from a large pool of different material, giving the method a great versatility, in addition to its simplicity and low cost. In addition, the assembly process can occur at room temperature, under mild conditions and entirely in aqueous solutions and thus does not require the use of organic or harmful solvent. Although several types of LbL exist relying on hydrophobic, hydrogen, covalent, metal-ligand or other interactions, it mainly is conducted through electrostatic interactions and that will also be the case in this study. The general method will be explained below, followed by the characterization of the multilayer formed. [22], [23]

3.2.1 The general method

The LbL assembly based on electrostatic interactions uses polyelectrolytes (PEs) as building blocks and the attraction between their opposite charges as binder to build a multilayer. This method permits to build the structure one layer at a time. The first PE interacts with the surface and then the construction is driven by the interaction of the two PEs of opposite charge. However, some weak bonds like hydrogen or hydrophobic bonds can also contribute to the adsorption steps. [22], [23]

Although the electrostatic interactions play an important role, it is more the entropy that drives the assembly of the layers. Indeed, upon PE adsorption, there is a release of counterions and some hydration water molecules, which increases the entropy. Of course, the fact that the PE is now adsorbed on the surface and not in solution anymore decreases its entropy but globally, the entropy increases upon PE adsorption. [20], [23]–[25]

There are several methods for PE deposition including dip-coating, spin-coating, spraying and perfusion. The most widely used method is the dip-coating. It permits the use of surfaces with a complex geometry. However, it needs a larger amount of material than the other techniques and it is a time-consuming method. [22] This LbL method works by dipping the surface on which the multilayer will be constructed, in several solutions of PEs. The surface is dipped a certain time to permit the adsorption of the PE in solution on the solid surface to form the first layer. For this work, the reverse situation was exploited: a 96-well plate surface did not move but the solution of PE in the wells was changed for each adsorption step. This

method is illustrated in Figure 6. The rectangle opened at the top represents a well. The first solution of positively charged PE is placed in the well and is adsorbed on the negatively charged microplate surface. At this point, there is a charge overcompensation leading to an inversion of the global surface charge.

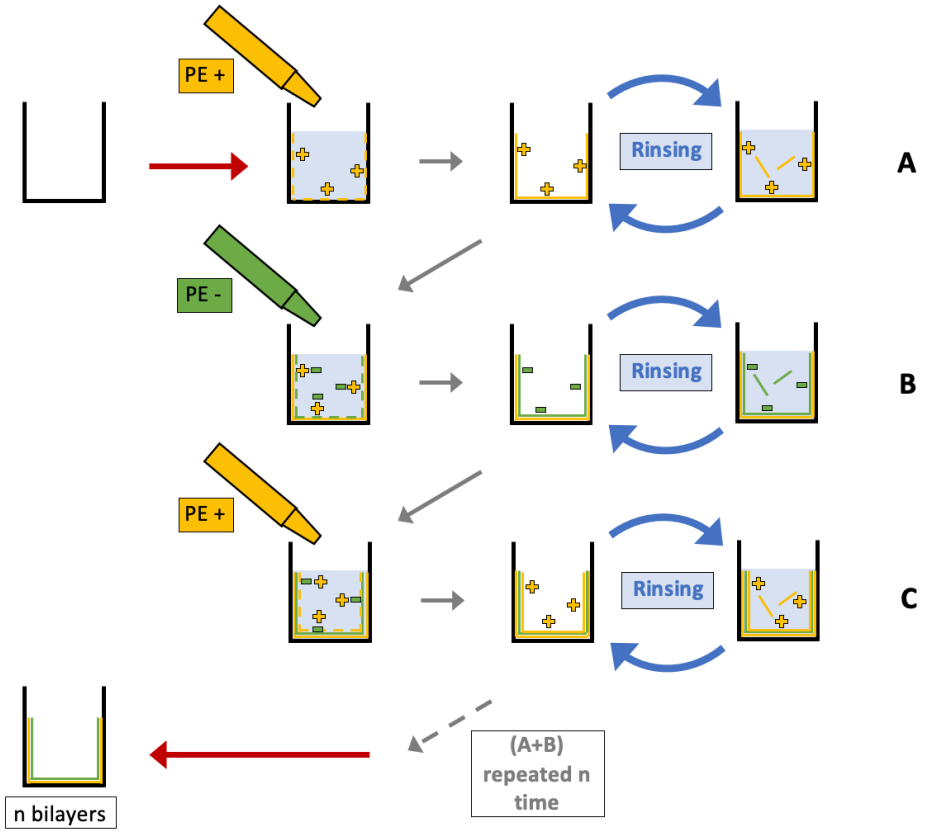

Figure 6 : LbL assembly of a multilayer formed of two oppositely charged PEs. A) The first positively charged PE interacts with the well walls leading to a surface globally positively charged. A rinsing step eliminates the too weakly bound PEs. B) The negatively charged PE is next added and interacts with the first positively charged PE leading to the overcompensation of negative charges of the surface. A same rinsing step occurs after that. C) The first adsorption step is reproduced to illustrate the continuity of the method. A) + B) form a bilayer and can be reproduced n times to reach the number of bilayers desired.

Then the first solution is removed, and the well is rinsed to eliminate the PE not bound or too weakly bound to the surface (Figure 6A). After that, the second PE, negatively charged this time, is placed in the well and can thus interact with the positively-charged surface, leading once again to its adsorption on the surface and to the overcompensation of the global surface charge (now negatively charged). This adsorption of two PE layers forms a bilayer (Figure 6B). After that, the first positively-charged PE is once again placed in the well and the same phenomenon occurs (Figure 6C). The multilayer keeps growing until the desired number of bilayers is reached. This method allows the construction of the bioactive coating with a number of bilayers needed to reach the LL37 amount required to have a wound healing effect while permitting its release in the wound area.

3.2.2 Polyelectrolyte multilayers (PEM)

a) PEM properties

The key parameters influencing LbL assembly are the type of interactions present, the environmental conditions and the choice of the surface and materials. [22] As the interaction type was already determined as electrostatic, the assembly conditions will be discussed here, followed by a description of the material used.

A good understanding of the effects of the different environmental factors on the PEM is crucial to characterize the PEM and discuss its properties. Borges et *al.* [22] have provided a quite complete review of those factors and their influence over the stability, structure, properties, and growth of the PEM. They can be divided in two categories: the environmental condition factors i.e. the physicochemical parameters that are the pH, ionic strength, temperature, adsorption time, electrolyte species, and solvent quality; and the intrinsic PE properties such as charge density, molar mass, and architecture. These parameters are presented in Table 1 and will be briefly described here with an emphasis on their effect on PEM growth and thickness. As the pH and the ionic strength are the most important ones, they will be a little bit more developed.

As the LbL method is based on weak electrostatic interactions, the PEM will be highly sensitive to the pH. [24] Rubner et *al*. [26] have shown that by slightly changing the pH, it is possible to construct multilayers with different thicknesses. Their multilayers were constructed with weak PEs which were poly(allylamine hydrochloride) (PAH) as the cationic PE and poly(acrylic acid) (PAA) as the anionic PE. This modification of the multilayer thickness is possible because a change of pH will induce a change in the charge density of the PEs. If the pH increases, the anionic PE (PAA) will present more negative charges (until it becomes fully charged) and the charge density of the cationic PE (PAH) will decrease. So, to overcompensate those numerous PAA negative charges, more PAH is needed, resulting in an increase in the PAH layer thickness. It is important to add here that at some pH, certain PE can take a preferable conformation (loop, coil, etc.) that can also affect the PEM thickness.

The ionic strength of the used solutions will also impact the building of the multilayer as it represents the density of ions present in the solution. Those ions can induce a screening of the PE charges, decreasing the adsorption capacity of the next PE layer. This competition between the PE and the external salt ions for the adsorption on the precedent PE of the multilayer can leads to the dissociation of the PEM as studied by Dubas et *al.* [27]

Table 1 : The physicochemical parameters and the intrinsic PE parameters that influence PEM formation and properties and a quick summary of their effects on the PEM thickness.

Physicochemical parameters	pH	• Change in pH affects the number of charges present on the layers and thus modifies the thickness of PE needed to overcompensate those charges.	Rubner et *al.* [26]
	Ionic strength (I)	• The screening of the salt ions induces a competition between the PE and the external salt ions for the adsorption on the multilayer.	Dubas et *al.* [27]
	Temperature	• Increase of temperature induces a swelling of the film, allowing better interpenetration.	Tan et *al.* [28]
	Adsorption time	• More time for the low molar mass PE to diffuse into the PEM.	Yang et *al.* [29]
	Electrolyte species	• Chaotropic counter anions interact more with the PE leading to an increase of PEM thickness.	Salomäki et *al.* [30]
	Solvent quality	• A poor quality solvent induces poor interactions between the PE and the solvent leading to a collapse of the PEM film.	Poptoshev et *al.* [31]
Intrinsic PE properties	Charge density	• Can be tuned by the pH and thus interferes in the same way.	Borges et *al.* [22]
	Molar mass	• PE of low molar mass favors its diffusion into the PEM.	
	Architecture	• The ramification of a branched PE affects the LbL assembly as there is a competition for sites.	Houska et *al.* [33]

The three next physicochemical parameters are based on the same phenomenon. They all interfere with the diffusion capacity of a low molar mass PE through the PEM, illustrating the dynamic aspect of the multilayer construction. If this diffusion is possible (if the PE molar mass is low enough), the film thickness will grow exponentially as opposed to a linear growth of the film thickness if this diffusion is not possible. [22] Tan et *al.* [28] show that the increase of temperature will favor the swelling of the film that will allow an increase of interpenetration between the PE layers. Yang et *al.* [29] investigate the effect of adsorption time and show that if the PE has a low molar mass, the PEM construction is more time-dependent due to the possible diffusion of the PE through the film. For the electrolyte species, it is more the nature of the used counter ions that will affect the PEM. Indeed, Salomäki et *al.* [30] have varied the nature of the counter anions following the Hofmeister series from cosmotropic to chaotropic anions. They have found that the chaotropic agents, which interact very poorly with water, screen strongly the PE charges and thus induce the PE deposition in a loopy conformation on the surface leading to a thicker PEM. Even if there is not yet protein in the PEM discussed here,

it is important to keep in mind that the chaotropic ions can disturb the 3D structure of proteins, which can be problematic. Finally, if the solvent quality is decreased, it can decrease the PEM thickness as shown by Poptoshev et *al.* [31] who have changed the concentration of ethanol in the PE solutions and compared the results obtained with the ones using water. They found that the decrease of the solvent quality (by increasing the volume of EtOH) leads to poor interactions between the PE and the solvent inducing a PEM collapse resulting in a decrease of the film thickness.

For the intrinsic PE properties, the charge density can be tuned by the pH and thus will affect the PEM in the same way. The PE charge densities can induce a change in the thickness of the layers and thus change the organization of the multilayers. [32] The molar mass and the architecture will also influence the PE diffusion phenomenon through the PEM. A low molar mass will favor diffusion, leading to an exponential PEM growth. The increase of the number of chain arms in a branched PE made the penetration more difficult. In addition, Houska et *al.* [33] investigated the chain length on the building of protein/PEM assemblies and show that the chain length of the polyanion affects the LbL processes due to the competition between the already adsorbed protein and the protein still in solution for the polyanion sites.

Now that the PEM formation parameters are clearly stated, the next sections will focus on the material chosen for the LbL assembly done in this work, especially the incorporation of a protein into the multilayer.

b) Incorporating proteins in PEMs

The insertion of proteins in PEMs can be tricky due to their amphiphilic nature and their heterogeneous charge distribution. Positive and negative charges present on the protein will favor either the attraction or the repulsion of the PE of the previous layer, decreasing the adsorption efficiency. In addition, the polyampholyte nature of the protein decreases its number of possible conformations in the PEM. A solution to overcome this charge distribution issue is to use protein-polyelectrolyte complexes (PPCs) as building blocks in the LbL assembly. The PPCs were widely studied by Aurélien vander Straeten during his thesis as described below. [34]

3.3 Protein-polyelectrolyte complexes

3.3.1 PPCs formation

PPCs are formed by mixing a protein with a PE of the opposite charge. The goal is to trap the protein inside a PE ring that will standardize the global surface charge of the protein. The ratio of negative to positive charges can be adjusted in function of the density of charges

of the protein. Thanks to its charge homogeneity, this new building block thus improves its interactions with the other PE of the multilayer construction, that is obviously charged oppositely to the one used in the PPCs. This complex will also give an additional protection to the protein from denaturation and maintains its antimicrobial activity. [32]

As the LL37 is globally positively charged, a negatively-charged PE is thus required to form the PPC. In this work, alginate (ALG) will take the role of the negatively-charged PE. The PPCs(LL37-ALG) formation is illustrated in Figure 7. It will be used as the negative building block for the LbL assembly and be alternated with layers of chitosan (CHI) working as the positively-charged PE. These PE are both described here under.

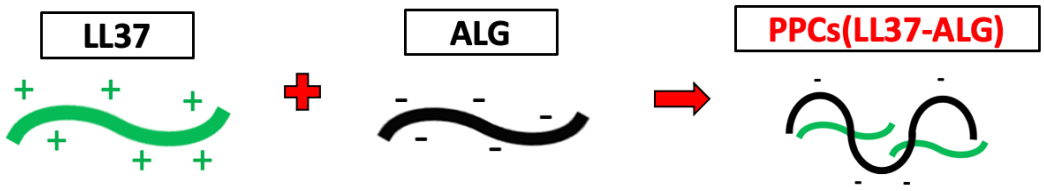

Figure 7 : PPCs(LL37-CHI) formation from LL37 and ALG.

3.3.2 Polyelectrolytes

a) Alginate

Alginate is a natural anionic polymer. It comes from brown seaweed and shows great biocompatibility and low toxicity. It is a low-cost PE and is usually produced in the form of a sodium salt: $C_6H_7NaO_6$ as illustrated in Figure 8A. It presents a pKa of 3.5. Each monomer has a molar mass of 198 g/mol and presents one carboxyl function that can be negatively charged depending on the pH. It was already widely used as wound dressing to keep a moist environment around the wound area as well as in the form of a hydrogel and is thus a PE of choice for the construction of bioactive coatings. [35]

b) Chitosan

Chitosan is a polysaccharide derived from chitin, a natural component found in the exoskeleton of some insects and crustaceans. Its biocompatibility, biodegradability, film forming capacity and antibacterial activity explain its wide range of application domains such as biomedicine or tissue engineering. This polycationic polymer possesses reactive hydroxyl and amino groups and shows a pKa of 6.3. Its high charge density can vary in function of its degree of de-acetylation. For this work, a CHI de-acetylated at 95% was used as represented in Figure 8B. CHI presents interesting antimicrobial and antibiofilm properties that may reinforce the coating healing capacity. [36], [37]

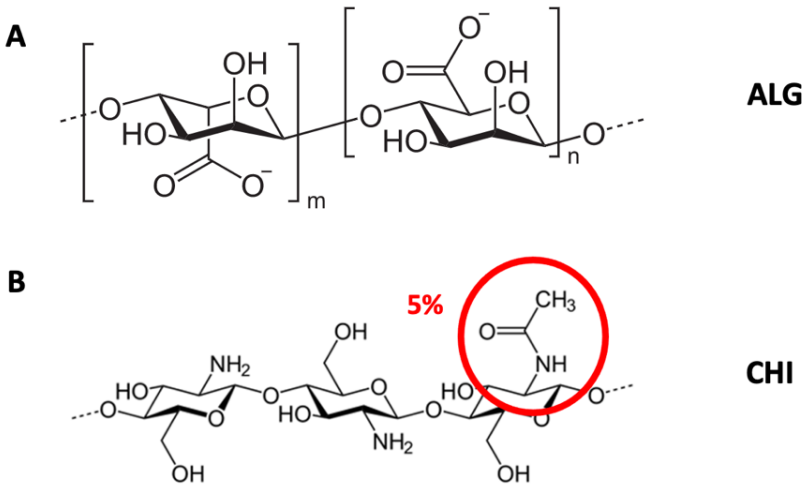

Figure 8: Chemical structure of A) Alginate and B) Chitosan.

3.3.3 PPCs in the multilayer

As they are charged object, the incorporation of PPCs in PEMs will be affected by the same parameters discussed above. A. vander Straeten studied the effect of the main parameters that are pH and ionic strength on the self-assembled LbL film composed of PAH-PPCs. The PPCs were formed by complexing poly(styrenesulfonate) (PSS) with lysozyme (Lys). The main results are exposed here and illustrated in Figure 9.

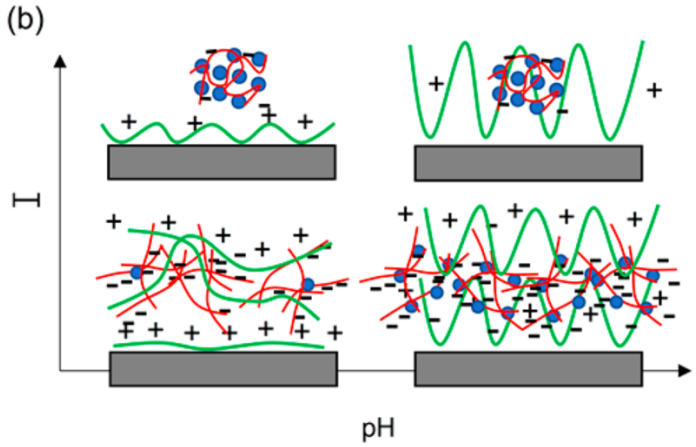

Figure 9 : Schematic representation of the [PAH-PPCs]$_{1,5}$ multilayer construction as function of the ionic strength and the pH. The Lys are in blue, the PSS in red, and the PAH in green. The surfaces with a cushion of [PAH-PSS]$_2$ are in grey.[32]

For high ionic strengths, they observed a low immobilization of Lyz and no LbL growth due to the screening of the PE charges. Then, at low I and low pH, there is a multilayer growth but a low amount of Lys was detected in the multilayer. This can be explained because the PAH is fully ionized at low pH and thus, the electrostatic interactions between PAH and PSS

are maximal which can displace the Lys, more weakly bound to the PSS. Finally, at low I and high pH, PAH presents a larger population of loops and tails than at low pH, that can be visualized in green in Figure 9. This allows a better charge overcompensation, resulting in a better conservation of the Lys into the multilayer. With these results, it is concluded that to immobilize a high protein amount, the conditions need to be sufficiently favorable so that the PSS conformation coexists with sufficiently attractive PSS-Lyz electrostatic interactions. The driving force of the LbL assembly was also reported to be solely based on PE-PE interactions, which provides a great attractiveness to PPCs as building blocks to incorporate all kinds of proteins into PEMs.

3.3.4 Study of the [CHI-PPCs(LL37-ALG)] multilayers

A. vander Straeten also studied the properties of $[CHI\text{-}PPCs(LL37\text{-}ALG)]_n$ multilayers in his thesis. He shows that the assembly using bare LL37 peptide and ALG fails to grow in a multilayer while much higher amounts of protein can be immobilized by using the PPCs(LL37-ALG) as building blocks. He manages to immobilize 0.42 µg of LL37/cm^2 per bilayer constructed on a planar surface. Then, he has tested the same construction on a dressing and computed this time a LL37 mass of 0.42 µg/cm^2 per bilayer, with a saturation occurring around 5 µg, corresponding to 9 bilayers. [34]

3.4 Quantification of immobilized LL37

The development of the effective LbL immobilization method triggers the necessity of developing a robust quantification method to evaluate the amount of proteins that is immobilized in the coating. The focus of this master thesis is set on the quantification of LL37 incorporated in PEMs. To do so, several protein quantification tests are available and two of them will be used in this work. Their principle will be explained in detail in the Materials and methods section that follows.

3.5 Multilayer disassembly

To quantify the protein amount in the multilayers, it is usually needed to desorb the multilayer from the surface. A explained previously, the change in some physicochemical parameters will impact the PEM construction and the stability of a formed PEM may also vary. Modifications of the conditions can sometimes lead to the desorption of the multilayer. For example, a change in pH can modify the charge of the PEs and decrease their interaction with each other up to their repulsion. Changes in temperature and ionic strength could also be used for desorption. However, in the quantification tests, there is usually a step of addition of a detergent to ensure multilayer desorption. A widely used detergent is sodium dodecyl sulfate (SDS) and its chemical structure is presented in Figure 10. Rahim et *al.* reported that the

desorption of PEMs by SDS results from electrostatic interactions between PEMs and SDS. They also reported that the rate and degree of PE desorption from the PEM films could be affected by the concentration and the choice of the surfactant, by the outermost layer of the PEM, and by the reaction time. [38]

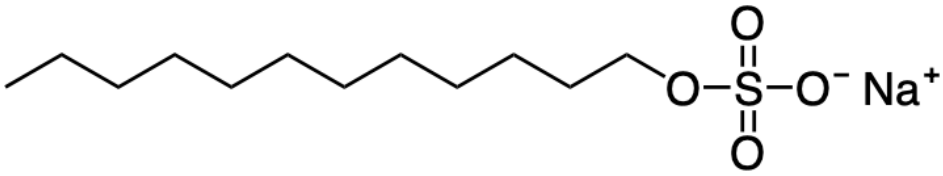

Figure 10 : Chemical structure of sodium dodecyl sulfate.

Objectives and strategy

This work will aim in a first time to validate the construction of the multilayer and then will study the quantification of the LL37 immobilized in that multilayer by using different quantification methods. To allow a better view of the objectives and the strategy, this section will be divided in multiple steps, representing the different objectives, linked together with some scientific questions which will in fact reflect the strategy used during this work.

How to immobilize LL37 in the coating?

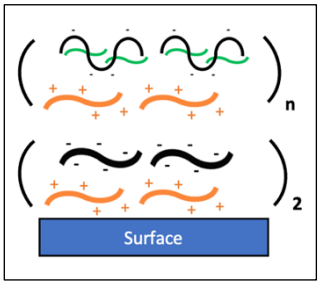

Firstly, it is important to validate the approach for the multilayer construction presented in the previous sections. And to do so, quartz crystal microbalance (QCM) can be used to visualize the evolution of the multilayer thickness in function of the adsorption steps of the different components.

How much LL37 is immobilized in the coating?

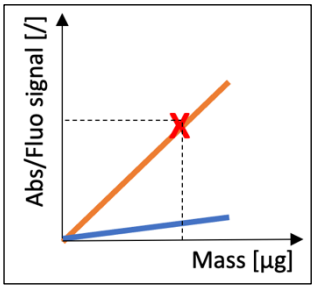

Secondly, as showed previously, LL37 needs to be in a sufficient amount to ensure its wound healing effect, which is of the order of 5 µg/cm^2. The second experimental step is thus to develop a robust quantification method of the LL37 immobilized in the multilayer, to know if the required amount is reached. This second interrogation leads to multiple experimental tests and to a combination of two different quantification methods that are BCA and NanoOrange assays, to compute a more accurate LL37 immobilized mass.

Is all the multilayer really quantified?

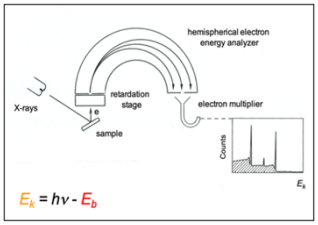

The LL37 mass obtained in the second experimental step is only accurate if all the LL37 immobilized in the multilayer is well quantified. In other words, one needs to be sure that all the LL37 is desorbed from the surface and quantified by the BCA and NanoOrange tests. A way to verify this is to use a surface chemical analysis method, like XPS, on surfaces having undergone the quantification tests. That will be the third experimental step of this master thesis.

How to validate the determined LL37 mass?

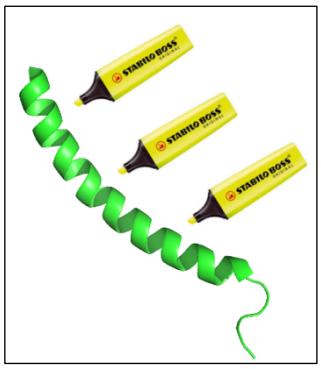

As the previous quantification tests always present some interference signal in addition to the one of LL37, it is interesting to try another quantification technique, like the one based on fluorescence. LL37 can be marked by fluorescence before being immobilized on the surface. The fluorescence signal that emerges from the multilayer is thus only due to the presence of the marked LL37. The approximations made on the determination of the LL37 mass with the other quantification methods could thus be avoided.

Materials and methods

The following sections present the technical information related to the experimentations carried out in this work. Firstly, the solutions of the components used in the multilayer and how the multilayer construction takes place are described. The different surfaces on which the multilayers were built are also detailed. Then, the methods used to quantify the amount of LL37 present in the coating are explained. Finally, the characterization methods utilized to have information about physicochemical properties of the multilayer like the thickness or the chemical composition are reported.

1. Multilayer construction

As described in the State of the art section, several parameters can impact the multilayer construction. Most of them will be kept constant: the ionic strength will be kept as low as possible (I≈0mM), the experimentation takes place at room temperature, the adsorption time will be fixed at 20 min per component (following the result of the QCM experimentation), the PEs are CHI and ALG and the solvent is water. However, the effect of the pH on the multilayer construction will be evaluated by making experimentation at pH 3.5 and 5.

1.1 Polyelectrolyte solutions

For all the solutions requiring to weigh a component, a microbalance (OHAUS, Explorer) was used and the used ultra-pure water was taken from a MilliQ machine (PURELAB Chorus), with a resistivity of 18,2 MΩ and a total organic carbon (TOC) comprised between 1 and 10 ppb.

1.1.1 Chitosan

In all experiments, a solution of 0.5 g/L was used for chitosan. The chitosan is 95% deacetylated and comes from Heppe Medical Chitosan Gmbh, Halle in Germany. To ensure good solubilization of the solid chitosan, a small volume of concentrated (cc) HCl (60 µL for 100 mL of solution) was added in the solution before placing it in a hot water bath at 60°C for 1 hour minimum (longer if all the chitosan is not well solubilized). Then the pH of the solution was rebalanced by adding a certain volume of ccNaOH (30 µL for 100 mL of solution). After homogenization, the solution was filtrated by 2 different types of syringe filters: firstly, with a cellulose filter of pore size of 5 µm (Ahlstrom, Barenstein, Germany) and then with a polyethersulfonate filter of pore size of 0.2 µm (VWR Chemicals, Leuven, Belgium). Finally, the solution pH was adjusted to the value wanted for the experimentations (3.5 or 5) by the addition of small droplets of ccNaOH. The pH was measured using pH-indicator strips

MColorpHast™ (Darmstadt, Germany). It is important to keep in mind that as we want the ionic strength of the solution to be as low as possible, we need to be careful when adjusting the pH to use minimal amount of ccHCl or ccNaOH. The solution was then stored in a cold room at 5°C and kept for maximum 2 weeks.

1.1.2 Alginate

The solution of alginate used in all the experimentations was also of 0.5 g/L. The utilized ALG has a molar mass of 198 g/mol per monomer residue and a total molar mass < 75000 g/mol (Pronova UP VLVM, NovaMatrix, Norway). ALG is soluble in water and the ultra-pure water used to solubilized it was already at the required pH (3.5 or 5) by addition of ccHCl. As ALG bear charges, its solubilization can be assisted by placing the gauge in a sonicator to disassociate the aggregates if needed. The same previous remark for the ionic strength also applies here. The solution was then stored in a cold room at 5°C and kept for maximum 2 weeks.

1.1.3 LL37

The LL37 aliquots were made at 0.450 g/L by C. Vranckx and frozen at -20°C. The solutions were diluted later if needed. LL37 presents the following sequence: LLGDFFRKSKEKIGKEFKRIVQRIKDFLRNLVPRTES and has a molar mass of 4493.26 g/mol (98,05% pure, ProteoGenix, France).

As for the LL37 marked by fluorescence, solutions of 1g/L were firstly made and then diluted later if needed. The LL37 marked with a fluorescein isothiocyanate (FITC) presents the following sequence: FITC-LLGDFFRKSKEKIGKEFKRIVQRIKDFLRNLVPRTES and has a molar mass of 4995,80 g/mol (96,55% pure, ProteoGenix, France). A representation of the chemical structure of FITC is exposed in Figure 11. FITC has a theoretical fluorescence excitation peak at 490 nm and a fluorescence emission peak at 525 nm as given by ThermoFischer.

1.1.4 Other solutions

The ccHCl stock solution has a concentration of 12M and comes from Prolabo, VWR Chemicals, Leuven in Belgium. As for the ccNaOH stock solution, it has a concentration of 10M and comes from Sigma Aldrich, Steinheim in Germany. The SDS solution was made by putting 10 g of SDS (99%, Sigma) in 200mL of ultra-pure water to have a solution at 5% of SDS.

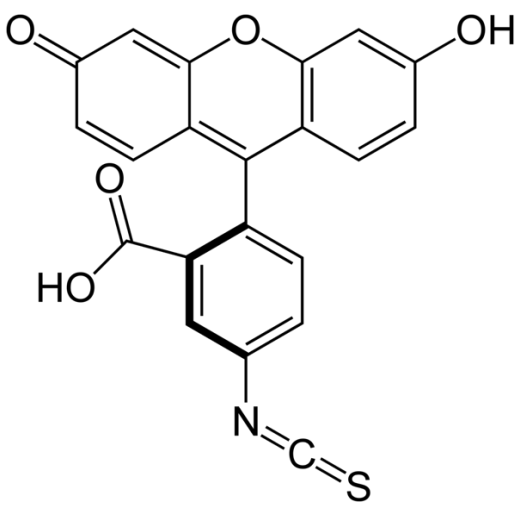

Figure 11 : Chemical formula of fluorescein isothiocyanate (FITC) used to mark LL37.

1.2 PPCs formation

As shown by Aurélien vander Straeten and recalled in the State of the art section, PPCs allow to override the charge heterogeneity of the protein. To be able to use PPCs as building blocks for LbL assembly, it is thus crucial to have a complete charge overcompensation of the protein by the PE used for complexation. This is possible by varying the ratio of negative to positive charge and it will be fixed here at 2 for all the experimentations. The charge of the LL37 at the different pH values can be calculated using the PDB2PQR server and the PROPKA tool. [38] LL37 has 10.395 positive charges per peptide at pH 3.5 and 7.02 positive charges at pH 5.

By fixing this ratio of 2 and knowing the properties of the used LL37 and ALG (molar mass, pKa, number of charges at certain pH, concentration of the solution, etc.), it is now possible to compute the volumes of each component needed to form the volume of PPCs required for each experimentation. The PPCs solutions were made daily by vortexing together the correct amounts of LL37, ALG and ultra-pure water to have the charge ratio of 2 and the volume of PPCs required for the different experimentations.

1.3 Multilayer assembly

Before starting the LBL construction as previously described, a cushion formed by two bilayers of CHI and ALG was made on all the surfaces as illustrated in Figure 12. This cushion allows to be sure that the different used surfaces present the same properties and permits to charge the well surface before starting the multilayer construction. Indeed, when using microplates, the first interaction between the chitosan and the microplate surface is mostly

of hydrophobic nature and only after that, the surface starts to be charged, allowing electrostatic interactions between the building blocks.

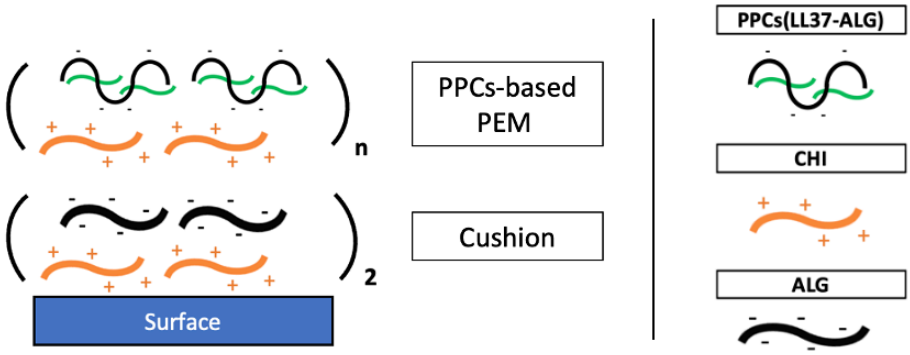

Figure 12 : Illustration of the presence of a cushion made of two bilayers of CHI and ALG on all surfaces before starting the construction of the multilayers containing PPCs. Schematic not at scale.

After the cushion construction, the assembly of the multilayer containing CHI and PPCs(LL37-ALG) started. However, the schematic describing the assembly presented in Figure 6 will be more detailed in this section. As the cushion ends with a negative layer of ALG, the next layer will be thus CHI. The surface is then rinsed three times with ultra-pure water at the pH of the experiment to remove the excess PEs. For each rinse, the microplate is shaken for 30 seconds. The solutions from the well were removed using a tip mounted on a syringe, connected to a vacuum pump linked to the tap. This set-up creates an aspiration at the end of the tips that sucks the solution when dipped in the well. A special attention was thus made to always touch the bottom of the well at the same place to minimize the degradation of the multilayer.

This method was followed to build until 25 PPCs-based bilayers. As it is a time-consuming method, the construction of all the multilayer could take several days. The microplate was thus placed in a cold room at 5°C during the night with ultra-pure water at pH 3.5 or 5 in the wells. The PPCs were prepared daily in function of the volume required for the number of bilayers constructed during the day.

Several multilayers were built with an increase of the number of bilayers to see the evolution of the multilayer step by step. Each kind of multilayer (with different numbers of bilayers) was prepared in triplicate to confirm good reproducibility. They were composed of either just the cushion or 1, 3, 5, 6, 9, 10, 12, 15, 20 or 25 PPCs-based bilayers. A triplicate of blank was also added to the microplate measurements. For each adsorption step, a volume of 100µL was put into the well for 20 minutes to allow adsorption of the component on the surface. Each rinse was also made with a volume of 100µL. To be able to compare the result of the future tests made on those different multilayers, the protocol was adjusted to finish all

the multilayer at the same time rather than finishing the smallest multilayers long before its measurement, waiting for the thicker ones to be constructed.

1.4 Surfaces

Different surfaces were used for the experiments performed in this work. In the following sub-sections, the treatment of those surfaces before starting the multilayer construction on them will be presented.

1.4.1 QCM sensors

For the QCM experiments, two different types of crystal were used, with sensors of two different nature: titanium and gold. The gold crystals were cleaned using a piranha solution (10 mL of H_2O_2 added to 20 mL of H_2SO_4) for 2 min to remove the organic contaminants. After their rinsing with ultra-pure water, they were placed in a berlin, immerged in ethanol (Ethanol 99%, VWR Chemicals), and sonicated for 10 min. Finally, after a second rinsing step, they were dried with N_2 and passed in a UV/O_3 cleaner (UVO Cleaner 42-220, Jelight Company, Irvine, United States) for 15 min. As for the titanium surfaces, the piranha solution was not used to avoid titanium oxidation. They were firstly carefully mechanically scrubbed with a lens filter imbibed in EtOH and then immerged in a solution at 1% in Hellmanex for 30 min at ambient temperature. They were then dried with N_2 and sonicated in EtOH solution for 10 min as for the gold surfaces. Finally, they were rinsed, dried with N_2 again, and then passed in UV/O_3 for 10 min.

1.4.2 Microplates

Several microplates were used during this master thesis and are listed in Table 2. The switch of plate type from n°1 to n°2 was due to a stock shortage of the initial plate type caused by the COVID-19 pandemic. However, the similarity of the chemical treatment applied to the two different plate surfaces was verified prior to use, to be sure to have comparable results for the different plates. All the four first kinds of plates are from Greiner Bio-one and composed of polystyrene. The fifth kind of plate is a custom-made plate ordered by V. Delmez and made of Teflon. This plate was used to prepare the titanium samples for the XPS experimentation and permits to use less solution to build the multilayer, when compared to the use of a more classical 24 wells microplate.

1.4.3 Titanium surfaces

The samples for the XPS measurement are made of Ti-6Al-4V titanium alloy (Grade 23; President Titanium, Massachusetts, United States). They were already cut out in squares with

a side of 1 cm, and already polished by C. Vranckx. To clean them, they were placed in a berlin, immersed firstly in a EtOH solution, and passed in a sonicator for 10 min. The previous action was repeated two times. Then, the surfaces were dried with N_2, immersed two times again in an acetone solution (Acetone 99.8 %, Merck, Darmstadt, Germany), and put again in a sonicator for 10 min. After a final N_2 drying, they were put into the UV/O_3 for 15 min. They were then placed in the microplate n°5 and the construction of the multilayer was carried out as explain above.

Table 2 : Different microplate types used in this work. A number is given to each of the microplate to be cited more easily in the next sections. The reference of each plate is reported with their brief description coming from the Greiner Bio-One platform. The experimentations done with each microplate are then detailed to give a first view at the readers of the material used but will also be specified in the results section. Finally, an illustration is added to give a better visualization of the different microplate types.

N°	Ref.	Description	Experimentations done	Illustration
1	655180	Cell culture microplate, 96 wells, PS, F-Bottom, clear, CELLSTAR®, TC.	• All the experiments when 25 bilayers were constructed.	
2	655098	Cell culture microplate, 96 wells, PS, F-Bottom, µCLEAR®, white, CELLSTAR®, TC.	• All the experiments when 15 bilayers were constructed.	
3	655077	Microplate, 96 wells, PS, F-Bottom, black, FLUOTRAC, high binding.	• All the fluorescent measurements from the top.	
4	655096	Microplate, 96 wells, PS, F-bottom, µCLEAR®, black, medium binding.	• Used for testing a fluorescence measurement from the bottom.	
5	/	Custom made microplate.	• Used to prepare the sample for the XPS experimentation.	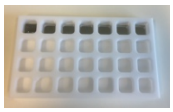

2. Quantification methods

As explained in the State of the art section, it is important to develop a robust quantification method for LL37 immobilized in the multilayer using LbL assembly. The choice and the principle of three different protein quantification tests used in this work will be presented in this section. A combination of the two first tests has also been conducted and will be discuss in the results section. All the absorbance and fluorescence measurements were performed using a microplate reader spectrophotometer (SpectraMax® iD3, Molecular devices). This part reports the theoretical operations of the different tests, but the specific

parameters used for each experimentation (wavelength, number of bilayers, etc.) will be described in the results and discussion section.

2.1 BCA protein quantification test

The bicinchoninic acid (BCA) protein assay test is widely used for the colorimetric detection and quantification of proteins over a broad concentration range: from 5 to 250 µg/mL with an adjusted protocol. This method is based on the reduction of Cu^{2+} to Cu^{+} by the protein in an alkaline medium. Then, the bicinchoninic acid and Cu^{+} form a purple-colored water-soluble complex that exhibits a strong absorbance at 562 nm as illustrated in Figure 13. This absorbance increases nearly linearly with the protein concentration. Unlike other protein quantification test, the BCA test allows protein quantification in presence of detergents such as SDS that will be used here to desorb the multilayer from the well surface.[39]

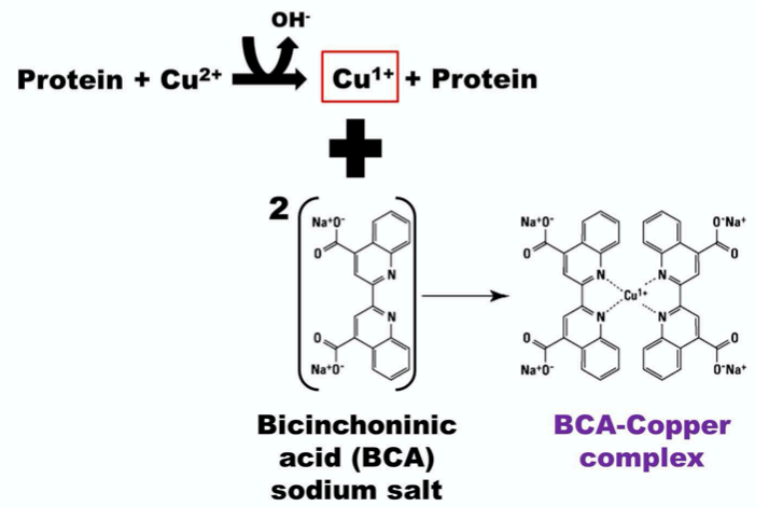

Figure 13 : Chemical principle of the BCA test. The protein reduces the Cu^{2+} in Cu^{+} that can interact with the bicinchoninic acid and form a purple complex that exhibits a strong absorbance at 562nm.[40]

BCA is sensitive to the amide groups present in the solution and to four particular amino acids: cysteine, cystine, tryptophan, and tyrosine which are not present in LL37. The absorbance signal of LL37 is thus due to its numerous peptide bonds and to the amide group of the asparagine (N) and the glutamine (Q), each present one time in the LL37 sequence.[39]

The multilayers were constructed from the cushion and up to 25 PPCs-based bilayers, in the microplate n°1 or n°2 and at a pH 3.5 or 5 (that will be specified in the result section for each experiment). To quantify the different components present in the different multilayers, three calibration curves were made with a known amount of either LL37, CHI or ALG. The protocol followed to establish the calibration curves and to perform the tests on the multilayers is presented in Table 3. For the calibrations, a computed volume of component was put into the wells, with 4µL of SDS, a volume of water calculated to keep the same total

volume in all the wells, and finally 200 µL of BCA reagent. In the wells in which the multilayers were constructed, 4 µL of SDS (5% in weight) were added to desorb the multilayer, then 16 µL of ultrapure water to reach the same volume as the one in the calibration curves. Finally, 200 µL of the BCA reagent were added in all the wells to reach a total volume of 220µL per well. The BCA reagent was made by mixing reagents A and B of the Thermo Scientific™ Pierce™ BCA Protein Assay Kit (Thermo Scientific, USA) in a proportion of 50:1 respectively. The microplate was then sealed by an adhesive tape (VWR, polyester, USA) and placed in a hot water bath at 60°C for 1 hour. After that, the plate was left for 20 min to return to room temperature before measuring its absorbance at 562 nm using the spectrophotometer, with 10sec shake before measurement and one measurement point per well.

Table 3 : Protocol followed to obtain the BCA calibration curves for the different components: first for the LL37 and then for CHI and ALG, presented in the same table as they follow the same protocol. The protocol followed in each well of the microplate for the BCA test of the different multilayers is also presented.

	CALIBRATIONS									
LL37	**µg LL37**	**0**	**0.9**	**1.8**	**2.7**	**3.6**	**4.5**	**5.4**	**6.3**	**7.2**
	µL LL37 (0.45 g/L)	0	2	4	6	8	10	12	14	16
	µL SDS (5%)	4	4	4	4	4	4	4	4	4
	µL WATER	16	14	12	10	8	6	4	2	0
	µL BCA REAGENT	200	200	200	200	200	200	200	200	200
CHI/ALG	**µg CHI/ALG**	**0**	**1**	**2**	**3**	**4**	**5**	**6**	**7**	**8**
	µL CHI/ALG (0.5 g/L)	0	2	4	6	8	10	12	14	16
	µL SDS (5%)	4	4	4	4	4	4	4	4	4
	µL WATER	16	14	12	10	8	6	4	2	0
	µL BCA REAGENT	200	200	200	200	200	200	200	200	200

	MEASUREMENTS	
MULTILAYERS	**Number of bilayers**	**n bilayers**
	µL SDS (5%)	4
	µL ULTRAPURE WATER	16
	µL BCA REAGENT	200

2.2 NanoOrange protein quantification test

The NanoOrange (NO) test allows a better sensitivity than other protein quantification tests while being simple to use and low cost. Indeed, it permits to detect proteins by fluorescence from 100 ng/mL to approximately 10 µg/mL when using a microplate reader. Usually, the techniques based on fluorescence offer higher sensitivity and lower background signals than absorbance-based techniques.[41] Those properties make the NO test a promising test to quantify the amount of LL37 present in the multilayer construction. The NanoOrange™ protein quantitation kit (Invitrogen, Molecular Probes, USA) is composed of two different components: a protein quantification reagent and a protein quantification diluent. The reagent is nonfluorescent in aqueous solution but when bound to proteins, it has an excitation peak around 470 nm and an emission peak around 570 nm.[42]

However, the exact way of how the reagent interacts with the proteins to allow their detection by fluorescence is unknown to us as the test is sold in the form of a commercial kit. When looking in the literature, one can see that there are two general methods for the detection of protein based on fluorescence. The first one employs nonfluorescent, reactive dyes that form a fluorescent covalent adduct when bound to amine groups. The second uses dyes that exhibit a fluorescence enhancement when they interact non-covalently with hydrophobic regions of proteins or detergent-coated proteins. The NO reagent appears to be a merocyanine dye that produces a large increase of fluorescence when it interacts non-covalently with detergent-coated proteins. [41], [43] This means that the NO test seems to be part of the second fluorescence method and the fact that the test is insensitive to the presence of a large quantity of amino acids (up to 10µg/mL) validates the non-selection of the method based on amine interactions. Nonetheless, not knowing the exact way of how the test works is not critical if it can detect proteins. Indeed, if the signal of fluorescence increases with the component concentrations, it can be used to access the component mass present in the different experiments.

However, once again, the nature of the detergent is unknown. The protein quantification diluent presents some detergent as it lathers upon agitation and as the proteins need to bind with detergent to interact with the dye present in the NanoOrange reagent. To compare its strength with the one of SDS, an adapted protocol was made by mixing the two tests and will be explained with the results.

The NO protein quantification tests done in this work followed the protocol described in Table 4. Calibrations were sometimes adjusted for certain experiments and this will be specified in the Results section when it is the case. The multilayers and the calibrations were firstly made in the microplate n°1. Then, 20 µL of ultrapure water was added to the wells containing multilayers. The volumes of ultrapure water for the calibrations were adjusted to

keep a total constant volume of 250 µL. Finally, a solution of reagent was made by diluting 10 time the NO diluent and 500 time the NO reagent from the kit into ultrapure water. To avoid photobleaching, from the moment that the NO reagent from the kit was used, the experimentation has taken place protected from the light. A volume of 230 µL of this new reagent was added to the different wells. The microplates were then sealed with an adhesive tape and put in a hot water bath at 80°C for 10 min. After that, they were cooled down at room temperature for 20 min. Then, 200 µL of each well were transferred to the microplate n°3 to allow fluorescence measurement. The fluorescence measurements were made using the spectrophotometer, at adjusted wavelengths provided by the kit: 485 nm for the excitation and 590 nm for the emission, 10 s shake before measurement and one point per well. [42]

Table 4 : Protocol for the NO protein quantification kit with the LL37/CHI/ALG calibrations. A dilution was made to have a solution of 0.10 g/L from a solution of 0.45 g/L.

	CALIBRATIONS										
LL37/CHI/ALG	**µg LL37**	**0**	**0.2**	**0.4**	**0.6**	**0.8**	**1.0**	**1.2**	**1.4**	**1.6**	**1.8**	**2.0**
	µL LL37 (0.10 g/L)	0	2	4	6	8	10	12	14	16	18	20
	µL WATER	20	18	16	14	12	10	8	6	4	2	0
	µL NO REAGENT	230	230	230	230	230	230	230	230	230	230	230

	MEASUREMENTS	
MULTILAYERS	**Number of bilayers**	**n bilayers**
	µL ULTRAPURE WATER	20
	µL NO REAGENT	230

2.3 Quantification of LL37 marked by fluorescence

LL37 is marked by a FITC at the N-terminal site. The FITC has a maximum excitation and emission wavelength at 490 nm and 525 nm respectively according to the literature. [44] As it is sensitive to photobleaching, all the experiment involving marked LL37 were conducted in a room protected from direct light.

Firstly, some calibrations were made in the microplate n°3 and n°4 to test the fluorescence response of marked LL37 and to find the best method to analyze the fluorescent LL37 present in the multilayer. Three calibrations curves were made in the two plate types. In the first calibration, a volume of 100µL of solution per well was used as explained in Table 5

(this volume corresponds to the component volume used during the LbL construction). Then the microplate was left to dry in a desiccator before being put in the spectrophotometer for fluorescence measurement. This last drying step permits to see if the LL37 fluorescence could be measured on the dry surface of the well or if marked LL37 needs to be in solution in order to detect its fluorescence. The second calibration uses a volume of 50 µL followed by the same drying step. This 50 µL represents the volume needed to entirely cover the bottom surface of the well while minimizing the contact with the edges of the well. The second calibration was thus made to evaluate the edge effect of the well in the fluorescence measurement. The third calibration uses 100 µL, but no drying step was made and the fluorescence of marked LL37 was measured in solution. The two different microplate types differ by the type of bottom of the wells: the n°3 has a dark bottom, allowing only measurements by the top of the wells while the n°4 has a clear bottom which thus permits measurements either from the top or from the bottom of the well. The fluorescence measurements were made by a plate reader spectrophotometer, firstly at the theoretical wavelengths (490/525 nm) and then at adjusted wavelengths (492/522 nm), with 10 s shake before measurements, and firstly with 1 point per well, and then with 5 points per well.

Table 5 : Protocol for the calibration with the LL37 marked. Here only presented for a total volume of 100µL. For the 50µL, the volume of water is just adjusted. The protocol for the fluorescence measurement directly on the multilayers is also presented.

	CALIBRATIONS								
MARKED LL37	**µg LL37**	**0**	**1**	**2**	**3**	**4**	**5**	**6**	**7**	**8**
	µL LL37 (0.50g/L)	0	2	4	6	8	10	12	14	16
	µL WATER	100	98	96	94	92	90	88	86	84
	MEASUREMENTS									
MULTILAYERS	**Number of bilayers**					**n bilayers**				
	µL WATER pH 3.5					200				

The same protocol for the construction of the different multilayers (cushion, 1, 3, 5, 6, 9, 10, 12, 15, 20 and 25 bilayers) at a pH of 3.5 was followed using marked LL37 instead of the classical LL37, to be able to compare the results. However, the amount of LL37 and ALG needed to form the PPCs were calculated with the new molar mass and concentration of marked LL37, to still reach a ratio of negative to positive charges of 2. The fluorescence measurement was made directly on the built multilayer, immersed in 100 µL of water at pH 3.5 as detailed in Table 5.

3. Characterization methods

In addition to the quantification methods used in this work, two characterization methods were also performed to have further information about the mass increase for each adsorption steps of the multilayer construction, or about the chemical composition of the surface before and after desorption of the multilayer.

3.1 Quartz crystal microbalance with dissipation

Quartz crystal microbalance (QCM) allows real-time interface characterization and is used for the study of soft or solvated interface between solid surfaces and bulk liquids. It can monitor dynamic changes in the interface organization and measure small mass variation at the surface of a sample.

QCM is based on the inverse piezoelectric effect: the application of an alternating voltage on a material leads to a cyclic deformation that results in an oscillatory motion. Here, the used QCM crystals were either in gold (commonly used in QCM experiments) or titanium (used in multiple biomedical applications in which the coating studied could be useful). If the frequency of the applied voltage matches the crystal's resonance frequency or one of its overtones, a standing wave is generated inside the crystal. The AT-cut crystals type used in this work vibrate in a thickness-shear mode with a resonance frequency of:

$$f_n = \frac{n * c}{2d}$$

Where n is the overtone order, c is the speed of sound in quartz and d is the crystal thickness. The QCM can be used as a microbalance thanks to its great stability and very low energy of dissipation. Indeed, the addition or removal of material from the crystal surface induces a shift in its resonance frequency as illustrated in Figure 14. The relationship between the mass of the crystal and its resonance frequency is linear and after making some hypotheses detailed below, the relationship can follow the Sauerbrey equation:

$$\Delta f = -\frac{n}{C} * \Delta \mathrm{m}$$

Where Δf is the frequency shift, n the overtone order, C the mass sensitivity factor (depending on the material properties of the quartz crystal) and Δm the mass change per unit area. The different adsorption steps of the multilayer construction can thus be detected during QCM experimentation.[45], [46]

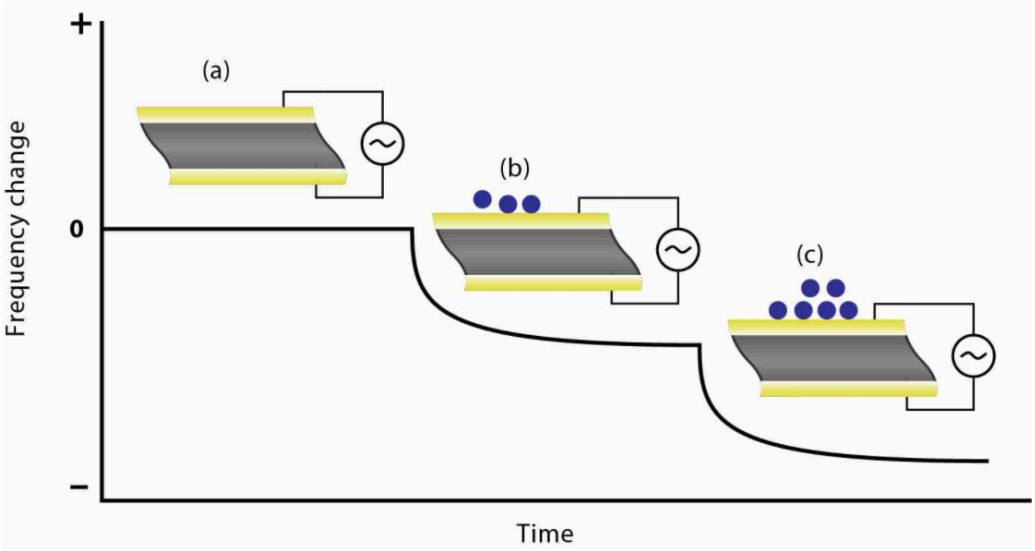

Figure 14 : Schematic representation of the variation of the crystal frequency upon adsorption of material on the surface of the crystal. A) The crystal oscillates at crystal resonance frequency. B) and C) Upon adsorption of material, there is a frequency shift of the crystal.[46]

However, the relationship between the crystal mass and the frequency shift depends on the film type. The limitation of the Sauerbrey's equation is that the adsorbed layer must be thin, homogeneous, and rigid. In that way, the energy dissipated by the film can be considerate as insignificant and the Sauerbrey's equation can be used. In soft and viscoelastic films, there are mechanical losses causing dissipation of oscillation energy, leading to a faster decay of the crystal oscillation. In that case, the Sauerbrey's equation cannot be used, and both the measurement of the frequency and the dissipation are needed to compute the accurate adsorbed mass.

The measurement of those two parameters is possible using a quartz crystal microbalance with dissipation monitoring (QCM-D). In QCM-D, the quartz is briefly excited to its resonance frequency and then an alternating voltage is applied. The energy losses are measured by recording the oscillation decay curve. From the decay curve, the resonance frequency (f) and the energy of dissipation (D) can be extracted. Then, the adsorbed mass and the viscoelastic properties can be modeled using the Voigt viscoelastic model. As the QCM-D enables real-time data acquisition, it can be very useful for the study of the multilayer construction on the crystal and the visualization of the different adsorption steps. [46]

The QCM-D used in this work is the Q-Sense E4 system (Biolin Scientific, Gothenburg, Sweden). [47] The solutions containing the components to be adsorbed on the surface are pumped through the measurement chamber in which one can place maximum four crystals as illustrated in Figure 15. The measurement chamber is connected to an electronic unit that controls the voltage applied on the crystals, itself linked to a laptop that computes the results. The crystals used are AT-cut 5 MHz crystal coated with either titanium or gold from Q-Sense

(QSensor QSX 310 Ti, QSensor QSX 301 Gold). [48], [49] They were pre-treated as explain above. The solutions are pumped at a rate of 20 µL/min. Gradually, as the layer is adsorbed on the crystal surface, there is a frequency drop and a rise in dissipation energy observed until the stabilization of the frequency. At that moment, water is pumped into the system for 10min to rinse the surface before the adsorption of the next layer. The construction of the multilayer continues with the same principle until the required number of bilayers is reached. In this experimentation, the crystals were coated with 5 bilayers of [CHI-PPCs(LL37-ALG)] to observe the construction of the multilayer. The results were then analyzed with the Q-Stomize software.

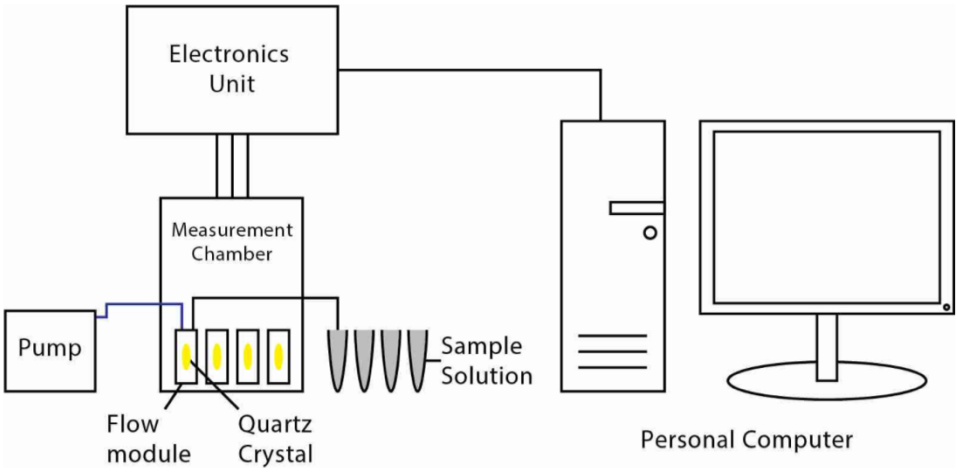

Figure 15 : Representation of the QCM-D instrument. The solutions are pumped into the measurement chamber in which the crystals oscillate under an alternative voltage controlled by the electronics unit, connected to a computer that recovers the data.[46]

3.2 X-ray photoelectron spectroscopy

X-ray photoelectron spectroscopy (XPS) is a surface analysis method that will give information about the chemical composition of the surface. XPS relies on the photoelectric effect in which an atom (A) is irradiated by photons of an energy (hv) producing an ion in an excited state (A^{+*}) after the ejection of an electron (e) at a certain kinetic energy (E_k):

$$A + h\nu \rightarrow A^{+*} + e$$

In XPS, an X-ray beam ensures the excitation of the sample, allowing the ejection of the electrons from core shells. The instrument is illustrated in Figure 16. The photoemitted electrons pass through a hemispherical electron energy analyzer where their kinetic energies are determined before being collected and counted in a detector. Finally, a spectrum of the electron number in function of their kinetic energies is computed. The electron kinetic energy and number will set respectively the position and the area of the peaks. [50], [51]

The electron kinetic energy (E'_k) measured by the spectrometer is related to its binding energy (E_b) with the atom by the following equation:

$$E'_k = h\nu - E_b - \phi_{sp} - E_c$$

Φ_{sp} is the spectrometer work function (the energy needed to bring the electrons when they are totally detached from the sample to the entry of the analyzer). E_c is the surface charge potential and is equal to 0 for conducting sample. As hv, Φ_{sp} and E_c are known and fixed, the E_k is thus only function of the E_b which is specific of an energy level of a define element. So, each peak of the XPS spectrum is singular to a specific element, allowing the XPS to characterize the element present on the sample surface. [50], [51]

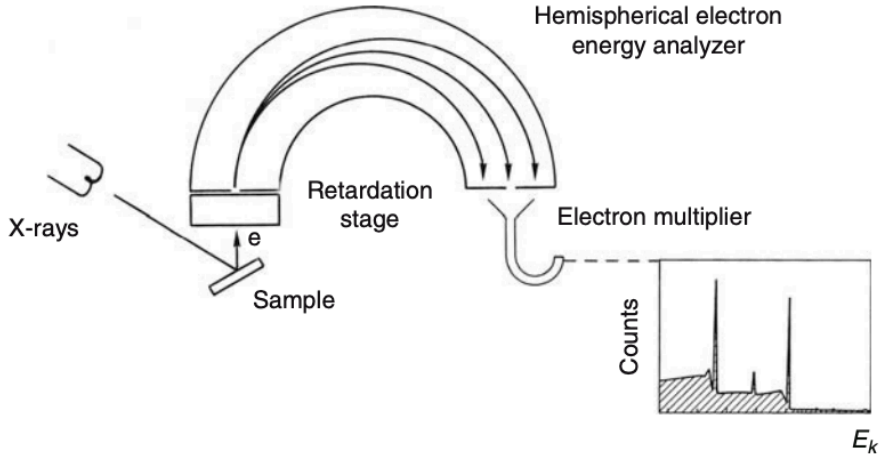

Figure 16 : Illustration of the XPS system. A X-ray beam excites the sample leading to ejection of photoelectrons, collected in a hemispherical electron energy analyzer ending with a detector to measure their kinetic energy and number respectively.[50]

The XPS can probe the thin layers at the outermost sample surface, up to 10nm. The atoms present deeper in the sample will be excited by the X-ray beam, but the emitted electrons will undergo inelastic collisions with other particles and will lose their energy. Sometimes those electrons still have enough energy to go out of the surface and will contribute to the background signal of the XPS spectra. During the XPS measurement, the sample is placed under an ultra-high vacuum to avoid at maximum the electron energy losses upon collisions between the electrons and gas molecules. [51]

The experimentations were performed on a SSX 100/206 photoelectron spectrometer from Surface Science Instruments (USA) equipped with a monochromatized and micro focused Al K_α X-ray beam (powered at 20 mA and 10 kV). The pressure in the chamber was around 10^{-9} Torr. Six different samples were analyzed, each composed of 15 bilayers of [CHI-PPCs(LL37-ALG)] constructed on titanium surfaces but having undergone different tests: BCA(SDS) 1 time, BCA(SDS) 2 times, BCA(HCl), BCA(NO), NO(NO) and a reference sample

where no test was done. Each of the parenthesis that follows the name of the test represents the technique used to desorb the multilayer and will be explained more deeply in the Results section that follows. The data were treated using CasaXPS (Casa Software LTD, UK) and the value for the C-(C-H) component of the C1s peak was fixed to 284.8 eV to correct the binding energy scale.

Results and discussion

The results section is divided in four parts. First, the QCM experiments will allow the visualization of the multilayer construction by measuring the increase of the multilayer mass after each adsorption step. Then, the amount of LL37 immobilized in the multilayer will be assessed, firstly by two different protein quantification tests (BCA and NanoOrange) and then, by combining them together. After that, some XPS measurements will be discussed to determine if all the material from the multilayers is well quantified during the previous tests. Finally, the results obtained from the experiments conducted on multilayers that were constructed with LL37 marked by fluorescence will be exposed and compared with previous results to complete the LL37 quantification study.

1. QCM experiments

The first experimental step of this work was to validate the good construction of the multilayers using PPCs as building blocks. The QCM instrument allows monitoring the change of the multilayer mass upon the different adsorption steps, giving a real-time characterization of the coating in formation. To do so, five bilayers of [CHI-PPCs(LL37-ALG)] were constructed on either a titanium or a gold surface, at pH 5, I≈0mM and with a negative-to-positive charge ratio of 2 for the PPCs formation, as described in Materials and methods section. The frequency shifts and the dissipation energy were measured and the results of the seventh overtone are presented. First, the hypothesis made to be able to use the Sauerbrey's equation need to be confirmed, then the increase of the adsorbed mass can be computed and the thickness of the hydrated film can be assessed by approximating the film density.

1.1 Validation of the Sauerbrey's hypothesis

To use the Sauerbrey's equation, the film needs to be approximated as rigid and laterally homogeneous, so that the energy dissipated by the film can be considered as insignificant. To validate this hypothesis, the ratio between the dissipation energy and the frequency shift can be computed and compared to a given value specific for a 5 MHz crystal [45]:

$$\frac{\Delta D_n}{|-\frac{\Delta f_n}{n}|} \ll 4 \times 10^{-7}\ Hz^{-1}$$

With ΔD, the energy dissipation shift, Δf, the frequency shift and n, the overtone number. When this hypothesis is validated, the film can be considered as rigid and the Sauerbrey's equation can be used to compute the areal mass density of the film. It is important to point

out here that the measured mass is the hydrated film mass as the measurements were performed in water. This amount of water can be significant. For the same number of constructed bilayers, Aurélien Vander Straeten pointed out in his thesis that water and ALG represent half of the film mass by bringing together QCM-D data and BCA and o-phthalaldehyde (*o*-Ph) assays. [34]

1.2 Adsorbed mass

The cumulation of the mass adsorbed on the crystal after each adsorption step can be visualized in Figure 17A. The first four adsorption steps, presented in purple in the graph, represent the cushion as discussed in the State of the art section and are followed by the construction of 5 bilayers of [CHI-PPCs(LL37-ALG)]. The y axis represents the total hydrated adsorbed mass per square centimeter on the crystal. After each adsorption step, there is an increase of the global mass, confirming the good multilayer construction using PPCs as building block. After 5 bilayers, the global hydrated mass of the film reaches 3.3 and 2.2 $\mu g/cm^2$ for the titanium and gold surface respectively. Upon cushion formation, the global mass decreases when ALG is adsorbed. This decrease illustrates the dynamic aspect of the multilayer construction which is not made of homogeneous layers but rather of interconnected layers due to the diffusion of components in the film during their adsorption. Here, the growth of the multilayer seems to be linear which is usually the case for films with less diffusion of components. The construction using bare LL37 and ALG as the second PE was also conducted but was stopped after the fifth adsorption step as the frequency did not stabilize well, leading to the failure of the multilayer construction (data not shown). This difficulty for the frequency to stabilize also illustrates the dynamic aspect of the multilayer construction. The frequency of the crystal takes between 20 to 25min to stabilize for each component. So, this time corresponds to the one needed for one component to be adsorbed on the crystal and will thus be used in the next LbL assembly experiments. The shape of the multilayer construction is similar when building on the titanium or the gold surface, which proves the versatility of the LbL assembly and the efficiency of the cushion.

In Figure 17B, the mass adsorbed for each adsorption step on the titanium surface is presented. During the PPCs adsorption steps, there is more mass adsorbed on the crystal than for the CHI steps. This might be due to the fact that the PPCs are composed of 2 components (LL37 and ALG) while there is only CHI on the other side. These data suggest that LL37 is well immobilized in the multilayer, even though QCM does not provide information on the nature of the compounds contributing to the mass increase.

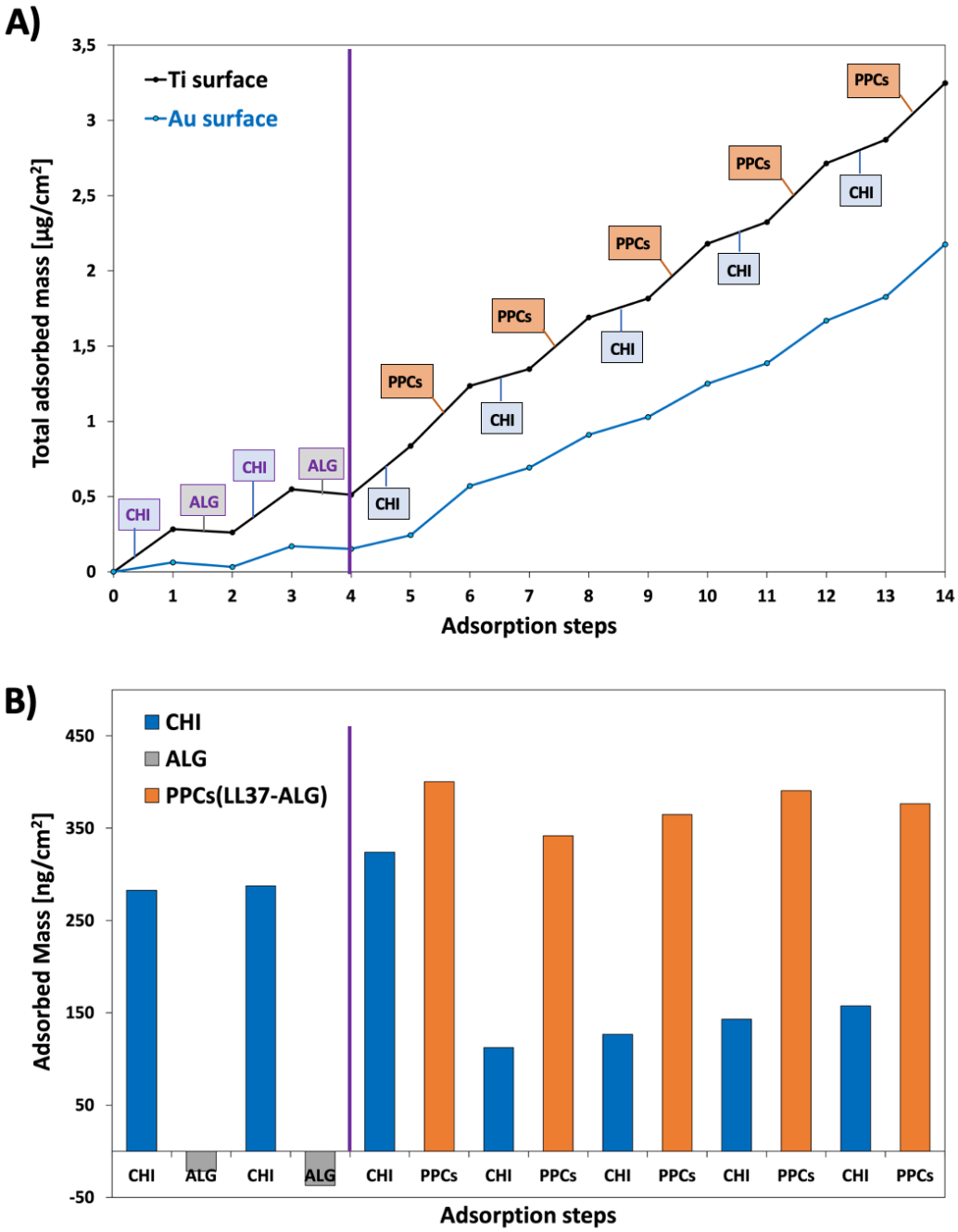

Figure 17 : QCM results: A) The increase of the adsorbed mass with the adsorption steps. In black, the construction on the titanium surface, and in blue on the gold surface. The different adsorption steps are detailed in the lables next to the curve. B) The adsorbed mass for each step. The purple line separates the cushion from the multilayer construction.

1.3 Thickness of the film

The thickness of the film can be assessed from the QCM data by approximating the density of the film to 1g/cm^3, which is a reasonable assumption often made for soft matter and due to the fact that the film is hydrated. [45] The following equation can be used:

$$h = m/\rho$$

Where h is the thickness of the film, m the adsorbed mass and ρ the film density. For 5 bilayers constructed on the titanium surface, the film reaches a thickness of 32.5 nm.

Since the mass of solvent is included in the adsorbed mass measured by QCM and since the contribution of the different components cannot be dissociated, it is difficult to know the precise mass of LL37 that is immobilized on the surface. This limitation leads to the search for other quantification methods like protein quantification assays from which the results are discussed in the following section.

2. Protein quantification tests

Two different protein quantification tests were performed in this work: the BCA test based on colorimetry, allowing the quantification over a broad concentration range (5 to 250 µg/mL) and the NanoOrange fluorescent test that is more sensitive and permits to detect lower concentrations of protein (100 ng/mL to 10 µg/mL). Both of those tests were firstly performed alone and then combined together to quantify the amount of the different components in the multilayer.

2.1 BCA protein quantification test

The first thing to do when performing protein quantification tests is to evaluate the different responses for all the components present in the multilayer, in order to reveal possible interferences. This is possible by making one calibration curve for each component, following the protocol explained in the Materials and methods section. Those calibration curves are exposed in Figure 18.

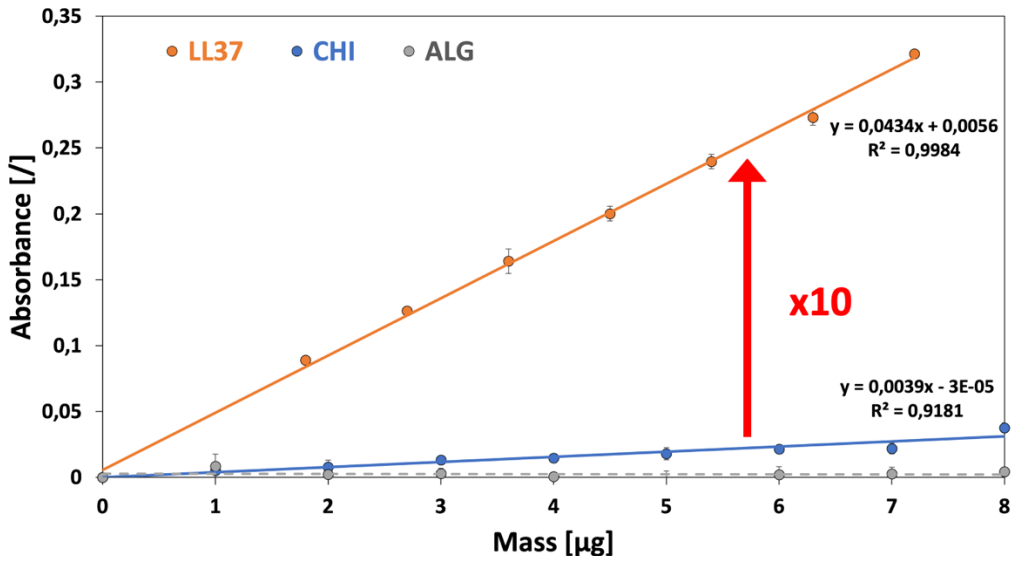

Figure 18 : BCA-calibration curves for pure LL37 (0-7.2µg) in orange, pure CHI (0-8µg) in blue and pure ALG (0-8µg) in grey measured at 562nm. The error bars represent the standard deviation on three measurements.

One can easily see that no signal was detected for ALG (in grey) and this was expected as the BCA test is sensitive to amide groups which are not present in ALG. On the other hand, both LL37 and CHI present some amide groups, respectively from the peptide bonds and from the 5% acetylated monomer residues as illustrated in Figure 19. However, the response of LL37 is 10 times higher than the one of CHI. This means that by using only the BCA test, it is possible to evaluate the LL37 mass with an error range of the order of 10%.

Figure 19 : Representation of the amide groups present A) in CHI or B) in LL37. [34]

As there are two components responding to the test, it is interesting to analyze if they did not interfere with each other when they are both present in the solution tested. To do so, known amounts of both LL37 and CHI are put in the same well of the microplate n°1 and tested following the BCA test protocol. The ratio of µgLL37/µgCHI tested are respectively: 8/0, 7/1, 6/2, 5/3, 4/4, 3/5, 2/6, 1/7 and 0/8. At the same time, a calibration curve for LL37 and for CHI were estabiched, giving the absorbance of the two components alone. One can thus compare the sum of the two absorbances measured when the components were alone, with the absorbance measured when they are in solution together. The results are exposed in the Figure 20. The signal of LL37 is in orange and the one of CHI in blue. The signal when they are both in solution is in grey.

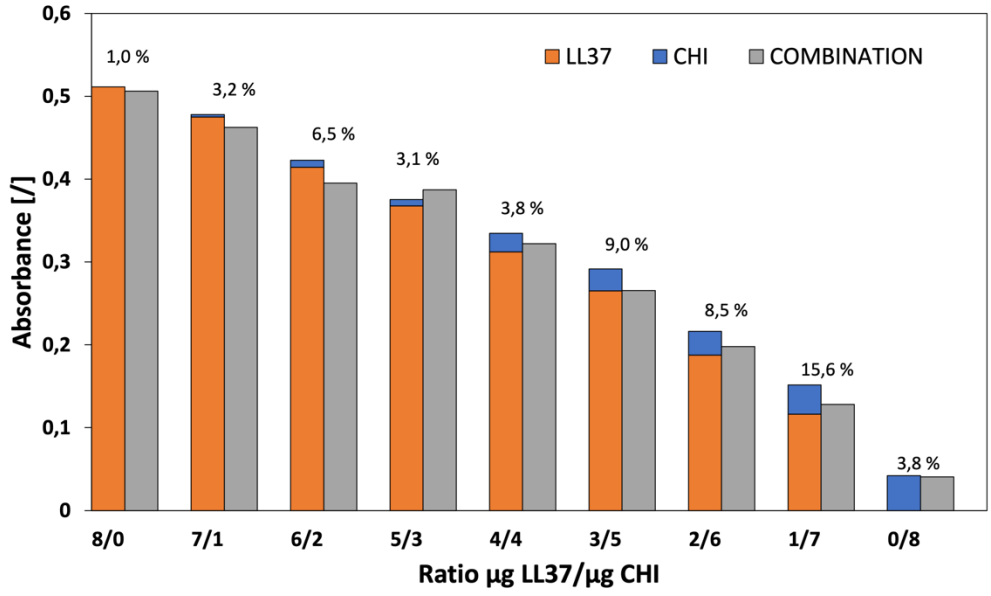

Figure 20 : Evaluation of the interferences between LL37 and CHI in the BCA test for different ratio of µgLL37/µgCHI. The response of LL37 alone is in orange, the one of the CHI alone, in blue and their combination in the ratio indicated is in grey.

One can observe that the absorbance measured when both LL37 and CHI are present at the same time is usually a little bit lower than their sum. However, the differences (expressed in percent at the top of each LL37/CHI ratio) remains quite low. In addition, each of the measurements was only performed one time. The error increases when the quantity of component decreases which is consistent because the absorbances measured are thus lower and lower. Indeed, as the quantity of components come closer to the limit of quantification, the possible error on their measurements increases. The same experiment for a calibration between 0 and 2µg presents more important errors and is exposed in Annex 1. One can conclude that CHI and LL37 seem to decrease the absorbance signal when they are combined, but this interference remains low and additional data would be needed to prove that this is truly significant.

A BCA test was then performed on several multilayers composed of either just the cushion, 1, 3, 5, 6, 9, 10, 12, 15, 20 or 25 bilayers of [CHI-PPCs(LL37-ALG)] constructed either at pH 3.5 or 5. The adsorption time for each step was fixed to 20min in agreement with the results found in QCM. The LL37 mass can be approximated by reporting the absorbance values directly on the calibration curve of the pure LL37, considering the response of CHI as insignificant. The LL37 mass can thus be plotted in function of the number of formed bilayers as presented in Figure 21. As each well developed a surface of 0.93 cm^2 when filled with 100 µL solution, a correction was applied to express the immobilized mass directly per cm^2.

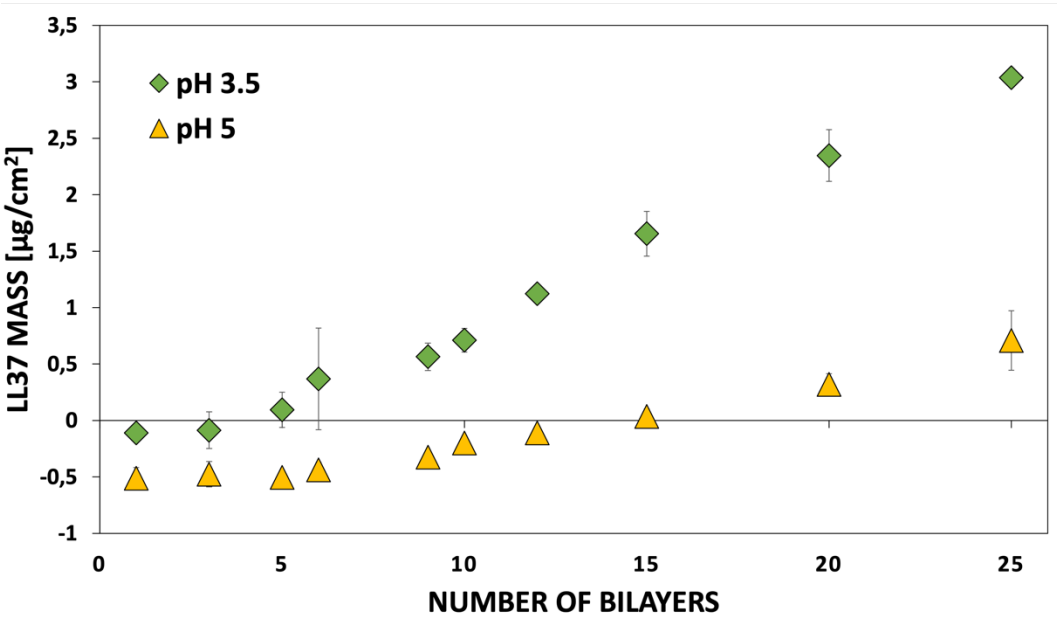

Figure 21 : Evolution of the LL37 mass as a function of the number of bilayers constructed at pH 3.5 in green and pH 5 in yellow.

Firstly, one can observe that the LL37 mass increases with the number of bilayers, confirming the continuous immobilization of LL37 upon multilayer construction, as previously discussed in QCM experiments. Then, one can see that the mass increases linearly reaching a

mass of 3.04 ± 0.07 µg/cm^2 for 25 bilayers, which means that until 25 bilayers, no saturation occurs. However, some mass values are negative which is of course not possible. The most likely explanation of those negative values is that the limit of quantification (LOQ) is situated between 10 and 12 bilayers (for pH 3.5), meaning that the mass values below are too small to be quantified. The fact that the linear response also started around 10 to 12 bilayers illustrated it well. This implies that the values below 10 bilayers are very close to the blank values and in this case even lower, leading to negative mass values.

Then, one can compare the two experiments conducted either at pH 3.5 or pH 5. The mass of LL37 immobilized at pH 3.5 is way higher than the one at pH 5, which is always lower than the LOQ. At pH 5 however, the same linear trend is observed than at pH 3.5, leading to an increase of the LL37 immobilized amount with the number of bilayers. This difference shows that the construction of the multilayer is strongly influenced by pH. Indeed, the pH will influence the degree of ionization (α_0) of the components and thus their charge densities. Based on the pH and the pKa, α_0 can be computed for each component as described in Table 6. When decreasing the pH, the number of positive charges of the LL37 increases and the degree of ionization of ALG decreases. This requires using a higher amount of ALG to overcompensate the LL37 charges with a ratio of 2. The ionization degree of CHI also increases upon decreasing the pH. This increases of charge density could explain the better interaction between the building blocks, leading to the increase of the LL37 immobilized amout.

Table 6 : The different ionization degrees or positive charges of the components at pH3.5 and pH5 alongside their pKa.

	pKa	Charge/α_0 at pH 3.5	Charge/α_0 at pH 5
LL37	/	10.4	7.02
ALG	3.5	50%	97%
CHI	6.3	99.8%	95.2%

However, the approximation made earlier that the absorbance signal measured in the wells only comes from LL37, meaning that the signal from CHI is negligible, can be debated. Indeed, the signal rather comes from both components. To discuss the approximation made here, the other way around could also be considered. If only the CHI signal was responsible for all the measured absorbance signal, it would mean that only CHI is present in the multilayer. To obtain the same signal, a mass of 33 µg of pure CHI should be immobilized on the surface. If the bulk density of dried CHI is approximated to 0.3 g/cm^3, it would give a thickness of 1100 nm. [52] However, as the film is highly hydrated, the density of the film can rather be approximated to 1 g/cm^3, and the thickness will thus be of 330 nm. This value can be compared to the one measured in the QCM experiment where the thickness of the multilayer reached about 30 nm for 5 bilayers. As the growth was observed to be constant, one can extrapolate the thickness that will be reached after 25 bilayers which is thus of 150

nm. The thickness computed if there was only CHI in the multilayer is more than two times higher than the prediction of the QCM. The second hypothesis that CHI alone would give the absorbance signal in the BCA test, is thus not compatible with the other data. Hence, the real composition of the absorbance signal is rather a combination of LL37 and CHI signal. This means that the LL37 mass presented in Figure 21 is the maximum possible amount of LL37 present in the multilayer when it is quantified with a BCA test. So, another quantification test can be assessed to try to remove this approximation of the LL37 mass computed by BCA test and that is what has been conducted in the next section.

2.2 NO protein quantification tests

The NO quantification test was chosen as the second test for its great sensitivity. As it is a commercial kit for which the exact detection method is unknown, it is even more important to realize careful calibrations to see how the different component interact with the test. As the maximal concentration of the test was around 10 µg/mL, a first calibration curve was made between 0 and 10 µg for a volume of 250 µL per well, thus representing a concentration between 0 and 40 µg/mL to verify the maximal concentration of LL37 that the test can quantify (data shown in Annex 2). The calibration curve was first measured with the theoretical set of wavelengths of 470 and 570 nm for the excitation and the emission respectively (470/570) and then, with the more accurate wavelengths of 485/590 nm provided by the kit supplier. As excepted, the fluorescent test saturates above 10 µg/mL.

Therefore, a more accurate calibration between 0 and 2 µg (representing a concentration between 0 and 8 µg/mL) was made for each component, measured at 485/590 nm, and presented in Figure 22. Firstly, one can observe that, as it was the case with the BCA test, ALG does not respond to the test. Then, one can see that the CHI also responds to this second test, meaning that there is still an additional signal to the one of LL37, just as in the BCA test. However, the CHI response is here even higher than the one of LL37, by a factor 2.

The repartition of the different points from either side of the line can also be discussed. As the points seem to have a curve shape by simple visual inspection, the use of a linear trend to calibrate the data can be assessed by doing a linearity test of lack of fit (LoF). The LoF computation was done for the CHI and the LL37 data and the results are taken back in Annex 3. As the calculated F statistics are in both case lower than the F statistics found in the F distribution table (for a degree of freedom of 6 and 16 for the numerator and denominator respectively), there is no LoF and the hypothesis that the data can be assessed by a linear trend is validated.

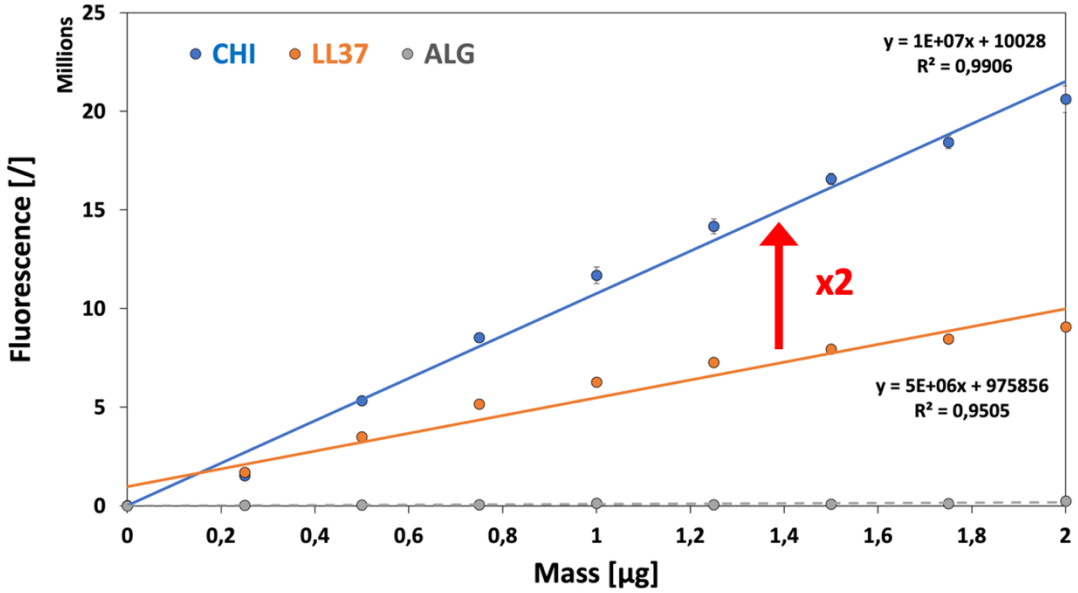

Figure 22 : NanoOrange calibration curves for pure LL-37 (0-2µg), pure CHI (0-2µg) and pure ALG (0-2µg) at 485/590nm.

A NO test was performed on several multilayers composed of either the cushion, or 1, 3, 5, 6, 9, 10, 12, 15, 20 or 25 bilayers [CHI-PPCs(LL37-ALG)] in the microplate n°1, as carried out with the BCA test. The adsorption time was also of 20 min and this experiment was conducted two times, at pH 3.5 and 5 respectively. The fluorescence was measured at 485/590 nm (1 point per well), and the results are reported in Figure 23. The increase of fluorescence is way higher at pH 3.5 than pH 5, in agreement with the BCA test. The standard deviation is higher at pH 5 and most of the values are below the LOQ for this latter pH value.

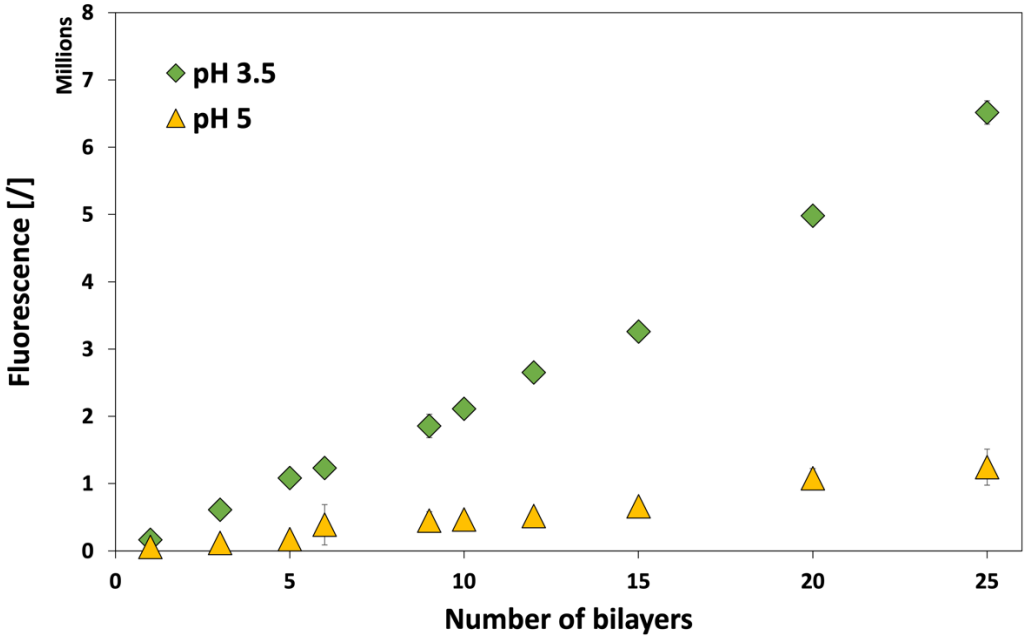

Figure 23 : Increase of the fluorescence signal as a function of the number of bilayers constructed either at pH 3.5 in blue or pH 5 in orange. The blank was already subtracted from all the values.

An interpretation of the data can be made by reporting the fluorescence measurements of the bilayers on the calibration curves. This was done in Figure 24, for 10, 12, 15, 20 and 25 bilayers constructed at pH 3.5 and the *x*-axis is zoomed between 0 µg and 1.2 µg to allow better visualization. As the fluorescence signals are the combination of LL37 and CHI signal, the two extreme points can be evaluated, where either only CHI or LL37 is responsible for all the measured fluorescence signal. This is represented by reporting the fluorescence measured on either the CHI or the LL37 calibration curve. The recovered data are exposed in Table 7 alongside the mass of LL37 found by the BCA test.

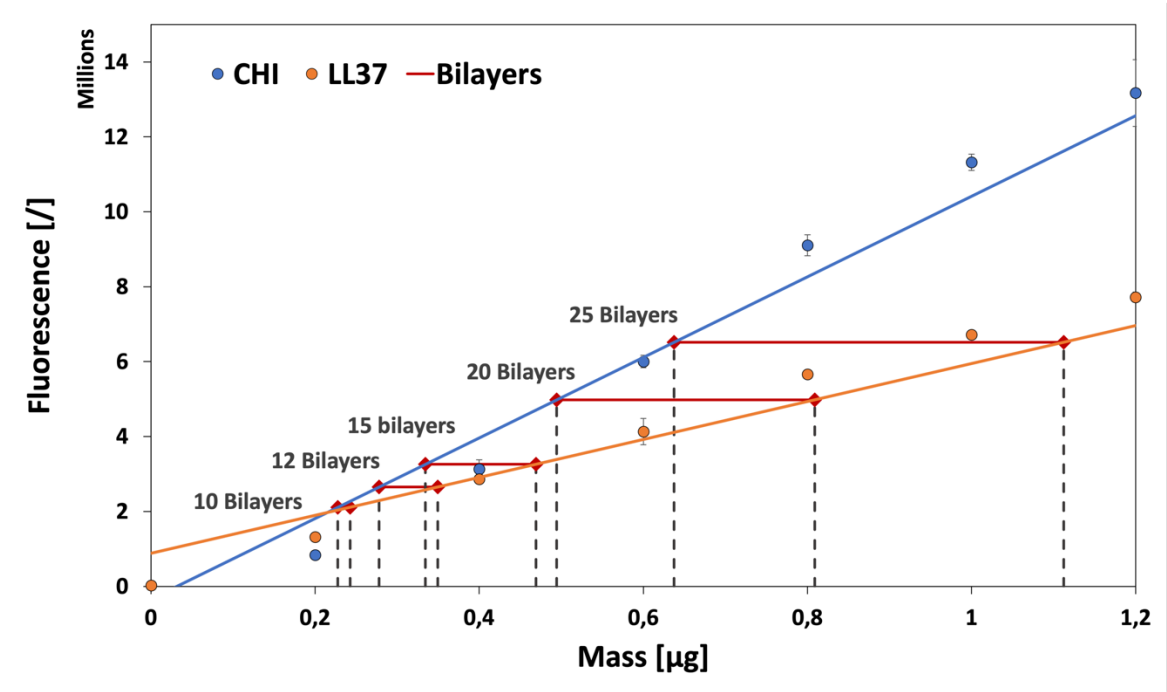

Figure 24 : Evaluation of the maximum mass [µg] if all the fluorescence signal comes from either only the LL37 or only the CHI. The fluorescent signal is in red for 10 to 25 bilayers constructed at pH 3.5, as the CHI calibration curve is in blue and the LL37 calibration curve in orange.

An interesting outcome is that if LL37 is the only component responsible for the measured fluorescence value, meaning that there is only LL37 in the multilayer (and water and ALG but not detected), the maximum LL37 mass computed with the NO test is always way lower than the LL37 mass approximated from the BCA test (neglecting the possible contribution of CHI). Two hypotheses can explain this phenomenon: firstly, the BCA test may overestimate the LL37 mass present in the multilayer which is why the value computed are higher. The other part of the signal will thus be due to the presence of CHI. This hypothesis was already discussed in the BCA results, and leads to high values for CHI mass which is unlikely when compared to QCM data. Secondly, the NO test may underestimate the LL37 mass present in the multilayer. This underestimation could come from an uncomplete desorption of the multilayer during the test, leading to an underestimation of the LL37 really immobilized in the multilayer. This second hypothesis will be developed in more details in the next section.

Table 7 : Maximal LL37 and CHI masses values [µg/cm²] obtained from the NO test for 10, 12, 15, 20 and 25 bilayers constructed at pH 3.5. Report of the values obtained for the BCA test to allow comparison.

	10 Bilayers	12 Bilayers	15 Bilayers	20 Bilayers	25 Bilayers
NO MAX CHI [µg/cm²]	0.245	0.299	0.360	0.532	0.685
NO MAX LL37 [µg/cm²]	0.261	0.376	0.504	0.870	1.196
BCA MAX LL37 [µg/cm²]	0.71	1.12	1.66	2.35	3.04

The same interpretation for the experiment made at pH 5 was not conducted because the measured fluorescence values were below the LOQ. However, we found that the values increase with the number of bilayers but are way lower than the one obtained at pH 3.5. Indeed, the value for 25 bilayers constructed at pH 5 is equal to the value of 6 bilayers constructed at pH 3.5 as illustrated in Figure 23. This observation is in line with the results of the BCA test showing that the construction of the multilayer works better at lower pH thanks to the increase of the CHI charge density, allowing a better interaction between the building blocks.

2.3 Combination of the BCA and NO tests

As both BCA and NO tests give a response for both LL37 and CHI, it becomes interesting to combine their results by solving a system of two equations with two unknown values to determine the mass of LL37 and CHI comprised in the multilayers.

2.3.1 System of two equations with two unknowns

The system of two equations with two unknowns is the following one:

$$A^{BCA} = m_{LL37}S_{LL37}^{BCA} + I_{LL37}^{BCA} + m_{CHI}S_{CHI}^{BCA} + I_{CHI}^{BCA}$$
$$F^{NO} = m_{LL37}S_{LL37}^{NO} + I_{LL37}^{NO} + m_{CHI}S_{CHI}^{NO} + I_{CHI}^{NO}$$

Where A^{BCA} is the absorbance measured for the multilayer after a BCA test, F^{NO} is the fluorescence measured for the multilayer after a NO test, m are the masses of the different components, S are the slopes of the calibration curves and I their intercepts. The results after the computation of that system are shown in Table 8 for pH 3.5 and 5 and compared with the values found using the BCA test only.

Firstly, one can observed that solving the system often gives negative values for CHI mass at high number of bilayers and LL37 at low number of bilayers, which is not possible. We will focus on the case of CHI as it occurs when the total amount of adsorbed matter must be high enough to ensure valid measurements. Three hypotheses can be made to explain those negative values. The first one is that the absorbance values for the CHI are too low in the BCA test to enable good solving of the system. Indeed, the absorbance values for the calibration curve of CHI (0-8 µg) are below the LOQ. This low signal from CHI is expressed in the system in the term $m_{CHI}S_{CHI}^{BCA}$. To evaluate if this term is well very low, it is possible to compare the responses of the system computed either with the slope of CHI measured in BCA or with the slope fixed to 0 (fixing by the same time the signal for the CHI in BCA to 0). The values for the 25 bilayers are: 3,102 µg of LL37/cm^2 and -0,865 µg of CHI/cm^2 with the slope of the CHI measured in BCA (=value from the Table 8) versus 3.038 µg of LL37/cm^2 and -0,835 µg of CHI/cm^2 when the slope is fixed to zero. Their similarity proves the fact that the response for the CHI to the BCA test is very low.

Table 8 : LL37 and CHI mass obtained after solving the system of two equations, at pH 3.5 and pH 5. The LL37 mass obtained with the BCA test alone is also reported here to allow comparison. Negative mass values are presented in red.

pH 3,5	Number of Bilayers									
	1	3	5	6	9	10	12	15	20	25
CHI [µg/cm^2]	0.027	0.063	0.023	-0.097	-0.129	-0.175	-0.321	-0.521	-0.684	-0.865
LL37 [µg/cm^2]	-0.139	-0.120	0.066	0.351	0.552	0.703	1.129	1.682	2.392	3.102
BCA-LL37 [µg/cm^2]	-0.11	-0.09	0.10	0.37	0.57	0.71	1.12	1.66	2.35	3.04

pH 5	Number of Bilayers									
	1	3	5	6	9	10	12	15	20	25
CHI [µg/cm^2]	0.121	0.110	0.129	0.120	0.071	0.012	-0.027	-0.084	-0.180	-0.352
LL37 [µg/cm^2]	-0.360	-0.324	-0.353	-0.287	-0.171	-0.041	0.053	0.204	0.495	0.897
BCA-LL37 [µg/cm^2]	-0.49	-0.46	-0.48	-0.42	-0.31	-0.18	-0.09	0.06	0.34	0.73

The second hypothesis is that the value for CHI can be underestimated when using the NO test. Indeed, as the response of CHI is two times higher than the one of LL37, if the fluorescence value measured for the multilayers is underestimated, the underestimation is two times higher for CHI than for LL37. The fact that the NO test could not quantify all the multilayer could explain the negative mass values for CHI. To assess this hypothesis, it is possible to conceive a new quantification test based on the BCA and NO tests to evaluate their ability to quantify all the multilayer. This experiment will be conducted in the next section. For now, to see if the NO test underestimates the quantity of component really present in the multilayer, it is possible to manually increase the fluorescence signal (F^{NO}) in the system of two equations. Indeed, increasing the F^{NO} is equivalent to overestimate the fluorescence measured by the NO test and thus allows to see if there really is an underestimation of the F^{NO} during the NO test. So, after having evaluated several multiplication factors, one can deduce that a minimal multiplication factor of 2.5 of the fluorescence signal is needed to start having positive masses values for CHI after solving the system of two equation. That means that there is a possible underestimation of the F^{NO} by minimum a factor 2.5 when using a NO test.

The last possible hypothesis is that no CHI is present in the multilayer, meaning that upon the adsorption steps, all the CHI is desorbed or diffuses out of the film, acting like a

sacrificial layer permitting the adsorption of LL37. This would be quite surprising as the CHI serves as a building block allowing the inversion of the global surface charge during the LbL. However, Alix Mertens has reported in her master thesis that no CHI was detected by XPS when analyzing surfaces covered with 6 bilayers of [CHI-PPCs(LL37-Heparin)]. Nonetheless, for each measurement, the outermost layer was made of PPCs of unknown thickness. This could mean that the CHI was not detected because the layer of PPCs was thicker than 10 nm but that it is still present in the multilayer. Future experiments are thus needed before approving this hypothesis.

Finally, when comparing the LL37 mass obtained from the system of two equations and the one coming from the BCA test alone, one can observe that there are almost equal. This similarity indicates that the BCA test alone seems to already estimate well the mass of LL37 present in the multilayer, assuming that the system of two equations is applicable, but also attests that CHI contribution is quite weak.

2.3.2 New quantification test based on the BCA and NO test components

The system of two equations presented above is only applicable if the multilayer is quantified in the same way by the two tests. In other words, it requires to compare the desorption of the multilayer in the two tests, which means comparing the effect of the detergent used in each method.

To test the strength of the detergent present in the NO diluent, an experiment was conducted where the BCA and NO test components were combined. The NO diluent that contains the detergent replaced SDS in the BCA test. The other way around (replacing the NO diluent by SDS in the NO test) was not possible due to the sensitivity of the NO test to the presence of detergent. This high sensitivity to detergent is because a too high detergent concentration can produce micelle formation and induce high fluorescence background. [41] Then, the comparison between the mass detected with either the BCA with SDS (BCA(SDS)) and the BCA with the NO diluent (BCA(NO)) will allow to see if the multilayer is desorbed in the same way for the 2 different tests. A NO test was also conducted to use the system of two equations, once with the BCA(SDS) and once with the BCA(NO).

A construction of 15 bilayers at pH 3.5 was made in 9 wells of the multiplate n°2 and tested with the three different tests: BCA(SDS), NO, and the mixed BCA(NO) test (each test has a triplicate of 15 bilayers). The BCA(NO) protocol was adjusted to have the same volume of detergent as in a classical NO test where 230 µL of reagent is normally used, composed at 10% of the diluent, which gives a diluent volume of 23 µL per well. So, the same volume needs to be put in each well of the BCA(NO) test. Hence, in the wells in which the BCA(NO) test will be made, there are 20 µL of ultrapure water (same as in all the tests and permitting to adjust

the volume in the calibrations), 23 µL of NO diluent and 207 µL of BCA reagent to keep the final volume at 250 µL. The test follows then a classical BCA test protocol: 1 hour in a hot water bath at 60°C followed by a 20 min rest at room temperature before measuring the absorbance at 562 nm (30 s shake and 1 point per well).

As there is a factor 5 between the LL37 and the CHI calibration curves made with the adapted BCA(NO) protocol (Annex 4), it is not possible to make the same approximation for the LL37 mass as in a classical BCA test. Therefore, the NO test was made to use the system of two equations to compute the mass of the LL37 and CHI. The masses found by solving the system of two equations are exposed in Table 9. Two remarks can be made for those results. Firstly, the comparison between the 2 tests seems to indicate that the BCA using the NO diluent quantified more LL37 than a classical BCA(SDS). However, this does not tell that the NO test quantifies more LL37 than the BCA(SDS) test. Secondly, the value of LL37 mass found with the BCA(SDS) in this experiment (0,786 µg/cm^2) is lower than the one found for the same number of bilayers in the previous experiment (1,682 µg/cm^2 from Table 8). This change may be due to the switch of the microplate type for the construction of the multilayers or to the standard deviation. Thus, it will be interesting to realize another time this experiment and to compare the two sets of data. As in the previous results, the masses of CHI obtained after solving the system are also negatives.

Table 9 : CHI and LL37 masses obtained after solving the system of two equations, firstly with the BCA(SDS) and then with the BCA(NO).

	15 Bilayers	
	CHI mass [µg/cm^2]	LL37 mass [µg/cm^2]
BCA(SDS)	-0.053	0.786
BCA(NO)	-0.387	1.582

2.4 Conclusion of the protein quantification tests

The BCA test presents a response that is 10 times higher for LL37 than for CHI, leading to an error range of about 10% on the LL37 mass. The two components do not much interfere with each other in the BCA test. The construction of multilayers works better at pH 3.5 than pH 5 and permits to immobilize at maximum of 3.1 µg/cm^2 after 25 bilayers. This is probably due the change of charge density that allows better interactions between the building blocks. The NO test, on the other hand, presents only a factor 2 between the response of LL37 and CHI and seems to quantify less LL37 than the BCA test maybe due to an incomplete desorption

of the multilayer. This hypothesis would explain the negative mass values found by solving the system of two equations obtained when combining the two tests. Those mass values are almost equal to the ones measured by the BCA test alone, meaning that the BCA test alone seems to already well quantify the LL37 present in the multilayer. However, the system of two equations only works if the tests desorb the multilayer in the same way which seems not to be the case as the BCA test using NO diluent quantifies more LL37 than the BCA test using SDS. As this last experiment is not sufficient to evaluate if the test desorbs all the multilayer, it would be interesting to evaluate the chemical composition that the surface possesses after it undergoes the different protein quantification tests and that is possible by using a surface analysis method such as XPS.

3. XPS experiments

To visualize the desorption capacity of the different tests, it is possible to perform XPS measurements on titanium surfaces after the different tests were carried out. XPS will thus give information about the chemical composition of the surface that remains after the quantification tests. To do so, 15 bilayers of [CHI-PPCs(LL37-ALG)] were constructed at pH 3.5 on 6 Ti surfaces in the microplate n°5. Then, several quantification tests were made and are reported in Table 10 with their particularities. Each of the test is mentioned via the first capital letters and the letters between brackets represent the desorption technique used for the test: SDS, HCl or the NO detergent noted (NO). Between the tests and the XPS measurement, the samples were rinsed 10 times with ultra-pure water to clean the surface from the different elements present in the test solution.

Table 10 : The 6 different samples measured in XPS with their particularity.

Name of the test	Particularity of the test
15 intact bilayers	This sample will serve as blank.
BCA(SDS) 1x	A classical BCA test with SDS as detergent.
BCA(SDS) 2x	Two BCA tests with SDS in a row on the same surface.
BCA(HCl)	A BCA test using HCl to desorb the multilayer instead of SDS.
BCA(NO)	The BCA test mixed with the NO test as discussed in the previous section.
NO(NO)	A classical NanoOrange test.

3.1 Survey spectra

Before analyzing individually several elements of the sample, a survey spectrum is acquired to evaluate the presence of those elements on the surface with an accuracy of 1%. In the survey, the following elements were detected: C, O, N, Ti, Cu, Na and will be then analyzed individually with an accuracy of about 0.1%. Al and V were also investigated as they also compose the Ti surface, but their peaks were not present in the survey and thus V and Al were not analyzed individually.

3.2 Elemental composition

The elemental composition of each sample is presented in percent in Table 11. Before going in more details for each element, several remarks can be made here. Firstly, it is important to remember here that the multilayer is not homogeneous and that the different elements detected above could reflect more the external layer composition than the one of the entire multilayer. As the XPS spot is 1.4 mm^2, the measurement could also be affected if there are preferential adsorption areas on the surface, leading to a lateral heterogeneity this time. Secondly, the first and the last measurement of the experiment for each sample was for the C peak. They comparison indicates that no shift has occurred, meaning that there was no degradation of the samples during the measurements. After that, when looking at the 15 intact bilayers, one can see that Ti is not detected. As XPS probes a depth of about 10 nm, it means that the surface is well covered with a multilayer thicker than 10 nm after the construction of 15 bilayers. As this agrees with the QCM experiment that already shows a thickness of 32.5 nm after the construction of 5 hydrated bilayers, it validates the good construction of the multilayer. Then, one can see that some Cu is detected for all the BCA tests, meaning that the 10 rinses were not enough to remove all the Cu coming from the BCA test. Finally, one can observe that the chemical composition of the 15 intact bilayers and the NO(NO) are surprisingly very similar, and this will be discussed later. The surface of these two samples also features a higher carbon content than all other samples.

Table 11 : Elemental composition of the 6 samples obtained after XPS measurement, expressed is percentage in the table. Bld = below detection limit.

	Ti	N	C	O	Cu	Na	Cl
15 intact bilayers	bld	4.0	52.4	43.5	bld	bld	bld
BCA(SDS) 1x	4.8	4.2	44.9	41.2	4.2	bld	0.6
BCA(SDS) 2x	5.3	3.4	45.1	39.6	5.3	0.5	0.9
BCA(HCl)	8.4	1.9	41.5	41.5	5.1	0.9	0.6
BCA(NO)	6.7	4.0	41.3	44.1	3.4	bld	0.5
NO(NO)	bld	4.2	52.6	43.3	bld	bld	bld

3.3 Titanium

In this experiment, the focus is set on the titanium peak because if more titanium is detected, more multilayer could have been desorbed. The shape of the Ti peak for each test is reported in Figure 25 to allow better visualization. Two points will be discussed here: the similarity between the NO(NO) and the 15 intact bilayers, and the difference in percentage of Ti detected for each test.

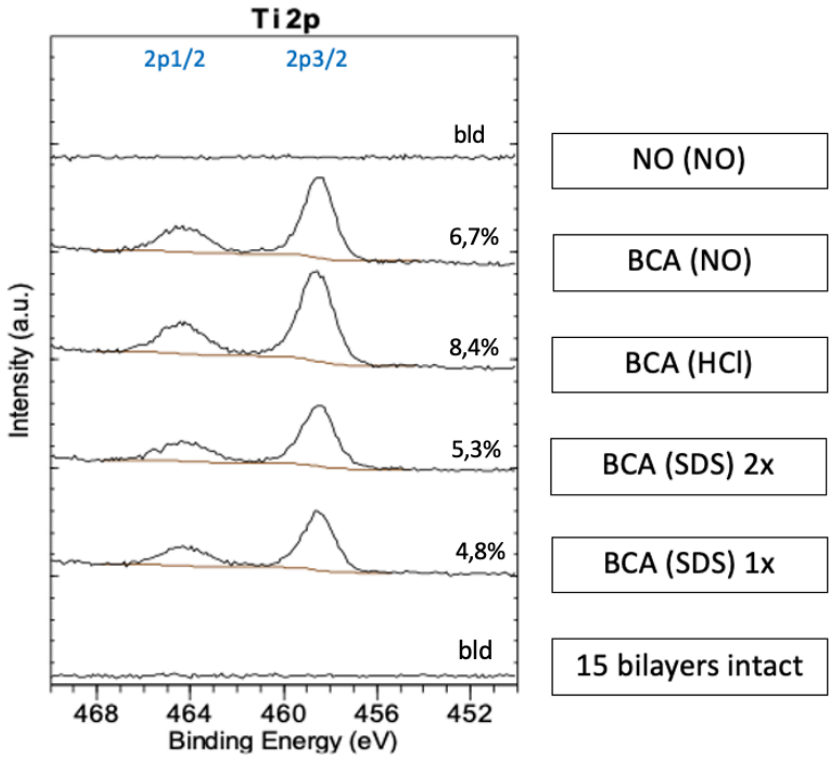

Figure 25 : Visualization of the shape of the Ti peak for each test alongside Ti percentage.

3.3.1 Similarity between the NO(NO) and the blank

Firstly, as noted previously, there is a great similarity between the NO(NO) and the 15 intact bilayers samples. In both cases, Ti is not detected, meaning that the titanium surfaces are covered with a continuous layer of a thickness higher than 10 nm. This result is quite interesting as it indicates that during the NO test, the multilayer is not totally desorbed and thus not totally quantified. This agrees with the second hypothesis made during the discussion of the NO experiment claiming that the negative mass values of the CHI could come from an underestimation of the fluorescence signal measured for the NO test. It also validates that the maximal LL37 mass computed with the NO test alone is lower than the one computed with

the BCA test alone. The fact that the NO test is not able to quantify all the multilayer questions the capacity of the system of two equation to assess LL37 and CHI masses.

3.3.2 Different percentages of Ti detected in function of the tests

The second point discussed here is the different percentages of Ti detected for each test. The detection of Ti can be explained by two phenomena: the layer on the surface is thinner than 10nm and/or the layer present some discontinuities resulting from the desorption method. The percentage of Ti detected increases as follow: BCA(SDS) 1x < BCA(SDS) 2x < BCA(NO) < BCA(HCl) with respectively those values: 4.8% < 5.3% < 6.7% < 8.4%. Those values can be compared to the percentage of Ti found when just the titanium sample is measured in XPS. Alix Mertens has done this experiment last year and has found a percentage of 11.4%. [53] Her results obtained for the Ti wafer is cited in Table 12. So, none of the tests made here reaches the 11.4% that she detected. However, one cannot conclude if all the multilayer is desorbed, as there can be numerous contaminants on the surface coming from the different tests. It will be thus interesting to make the different tests on Ti sample with no multilayer construction and then to measure them by XPS to see the impact of the contaminants coming from the tests.

In addition, without knowing the initial and final thickness of the built multilayer, it is difficult to evaluate the quantity of the multilayer desorbed by the tests. What can be observed here, is that the BCA(SDS) 2x presents a higher Ti signal than when it was only done once. That seems to indicate that the first BCA test did not desorb the entire multilayer and the second BCA test allows to desorb more of the multilayer. The decrease of the N percentage agrees with that idea, nitrogen being attributed to the multilayer (LL37 or CHI).

Table 12 : Chemical composition of the used titanium wafer. Modified from Mertens et al.[53]

	Ti	N	C	O	V	Al	Ca
Ti wafer	11.4	0.9	42.0	43.5	0.3	1.7	1.2

Interestingly, one can see that the increase of Ti goes along with the increase of the C-(C,H) component of the C_{1S} peak as exposed in Table 13. The percentages of all the decomposed peaks are presented in Annex 5. This is because the Ti is rapidly contaminated by C-(C,H). As the C-(C,H) value for the NO(NO) does not change from the one of the blank, it comes validate the fact that the Ti surface is reached with all the BCA tests but not with the NO test.

Table 13 : Comparison of the %Ti and the %C-(C,H) of the different samples.

	Ti	C-(C,H)
15 bilayers intact	bld	6.8
BCA(SDS) 1x	4.8	16.1
BCA(SDS) 2x	5.3	19.7
BCA(HCl)	8.4	25.7
BCA(NO)	6.7	16.5
NO(NO)	bld	8.6

Another remark can be made here when looking at the Ti percentage for the BCA(SDS) 1x and the BCA(NO). Interestingly, more Ti is detected for the BCA(NO) (6,7% versus 4,8%). That means that when using the NO diluent in the BCA test, more multilayer is desorbed than with the SDS. This result can thus explain why more LL37 was quantified using the mixed BCA(NO) than by the classical BCA(SDS) in the previous protein quantification section.

Finally, it is interesting to point out here that even if Ti is detected, the detected percentages remain low. If the data is looked the other way around, one can say that we detect 95.2, 94.7, 91.6 and 93.3% of other elements during the XPS experiment. So, one needs to be careful when discussing the significance of the differences in the Ti percentages.

3.4 Nitrogen

For nitrogen, the percentage usually decreases when a test is made, excepted for BCA(SDS) 1x and BCA(NO). This is a little bit disturbing as the N quantity was expected to decrease as the quantification tests remove some LL37 and CHI. For the BCA(SDS) 1x, this might be due to the presence of the bicinchoninic acid on the surface as it possesses two nitrogen atoms in its carbon cycles. However, the quantity of bicinchoninic acid should be very high to compensate all the N gone with the removing of CHI and proteins. In addition, if some aromatic carbons were present on the surface, one should observe a shake up at 291 eV with an intensity of 5 to 10% of the one of the carbon peak. However, it was not the case here, meaning that no bicinchoninic acid is clearly present on the surface. So, the increase of the N percentage rather comes from contamination. For the BCA(NO), it is much harder to tell because the molecules present in the NO diluent are unknown to us.

The next information brought by the N peak is the impact of the pH, at which the tests are performed, on the desorption. Indeed, when decomposing the N peaks, one can see in Table 14 that for the BCA tests, all the N atoms are deprotonated due to the alkaline conditions required to perform the test. In the NO(NO) and the 15 intact bilayers, on the other hand,

there is still some protonated N. Thus, as the BCA test using the NO diluent (BCA(NO)) still manages to desorb the multilayer, it shows that the pH can play an important role in the desorption, and it raises the interrogation if only the pH change during the BCA test is sufficient to desorb the multilayer. To know that, additional experiments need to be done where only the BCA reagent is used, without any detergent, but this was not done in this work.

Table 14 : Decomposition of the N peaks of the different sample. The compositions are expressed in %.

	NH+	N-(C,H)
15 intact bilayers	2.6	1.4
BCA(SDS) 1x	bld	4.2
BCA(SDS) 2x	bld	3.4
BCA(HCl)	bld	1.9
BCA(NO)	bld	4.0
NO(NO)	2.5	1.6

3.5 Other elements

For the other elements, it is more difficult to extract information. As for oxygen, the chemical shifts of the different O peaks are low, causing the decomposition and interpretation of the peak very difficult. The detection of traces of Na and Cl can come from the HCl or NaOH solutions used to adjust the pH or from the HCl used in the desorption for the BCA(HCl). Na can also come from the SDS as it is the counter ions. However, as no sulfur was detected in the survey, one can assume that the sulfur part of the SDS is not present on the surface.

3.6 Conclusion of the XPS experiment

The great similarity between the NO(NO) and the blank validates the hypothesis that the diluent used for the NO test does not desorb and thus this test does not quantify all the multilayer leading to the computation of negative mass values for CHI. This confirms that the system of two equations can thus not be used to assess the mass of LL37 and CHI. By comparing the detected percentage of Ti with the percentage detected on the wafer alone, it seems that all the multilayer is not desorbed during the test. To validate this observation, it is necessary to use a direct quantification method for the LL37 to verify it the previous tests quantified the correct amount of LL37 present in the multilayer. This explains the necessity to run some experiments with LL37 marked by fluorescence to complete the quantification study of the coating.

4. Experiments with LL37 marked by fluorescence

The advantage of using LL37 marked by fluorescein isothiocyanate (FITC) is that the measured fluorescence will be directly related to the mass of LL37, allowing an accurate measurement without the interference of CHI that occurs in the other protein quantification tests as previously discussed. As the experiments done here were the first with marked LL37 ordered by the lab, several calibrations and measurements were made to evaluate the best quantification method to use. After that, the same series of multilayers as in the protein quantification tests were constructed using marked LL37, and the results were compared.

4.1 Calibration curves

To identify the best measurement method, three different calibration curves (0-8 µg) were established. The first one tests the measurement on dried drops of marked LL37 solution and for a volume equal to the one used for the multilayer construction. The calibration was thus made with a total volume of 100 µL of LL37 solution, which was dried in a desiccator before being measured in the spectrophotometer with the suggested set of wavelengths of 490/525 nm. The second one is the same as the first except that the volume used is the minimal volume needed to entirely cover the bottom of the well. This will permit to assess if there is an edge effect when marked LL37 is also present on the edges of the well. As the microplate was hydrophobic, the minimal volume required to entirely cover the bottom of the well was 50 µL and then the microplate was left to dry in a desiccator before measurement. The third calibration curve evaluates the response of marked LL37 in solution. It was thus performed with a volume of 100 µL and measured directly. The three calibration curves were acquired twice: with the microplate n°3 and with the microplate n°4 to compare the fluorescence measurement from the top or from the bottom of the wells. The measurements (5 points per well) for the three calibrations in the dark microplate (n°3) are shown in Figure 26 and the comparison between the measurements made from the top and from the bottom of the calibration in solution is presented in Figure 27.

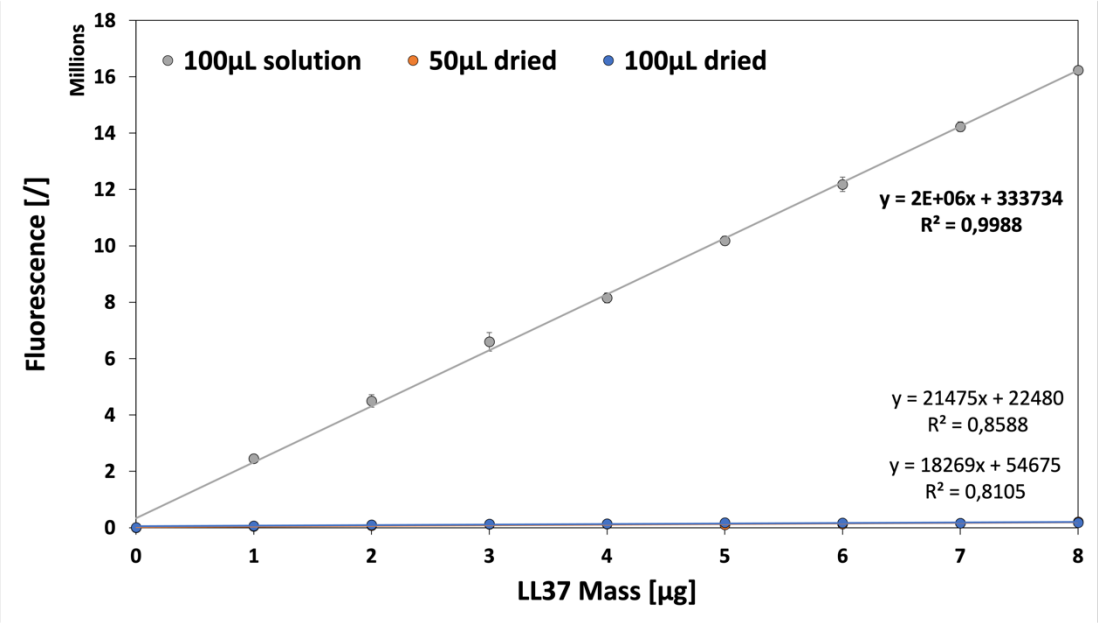

Figure 26 : Test of three calibration curves for the LL37 marked by fluorescence [0-8 µg]. The first one with 100 µL dried is in blue, the second one with 50 µL dried is in orange and the third one with 100 µL in solution is in grey. The first one and the second one are nearly superimposed. Measured with 5 points per well and at 490/525 nm.

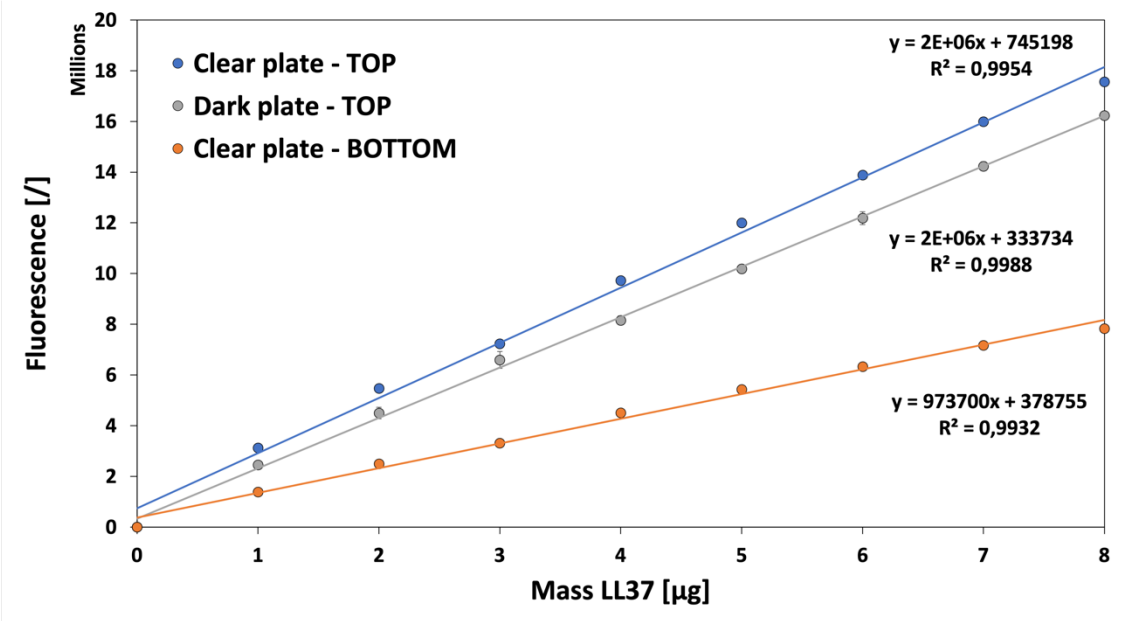

Figure 27 : Calibration curves of marked LL37 in solution on different microplate. Measurements are carried out from the TOP and from the BOTTOM of the well. The measurement for the dark plate, from the top is in grey, the one in the clear plate from the top in blue, and the one for the clear plate from the bottom is in orange.

Firstly, one can easily see that only the measurement of the LL37 marked in solution (the third tested calibration) gives a usable calibration curve. Indeed, the calibrations made on dried LL37 solutions present low fluorescence signal probably due to some quenching with polystyrene occurring because marked LL37 is in close contact with other molecules. Then, one can compare the measurement from the top in the dark and clear microplate with the one from the bottom in the clear microplate and conclude that the measurements from the

top of the wells gives higher fluorescence signal. As the calibration curves in the clear and dark microplates are quite similar for measurements from the top, the following experiments will use the dark microplate (n°3) for the construction of the multilayer because that is the one that was in stock in the lab. As both dried experiments present similar and weak fluorescence signals, it is hard to evaluate the edge effect as wanted. It is also possible that there is no edge effect because marked LL37 may stay as long as possible in solution upon the drying step and thus could be more adsorbed on the bottom than on the edges.

The chosen calibration method is thus the one where the LL37 is in solution. Therefore, as in the protein quantification tests, an additional desorption step is required before measuring the fluorescence of LL37 present in the multilayer. Then, the measurement parameters can be tested and in particular the set of wavelengths. To assess them, a spectrum was made on three well containing 3 µg of marked LL37 in a volume of 100 µL. The excitation was evaluated between 480 and 495 nm with a detection fixed at 525 nm and the emission was assessed between 510 and 560 nm with an excitation of 490 nm. The spectrum is presented in Figure 28, and no data was recorded between 510 and 518 nm due to the saturation of the spectrophotometer. One can observe that the spectrum does not present an emission and excitation peak. However, as the spectrophotometer recommends a gap of wavelength superior to 40 nm between excitation and emission to allow good quantification, it was not possible to determine the exact peak location. Nonetheless, the set of wavelengths could be adjusted to increase the fluorescence signal and passed from 490/525 nm to 492/522 nm.

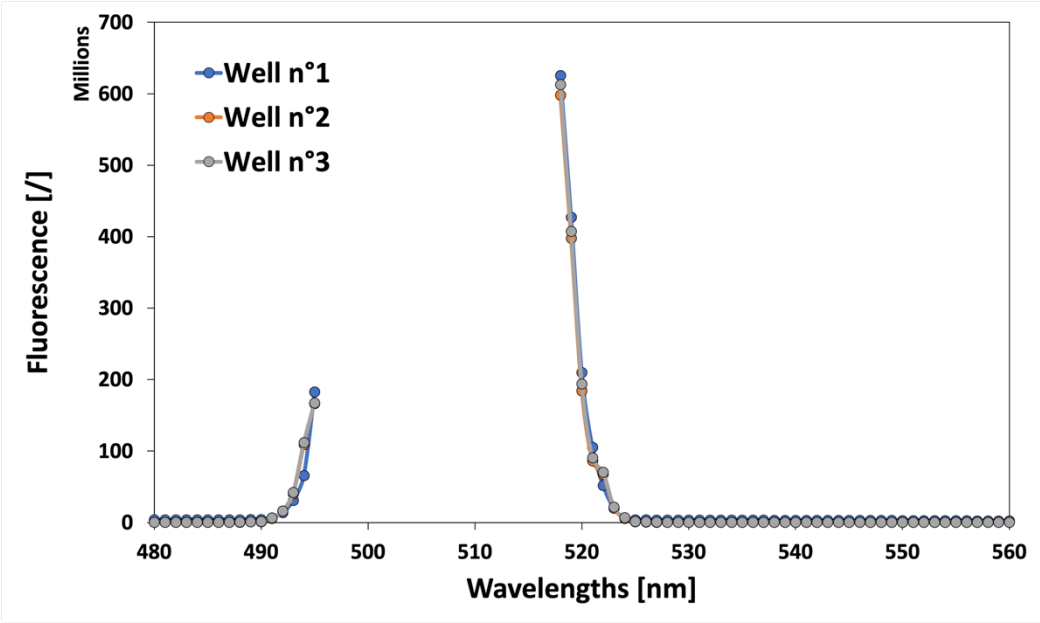

Figure 28 : Spectrum of 3 wells comprising 3 µg of marked LL37 each, in a volume of 100 µL. The excitation wavelength is scanned from 480 to 495 nm while being detected at 525 nm. The emission wavelength is scanned from 510 to 560 nm while being excited at 490 nm. There is no data represented between 510 and 517 nm because there is a saturation of the spectrophotometer.

As a supplementary information, the calibration curves were measured a second time after that the calibration samples were heated at 60°C during 1h to see if the calibrations were stable and that was well the case (data not shown).

4.2 Test on multilayers

The same series of cushion, 1, 3, 5, 6, 9, 10, 12, 15, 20 or 25 bilayers [CHI-PPCs(LL37-ALG)] was constructed at pH 3.5 on the microplate n°3 with marked LL37 this time. The fluorescence was first measured at 492/522 nm directly on the multilayers immersed in water at pH 3.5, without any previous desorption step to see if marked LL37 could be quantified directly in the multilayer. The results are presented in Figure 29. Firstly, one can see that the value of the blank is higher than all the values measured for the multilayers. This means that all the measurements are below the limit of detection and thus cannot be interpreted here. This high blank value will be discussed in the next section. Then, as the direct measurement on the multilayers does not allow the quantification of the LL37, as shown previously with the dried calibration curves, one can try to put the LL37 in solution and this was done by using the BCA test conditions on the same multilayers to desorb immobilized LL37, followed by fluorescence measurements to quantify LL37. These results will be discussed later.

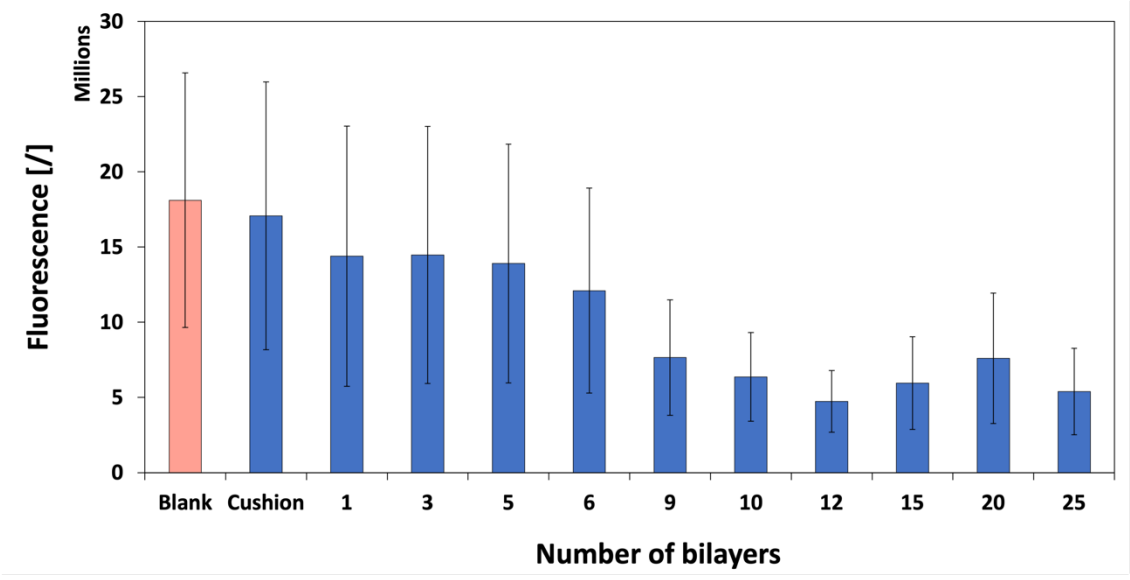

Figure 29 : Evolution of the fluorescence signal as a function of the number of bilayers constructed at pH 3.5 measured at 492/522nm.

4.3 High blank values

The high value for the blank observed in Figure 29 could come from the change in the set of wavelengths. To evaluate this possibility, one can compare the calibration made earlier at 490/525 nm with the one done here at 492/522 nm. However, it is important to point out that the volume was different for the two calibrations. The one at 492/522 nm has indeed a volume of 200 µL while the one at 490/525 nm has a volume of 100 µL. Their values are compared in Table 15. As expected, the value for the blank is more increased than the values for marked LL37, explaining the high blank value encountered in the experiment at 492/522 nm. One can conclude that the problematic high blank values are probably due to the adjustment of wavelengths. To confirm this interpretation, additional experiments measuring the fluorescence at the two set of wavelengths of both marked LL37 and water in the same volume can be conducted. If the factor of multiplication is way higher for the water than for the LL37 marked, the previous interpretation is correct.

Table 15 : Comparison of the fluorescence signals expressed in 10^6 made either at 490/525nm or at 492/522nm. The multiplication factors between the values from the first calibration and the ones from the second is also reported.

		Marked LL37								
		Blank	**1 µg**	**2 µg**	**3 µg**	**4 µg**	**5 µg**	**6 µg**	**7 µg**	**8 µg**
Fluo (10^6)	**490-525 nm**	0.69	3.14	5.19	7.28	8.84	10.87	12.87	14.92	16.92
	492-522 nm	14.03	11.43	14.25	17.69	20.14	22.20	24.58	26.74	27.86
FACTORS		20.4	3.6	2.7	2.4	2.3	2.0	1.9	1.8	1.6

4.4 Desorption of the multilayer by a BCA test

Finally, as the quantification of marked LL37 directly in the multilayer does not work, it is possible to use the conditions of the BCA test to put the LL37 in solution and then to measure the fluorescence signal coming from the same wells. The use of the BCA conditions (high pH, heat at 60°C for 1 h and use of SDS) was needed to desorb the multilayer because the SDS alone was not able to desorb the multilayer. This was validated by an experiment that used only the SDS on 15 bilayers and was heated at 60°C for 1 h. Both fluorescence measurements acquired before and after the addition of SDS and the heating step at 492/522 nm were below the blank values. As there is some fluorescence measured after applying the BCA conditions (as presented below), it seems that the SDS and the heating step are not enough to place the marked LL37 in solution. In addition, as a desorption step is also required with the marked LL37 experiments, the use of the BCA conditions to desorb the multilayer will

allow to have the same type of desorption as in the BCA test, facilitating the comparison of the results.

Before making the BCA desorption experiment, a fluorescence measurement of a blank in the BCA condition (4 µL SDS, 16 µL water, 230 µL BCA reagent) was compared to a water blank value to be sure that the BCA conditions does not interfere with the fluorescence measurement. As the BCA blank value is more than 5 times lower than the water blank value at 492/522 nm, the experiment can thus be made, and the results are presented in Figure 30.

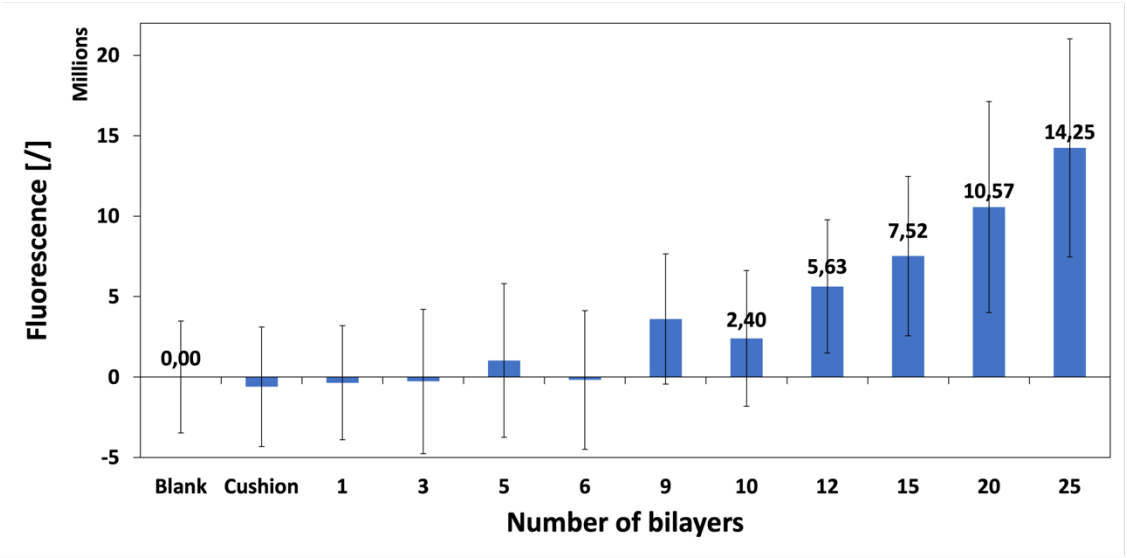

Figure 30 : Evolution of the fluorescence measured on the same multilayers after using the BCA test just to desorb the marked LL37 that is immobilized in the multilayer.

After removing the blank, one can see that the fluorescence signal continually increases from 10 bilayers to 25 bilayers. This trend validates the first hypothesis made in the QCM experiment that the amount of LL37 immobilized in the multilayer increases with the number of bilayers. Then, using the calibration curve made for the measurement in BCA conditions shown in Figure 31, it is possible to assess the mass of LL37 quantified by this method. Finally, it is also possible to compare these amounts with the ones of the BCA test alone. If one made the hypothesis that the mass of LL37 measured by the fluorescence measurement is the accurate mass of the LL37 present in the multilayer, it is possible to assess the repartition of CHI and LL37 in the multilayer. As the mass of LL37 is fixed by the fluorescence experiment, one can deduce the absorbance corresponding to those masses in the BCA test. The difference between the total absorbance measured and the LL37 absorbance found with marked LL37 gives the absorbance corresponding to the CHI mass that would be present in the multilayer. So, the Table 16 compares the mass found in the BCA test with the one from the marked LL37 experiment from 10 to 25 bilayers, alongside the possible mass of CHI present in the multilayer.

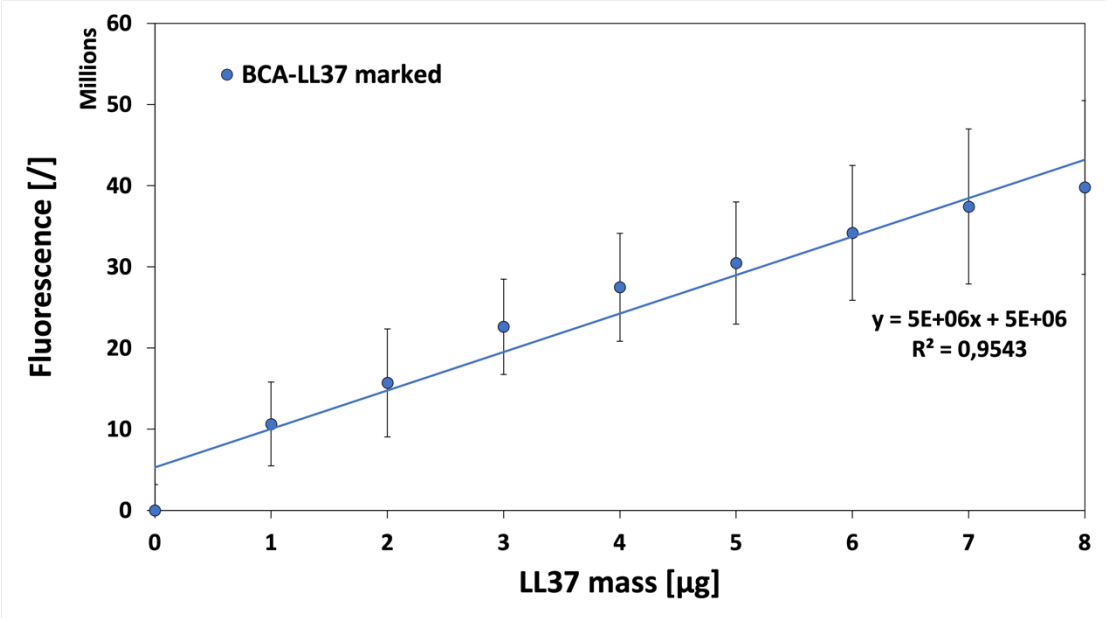

Figure 31 : Calibration curve for marked LL37 [0-8 µg] in the BCA conditions.

Firstly, the obtained LL37 masses are not similar. That can be due to the adjustment of the wavelengths that leads to a decrease of sensitivity that can be visualized by the negative mass found for 10 bilayers and by the high standard deviations. The lower quantified mass may also be due to a less good construction of the multilayer when using LL37 marked by FITC. Then, the remarkable high masses found for the CHI are due to the low slope of the CHI calibration curve. Both those remarks suggest that the hypothesis made that the LL37 mass measured with the fluorescence experiment is the accurate LL37 mass, may not be correct.

Table 16 : Comparison of the LL37 mass [µg/cm2] obtained from the BCA test and from the LL37 marked experiment. The mass of CHI present in the multilayer if the amount of LL37 found with the fluorescent measurement is accurate, is presented in blue.

	Number of bilayers				
	10	12	15	20	25
BCA - LL37 [µg/cm^2]	0.71	1.12	1.66	2.35	3.04
Marked LL37 [µg/cm^2]	-0.66	0.07	0.50	1.19	2.03
CHI [µg/cm^2]	3.71	11.73	12.89	12.90	11.29

4.5 Conclusion of the experiments with marked LL37

The preliminary experiments define that the best method to quantify marked LL37 was in solution and that the fluorescence signal was higher when measured from the top of the microplate. Then, the experiments where the wavelengths were adjusted show that it is preferable to use the wavelengths of 490/525 nm suggested by the literature to measure the fluorescence of marked LL37. As for the quantification of LL37, the preliminary experiments seem to quantify less LL37 than the BCA test. However, other experiments measured at the appropriate wavelengths are needed to validate this result but as the marked LL37 arrived tardily at the lab, there was no time left to conduct them.

General discussion

Three different points will be discussed here: firstly, the issue occurring with the system of two equations with two unknows, leading to the question of the quality of the desorption of the multilayer prior to quantification. Then, the actual amount of LL37 that is immobilized in the multilayer will also be discussed.

The goal of the quantification method used in this work was to combine the BCA test with the NO test to remove the approximation due to the presence of CHI on the LL37 mass computed by the BCA test alone. These two tests indeed feature a response from both analytes, though with different sensibilities: the BCA test gives a higher response for LL37 while, conversely, the NO test delivers a higher signal for CHI. As the NO test protocol seems to be insufficient to entirely desorb the multilayer and as the CHI signal in the BCA is low, it suggests that the system of two equations can thus not be used. This result leads to re-evaluate the capacity of the system of two equations to remove the approximation on LL37 mass that occurs if the BCA test is used alone, neglecting CHI contribution. Along the same line, vander Straeten et *al.* have used a similar system of two equations combining the BCA and the o-phthalaldehyde tests and have also rejected the method due to too low absorbance values (below the LOQ) of the o-Ph test. [34] However, preliminary experiments with LL37 marked by FITC could be the key to solve this problem. Indeed, as it has been shown that marked LL37 can be measured by fluorescence if it is in solution, it means that the creation of a new system of two equations combining this time measurements performed with marked LL37 and another quantification test sensitive to CHI could allow the mass of the components present in the multilayer to be determined. The second quantification method to be used in combination with marked LL37 remains to be chosen.

The failure of the quantification method based on the combination of BCA and NO assays, and on the resulting system of two equations, raises the problem of the desorption of the multilayer. Indeed, to quantify the multilayer entirely, it must first to be totally desorbed from the surface. This is also the case for marked LL37 as shown by the three tested calibration curves. As long as the desorption method is not known to be totally efficient, one can never be absolutely sure that the entire multilayer is desorbed, and that the quantification is accurate. In the literature, the desorption of PEMs using SDS shows the presence of holes in the multilayer, which can explain the increase of Ti percentage detected in the XPS experiment. [38] However, that would also mean that some of the multilayer remains adsorbed on the surface and is thus not detected when assays are carried out in solution. It will be interesting here to do some additional experiments to choose the optimal concentration and detergent required to achieve a better desorption of the multilayer.

Finally, from the BCA tests, neglecting the contribution of CHI, we can evaluate the amount of LL37 in the multilayer to be of the order of 3 µg/cm^2 after 25 bilayers of [CHI-PPCs(LL37-ALG)] at pH 3.5. One can see that the mass is in the same range of the 5 µg/cm^2 expected to be needed to improve wound healing. As the LL37 mass increases linearly with the number of bilayers, one could consider increase the number of bilayers to further increase the LL37 mass. However, it is important to keep in mind the application of the coating. Indeed, the multilayer will be constructed on the surface of a dressing which can lead to a possible saturation at the dressing surface notably due to the closer interactions between the PEs. This can limit the number of possible bilayers that can be built and thus the quantity of immobilized LL37. However, as the mass of LL37 is in the range of the one required to improve wound healing, it could enhance the wound healing capacity of the dressing. In addition, the LL37 will not act alone *in vivo*, so the interaction with other molecules could also bring some additional healing capacity.

Conclusion

To conclude this master thesis, the scientific questions raised in the objectives and strategy section will be answered, followed by the main results of the experiments conducted in this work.

The LL37 can be immobilized into the coating by using the LbL assembly with PPCs(LL37-ALG) and CHI as building blocks.

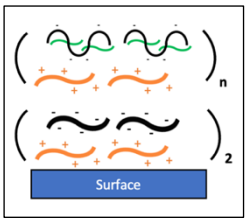

The linear increase of the hydrated mass of the film measured on 5 bilayers by QCM validates the good construction of the multilayer using PPCs(LL37-ALG) and CHI as building blocks. The presence of LL37 in the multilayer was validated with the BCA test and the experiments using LL37 marked by FITC.

Solving the system of two equations combining the BCA and NO tests gives a maximal mass of LL37 of 3.1 µg/cm^2 after the construction of 25 bilayers at pH 3.5.

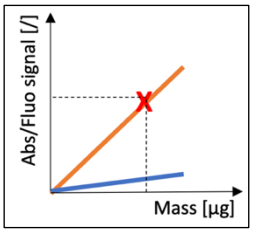

More LL37 was immobilized when the multilayers were constructed at pH 3.5 than at pH 5. The LL37 mass values computed by solving the system are almost equal to the ones measured by the BCA test alone, meaning that the BCA test alone seems to already well quantify the LL37 present in the multilayer.

The NO test seems to not desorb entirely the multilayer and thus may not quantify all the LL37 present in the multilayer.

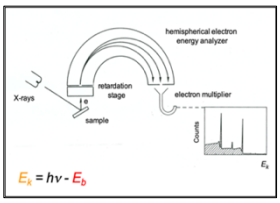

The chemical composition of the Ti surface cover with 15 bilayers is almost the same when no test was conducted and when the NO test was conducted. In both cases, no Ti was detected, suggesting that the NO test did not desorb the multilayer. Hence, the system of two equations combining data from BCA and NO assays cannot be used to remove the approximation on the mass of the LL37 due to the interference of CHI.

The development of a new system of two equations combining experiments using marked LL37 and another quantification test sensitive to CHI could quantify the CHI and LL37 mass.

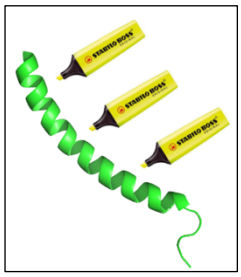

Preliminary experiments using LL37 marked with FITC show that the LL37 present in the multilayer can be detected by fluorescence measurement if it is desorbed from the multilayer. The best method of measurement was from the top of the well and using the wavelengths of 490/525 nm. The preliminary quantification test computed lower LL37 mass than the one recorded for the BCA test alone, but the fluorescence was measured at 492/525 nm which induced high blank value, decreasing the sensitivity. Future experiments are thus needed to validate the LL37 mass recorded by using this method.

The quantification method developed in this work is thus primordial to evaluate if sufficient LL37 is immobilized in the bioactive coating to ensure wound healing improvement, but it can also be a great tool in the study of the stability or the release of LL37 from the coating for example, giving numerous applications for the developed method.

Future work

Some future work can be made to complete this research. In the first time, other experiments can be conducted for the quantification study and then, the application of the coating on the surface of a dressing can be studied.

For the quantification study, it would be very interesting to do the same BCA test as before but to use this time a fully deacetylated CHI. This CHI is more expensive because it is harder to produce. However, a compression method was developed to produce a 100% deacetylated CHI. [54] With this CHI, the BCA test will only be sensitive to the LL37 present in the multilayer. By comparing those measurements with the ones done in this work, it will be finally possible to exactly know the part of the absorbance signal that comes from the CHI and induces the approximation on the LL37 mass when computed with the BCA test alone. This will thus indicate if the BCA test can be used alone to assess the LL37 mass. However, a validation of the construction of the multilayer is also necessary as the charge density of the CHI will change, and could affect the multilayer assembly.

The desorption method can also be investigated in more details. Indeed, a BCA test could be conducted on several multilayer without the SDS to see if the change in pH due to the BCA test conditions is sufficient to desorb the multilayer. To see that, a comparison of the results obtained with and without SDS can be made or XPS experiment on a blank and on the surfaces after the tests can also be conducted. The concentration of SDS was maintained constant in this work but some additional experiments could vary the concentration (in the range allowed by the test) to see the impact on the desorption in order to define the best desorption conditions.

It is important here to point out that the only parameter that was changed here as regards the LbL construction is the pH. Or, as explained in the State of the art section, there are several parameters that can be tuned and impact the multilayer construction or desorption. Variation of the temperature, or of the time of adsorption could be evaluated for example. The polyelectrolyte nature can also be adapted, as experimented by C. Vranckx who uses heparin instead of alginate, that shows promising results. So, those parameters offer a lot of buttons that we can turn to evaluate the best construction conditions.

Then, the experiments with LL37 marked by fluorescence are only preliminary and further work must be carried on. To start, the construction of the same series of multilayer

can be made again and measured at the original wavelengths (490/525 nm) to avoid having the high blank value issue, allowing more detection of the LL37 present in the multilayer.

Finally, the quantification study can be adapted for the coating constructed on a dressing. The construction of several multilayers at pH 3.5 on a Tegaderm Contact dressing can be made. The amount of quantified LL37 can be then compared to the one found by Aurélien vander Straeten in his thesis. As there are a lot of molecules in addition of LL37 that play a role in wound healing, some *in vivo* experiments are needed to validate the good improvement of the dressing.

Now that the bioactive coating is quantified by the method developed in this work, and constructed on the surface of a dressing, its healing capacity can be evaluated *in vivo*, by studying the release of LL37, if it is in its active form after the release and the healing time of a specific wound for example. The quantification study thus moves on to an activity study of LL37 on wound healing that raises new challenges.

References

[1] **J. B. Shah,** 'The History of Wound Care', *J Am Col Certif Wound Spec*, vol. 3, no. 3, pp. 65–66, Apr. 2012, doi: 10.1016/j.jcws.2012.04.002.

[2] **G. T. Lionelli** and W. T. Lawrence, 'Wound dressings', *Surgical Clinics of North America*, vol. 83, no. 3, pp. 617–638, Jun. 2003, doi: 10.1016/S0039-6109(02)00192-5.

[3] **G. Broughton**, J. E. Janis, and C. E. Attinger, 'A brief history of wound care', *Plast Reconstr Surg*, vol. 117, no. 7 Suppl, pp. 6S-11S, Jun. 2006, doi: 10.1097/01.prs.0000225429.76355.dd.

[4] **C. Daunton,** S. Kothari, L. Smith, and D. Steele, 'A history of materials and practices for wound management', *Wound Practice & Research: Journal of the Australian Wound Management Association*, Nov. 2012, Accessed: May 20, 2021. [Online]. Available: https://search.informit.org/doi/abs/10.3316/informit.058025628512911

[5] **T. Brocke** and J. Barr, 'The History of Wound Healing', *Surgical Clinics of North America*, vol. 100, no. 4, pp. 787–806, Aug. 2020, doi: 10.1016/j.suc.2020.04.004.

[6] **D. Queen**, H. Orsted, H. Sanada, and G. Sussman, 'A dressing history', *International Wound Journal*, vol. 1, no. 1, pp. 59–77, 2004, doi: https://doi.org/10.1111/j.1742-4801.2004.0009.x.

[7] **K. K. Chereddy** *et al.*, 'PLGA nanoparticles loaded with host defense peptide LL37 promote wound healing', *Journal of Controlled Release*, vol. 194, pp. 138–147, Nov. 2014, doi: 10.1016/j.jconrel.2014.08.016.

[8] **L. Steinstraesser** *et al.*, 'Host Defense Peptides in Wound Healing', *Mol Med*, vol. 14, no. 7, Art. no. 7, Jul. 2008, doi: 10.2119/2008-00002.Steinstraesser.

[9] **R. Ramos** *et al.*, 'Wound healing activity of the human antimicrobial peptide LL37', *Peptides*, vol. 32, no. 7, pp. 1469–1476, Jul. 2011, doi: 10.1016/j.peptides.2011.06.005.

[10] **R. E. W. Hancock** and H.-G. Sahl, 'Antimicrobial and host-defense peptides as new anti-infective therapeutic strategies', *Nature Biotechnology*, vol. 24, no. 12, Art. no. 12, Dec. 2006, doi: 10.1038/nbt1267.

[11] **Y. Kai-Larsen** and B. Agerberth, 'The role of the multifunctional peptide LL-37 in host defense', *Front Biosci*, vol. 13, pp. 3760–3767, May 2008, doi: 10.2741/2964.

[12] **A. W. Norman** and H. L. Henry, 'Chapter 9 - Calcium-Regulating Hormones: Vitamin D, Parathyroid Hormone, Calcitonin, and Fibroblast Growth Factor 23', in *Hormones (Third Edition)*, A. W. Norman and H. L. Henry, Eds. San Diego: Academic Press, 2015, pp. 189–221. doi: 10.1016/B978-0-08-091906-5.00009-4.

[13] **F. Costa,** I. F. Carvalho, R. C. Montelaro, P. Gomes, and M. C. L. Martins, 'Covalent immobilization of antimicrobial peptides (AMPs) onto biomaterial surfaces', *Acta Biomaterialia*, vol. 7, no. 4, pp. 1431–1440, Apr. 2011, doi: 10.1016/j.actbio.2010.11.005.

[14] **D. Vandamme**, B. Landuyt, W. Luyten, and L. Schoofs, 'A comprehensive summary of LL-37, the factotum human cathelicidin peptide', *Cellular Immunology*, vol. 280, no. 1, pp. 22–35, Nov. 2012, doi: 10.1016/j.cellimm.2012.11.009.

[15] **X. Li,** Y. Li, H. Han, D. W. Miller, and G. Wang, 'Solution Structures of Human LL-

37 Fragments and NMR-Based Identification of a Minimal Membrane-Targeting Antimicrobial and Anticancer Region', *J. Am. Chem. Soc.*, vol. 128, no. 17, pp. 5776–5785, May 2006, doi: 10.1021/ja0584875.

[16] **P. C. Biggin** and M. S. P. Sansom, 'Interactions of α-helices with lipid bilayers: a review of simulation studies', *Biophysical Chemistry*, vol. 76, no. 3, pp. 161–183, Feb. 1999, doi: 10.1016/S0301-4622(98)00233-6.

[17] **C. N. Anna Christina,** F. Wagner, S. Antonio, and S. C. Mariana, 'Antimicrobial Peptides from Anurans Skin Secretions', *Protein & Peptide Letters*, vol. 10, no. 3, pp. 227–238, May 2003.

[18] **O. Sørensen**, T. Bratt, A. H. Johnsen, M. T. Madsen, and N. Borregaard, 'The Human Antibacterial Cathelicidin, hCAP-18, Is Bound to Lipoproteins in Plasma*', *Journal of Biological Chemistry*, vol. 274, no. 32, pp. 22445–22451, Aug. 1999, doi: 10.1074/jbc.274.32.22445.

[19] **J. Johansson**, G. H. Gudmundsson, M. E. Rottenberg, K. D. Berndt, and B. Agerberth, 'Conformation-dependent Antibacterial Activity of the Naturally Occurring Human Peptide LL-37*', *Journal of Biological Chemistry*, vol. 273, no. 6, pp. 3718–3724, Feb. 1998, doi: 10.1074/jbc.273.6.3718.

[20] **UCL/SGSI, 'Biomatériaux'**, *UCLCatalogue des formations 2020-2021*, May 23, 2021. https://uclouvain.be/cours-2020-lgbio2030a (accessed May 23, 2021).

[21] **L. S. Wong**, F. Khan, and J. Micklefield, 'Selective Covalent Protein Immobilization: Strategies and Applications', *Chem. Rev.*, vol. 109, no. 9, pp. 4025–4053, Sep. 2009, doi: 10.1021/cr8004668.

[22] **J. Borges** and J. F. Mano, 'Molecular Interactions Driving the Layer-by-Layer Assembly of Multilayers', *Chem. Rev.*, vol. 114, no. 18, pp. 8883–8942, Sep. 2014, doi: 10.1021/cr400531v.

[23] **K. Ariga**, J. P. Hill, and Q. Ji, 'Layer-by-layer assembly as a versatile bottom-up nanofabrication technique for exploratory research and realistic application', *Phys. Chem. Chem. Phys.*, vol. 9, no. 19, pp. 2319–2340, May 2007, doi: 10.1039/B700410A.

[24] **J. J. Richardson**, J. Cui, M. Björnmalm, J. A. Braunger, H. Ejima, and F. Caruso, 'Innovation in Layer-by-Layer Assembly', *Chem. Rev.*, vol. 116, no. 23, pp. 14828–14867, Dec. 2016, doi: 10.1021/acs.chemrev.6b00627.

[25] **C. B. Bucur**, Z. Sui, and J. B. Schlenoff, 'Ideal Mixing in Polyelectrolyte Complexes and Multilayers: Entropy Driven Assembly', *J. Am. Chem. Soc.*, vol. 128, no. 42, pp. 13690–13691, Oct. 2006, doi: 10.1021/ja064532c.

[26] **S. S. Shiratori** and M. F. Rubner, 'pH-Dependent Thickness Behavior of Sequentially Adsorbed Layers of Weak Polyelectrolytes', *Macromolecules*, vol. 33, no. 11, pp. 4213–4219, May 2000, doi: 10.1021/ma991645q.

[27] **S. T. Dubas** and J. B. Schlenoff, 'Polyelectrolyte Multilayers Containing a Weak Polyacid: Construction and Deconstruction', *Macromolecules*, vol. 34, no. 11, pp. 3736–3740, May 2001, doi: 10.1021/ma001720t.

[28] **H. L. Tan**, M. J. McMurdo, G. Pan, and P. G. Van Patten, 'Temperature Dependence of Polyelectrolyte Multilayer Assembly', *Langmuir*, vol. 19, no. 22, pp. 9311–9314, Oct. 2003,

doi: 10.1021/la035094f.
[29] **Y.-H. Yang**, F. A. Malek, and J. C. Grunlan, 'Influence of Deposition Time on Layer-by-Layer Growth of Clay-Based Thin Films', *Ind. Eng. Chem. Res.*, vol. 49, no. 18, pp. 8501–8509, Sep. 2010, doi: 10.1021/ie100499x.
[30] **M. Salomäki**, P. Tervasmäki, S. Areva, and J. Kankare, 'The Hofmeister Anion Effect and the Growth of Polyelectrolyte Multilayers', *Langmuir*, vol. 20, no. 9, pp. 3679–3683, Apr. 2004, doi: 10.1021/la036328y.
[31] **E. Poptoshev,** B. Schoeler, and F. Caruso, 'Influence of Solvent Quality on the Growth of Polyelectrolyte Multilayers', *Langmuir*, vol. 20, no. 3, pp. 829–834, Feb. 2004, doi: 10.1021/la035485u.
[32] **A. vander Straeten**, A. Bratek-Skicki, A. M. Jonas, C.-A. Fustin, and C. Dupont-Gillain, 'Integrating Proteins in Layer-by-Layer Assemblies Independently of their Electrical Charge', *ACS Nano*, vol. 12, no. 8, pp. 8372–8381, Aug. 2018, doi: 10.1021/acsnano.8b03710.
[33] **M. Houska**, E. Brynda, and K. Bohatá, 'The effect of polyelectrolyte chain length on layer-by-layer protein/polyelectrolyte assembly—an experimental study', *Journal of Colloid and Interface Science*, vol. 273, no. 1, pp. 140–147, May 2004, doi: 10.1016/j.jcis.2003.12.056.
[34] **A. vander Straeten**, 'Protein-polyelectrolyte complexes for the surface immobilization of bioactive proteins', UCL - Université Catholique de Louvain, 2019. Accessed: May 20, 2021. [Online]. Available: https://dial.uclouvain.be/pr/boreal/fr/object/boreal%3A218057
[35] **O. Jeon**, D. S. Alt, S. M. Ahmed, and E. Alsberg, 'The effect of oxidation on the degradation of photocrosslinkable alginate hydrogels', *Biomaterials*, vol. 33, no. 13, pp. 3503–3514, May 2012, doi: 10.1016/j.biomaterials.2012.01.041.
[36] **P. H. Yassue-Cordeiro** *et al.*, '1 - Chitosan-based nanocomposites for drug delivery', in *Applications of Nanocomposite Materials in Drug Delivery*, Inamuddin, A. M. Asiri, and A. Mohammad, Eds. Woodhead Publishing, 2018, pp. 1–26. doi: 10.1016/B978-0-12-813741-3.00001-7.
[37] **D. Raafat** and H.-G. Sahl, 'Chitosan and its antimicrobial potential – a critical literature survey', *Microbial Biotechnology*, vol. 2, no. 2, pp. 186–201, 2009, doi: https://doi.org/10.1111/j.1751-7915.2008.00080.x.
[38] **Md. A. Rahim**, W. S. Choi, H.-J. Lee, and I. C. Jeon, 'Ionic Surfactant-Triggered Renewal of the Structures and Properties of Polyelectrolyte Multilayer Films', *Langmuir*, vol. 26, no. 7, pp. 4680–4686, Apr. 2010, doi: 10.1021/la9035634.
[39] 'MAN0011430_Pierce_BCA_Protein_Asy_UG.pdf'. Accessed: May 27, 2021. [Online]. Available: https://assets.thermofisher.com/TFS-Assets/LSG/manuals/MAN0011430_Pierce_BCA_Protein_Asy_UG.pdf
[40] **A. Lewies,** 'An in vitro evaluation of the antibacterial and anticancer properties of the antimicrobial peptide nisin Z', 2018. doi: 10.13140/RG.2.2.26416.66564.
[41] **L. J. Jones**, R. P. Haugland, and V. L. Singer, 'Development and Characterization of the NanoOrange® Protein Quantitation Assay: A Fluorescence-Based Assay of Proteins in Solution', *BioTechniques*, vol. 34, no. 4, pp. 850–861, Apr. 2003, doi: 10.2144/03344pt03.
[42] 'NanoOrange® Protein Quantitation Kit', p. 6.
[43] **M. D. Harvey,** V. Bablekis, P. R. Banks, and C. D. Skinner, 'Utilization of the non-

covalent fluorescent dye, NanoOrange, as a potential clinical diagnostic tool: Nanomolar human serum albumin quantitation', *Journal of Chromatography B: Biomedical Sciences and Applications*, vol. 754, no. 2, pp. 345–356, Apr. 2001, doi: 10.1016/S0378-4347(00)00627-7.

[44] 'Fluorescein (FITC) - BE'. //www.thermofisher.com/uk/en/home/life-science/cell-analysis/fluorophores/fluorescein.html (accessed May 24, 2021).

[45] **I. Reviakine**, D. Johannsmann, and R. P. Richter, 'Hearing What You Cannot See and Visualizing What You Hear: Interpreting Quartz Crystal Microbalance Data from Solvated Interfaces', *Anal. Chem.*, vol. 83, no. 23, pp. 8838–8848, Dec. 2011, doi: 10.1021/ac201778h.

[46] 'Quartz Crystal Microbalance (QCM)', *Nanoscience Instruments*. https://www.nanoscience.com/techniques/quartz-crystal-microbalance/ (accessed May 25, 2021).

[47] 'Q-SenseE4 product information.pdf'. Accessed: May 26, 2021. [Online]. Available: http://cdn.fct.unl.pt/sites/default/files/e4brochure.pdf

[48] 'Sensor spec sheet QSX310Ti.pdf'. Accessed: May 25, 2021. [Online]. Available: https://www.biolinscientific.com/hubfs/Pdf/QSense/QSensors/Sensor%20spec%20sheet%20QSX310Ti.pdf

[49] 'Sensor spec sheet QSX301Gold.pdf'. Accessed: May 25, 2021. [Online]. Available: https://www.biolinscientific.com/hubfs/Pdf/QSense/QSensors/Sensor%20spec%20sheet%20QSX301Gold.pdf

[50] **E. Matijevic**, Ed., *Medical Applications of Colloids*. New York, NY: Springer New York, 2008. doi: 10.1007/978-0-387-76921-9.

[51] **UCL/SGSI, 'Caractérisation de surface des matériaux'**, *UCLCatalogue des formations 2020-2021*, May 23, 2021. https://uclouvain.be/cours-2020-lbrna2102 (accessed May 23, 2021).

[52] **Y. I. Cho**, H. K. No, and S. P. Meyers, 'Physicochemical Characteristics and Functional Properties of Various Commercial Chitin and Chitosan Products', *J. Agric. Food Chem.*, vol. 46, no. 9, pp. 3839–3843, Sep. 1998, doi: 10.1021/jf971047f.

[53] **A. Mertens de Wilmars**, 'Characterisation of a coating composed of LL-37-heparin complexes and study of its antibacterial activity', 2020.

[54] **X. He**, K. Li, R. Xing, S. Liu, L. Hu, and P. Li, 'The production of fully deacetylated chitosan by compression method', *The Egyptian Journal of Aquatic Research*, vol. 42, no. 1, pp. 75–81, Mar. 2016, doi: 10.1016/j.ejar.2015.09.003.

Appendices

Annex 1:

Evaluation of the interferences between LL37 and CHI in the BCA test for different ratio of µgLL37/µgCHI. The response of LL37 alone is in orange, the one of the CHI alone, in blue and their combination in the ratio indicated is in grey.

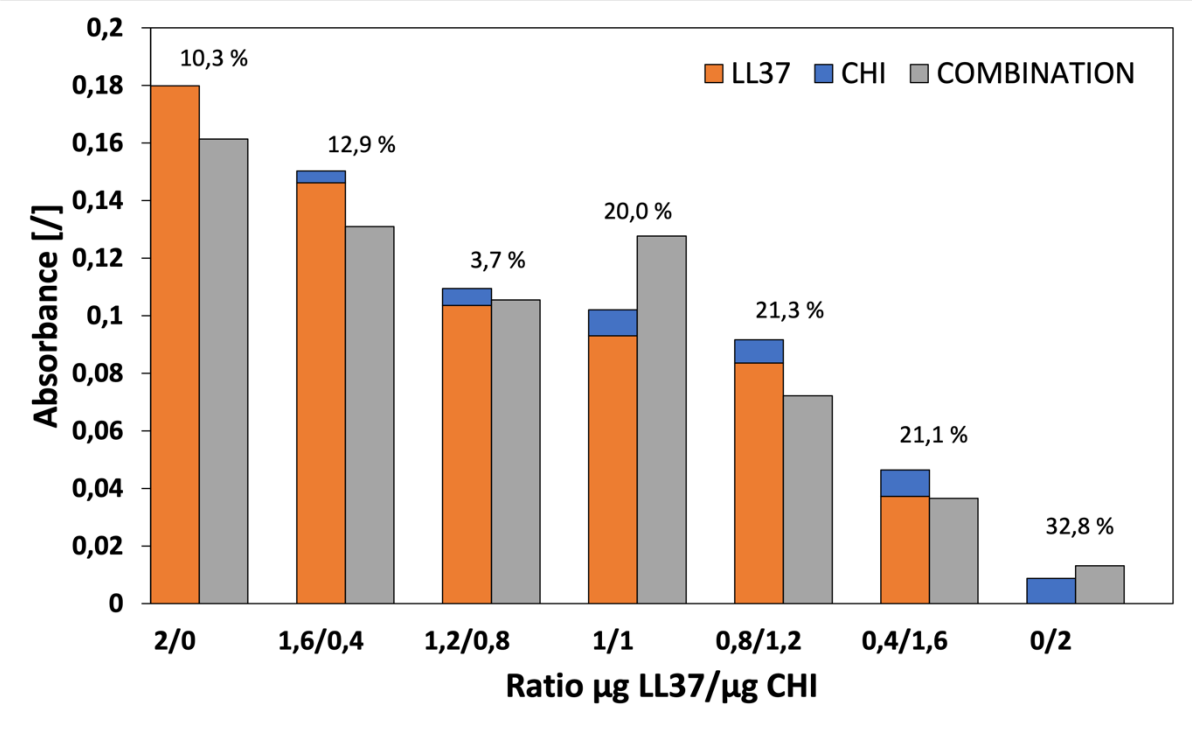

Annex 2:

First calibration curves for the NO test between 0 and 10 µg, firstly measured at 470/570 nm and then at 485/590 nm.

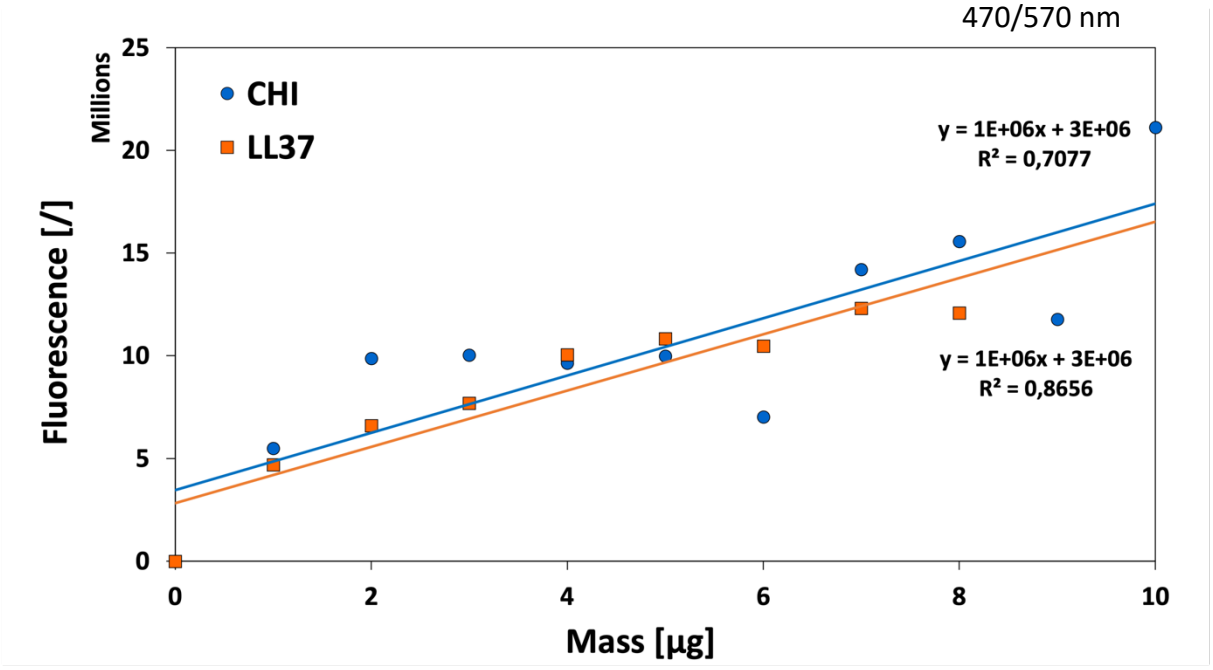

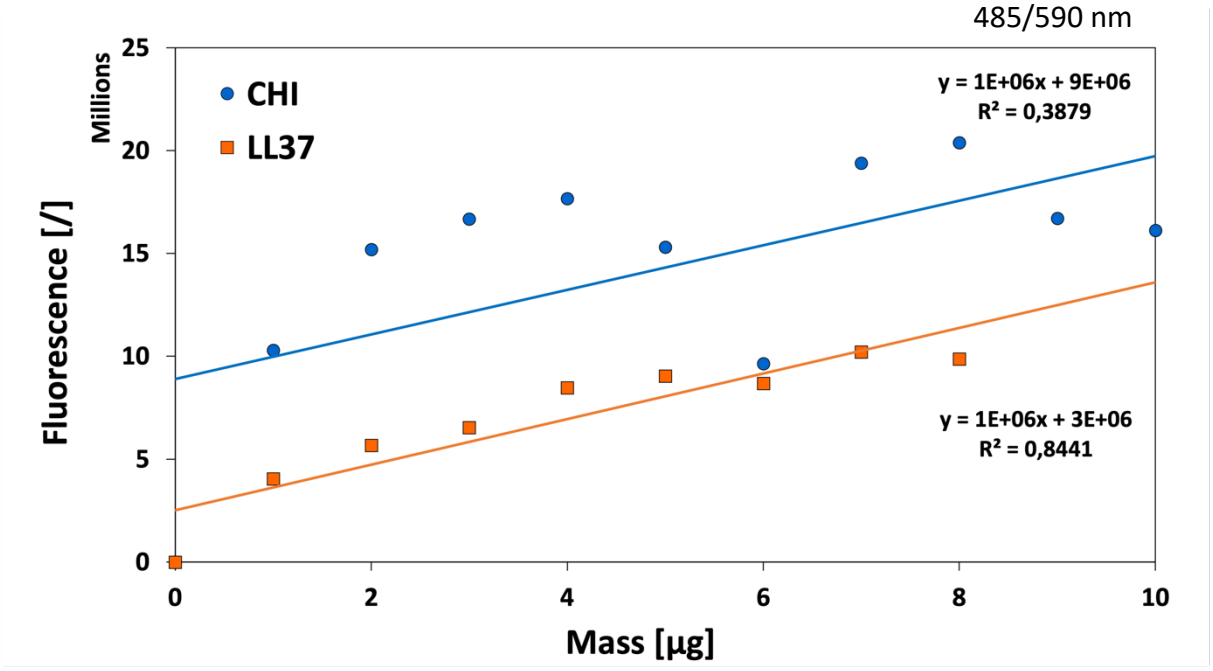

Annex 3:

Test LoF for the calibration curves of the NO test.

	MSS(LoF)	MSS(error)	Fcalc	Ftab = F^{6}_{16}
LL37	4,97978E+11	4,39822E+13	0,01132	4,2 For α = 0,01
CHI	6,85417E+11	1,81699E+14	0,00377	4,2 For α = 0,01

	MSS(LoF)	MSS(error)	Fcalc		Ftab = F^{6}_{16}
LL37	4,97978E+11	4,39822E+13	0,01132	<	4,2 For α = 0,01
CHI	6,85417E+11	1,81699E+14	0,00377	<	4,2 For α = 0,01

Annex 4:

Calibration curves for LL37 and CHI using NO diluent instead of SDS. There is a factor 5 between the calibration curves.

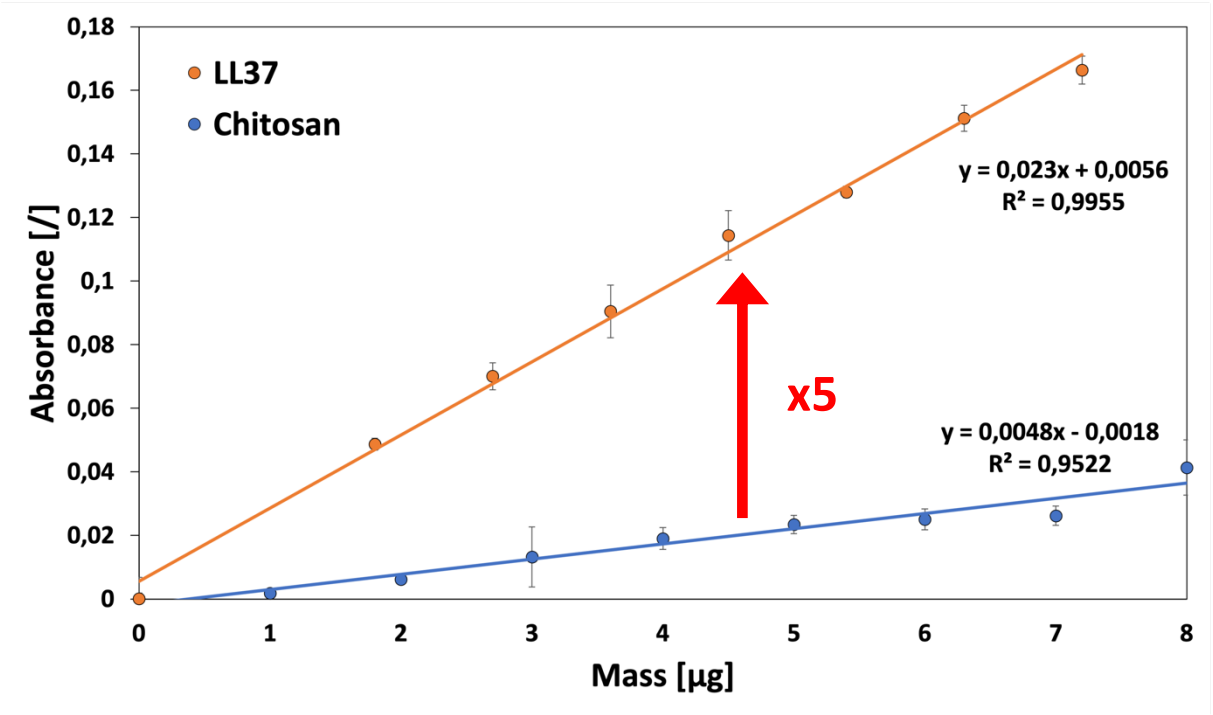

Annex 5:

The percentages of all the decomposed peaks of the XPS experiment.

	Na	Cu				O	Ti	N	
	Na 1s	Cu 2p3 Cu <II sat.	Cu 2p3 Cu <II	Cu 2p3 Cu <I	Cu tot.	O 1s	Ti 2p	NH+	N-(C,H)	N tot.
15layers	**bdl**	bdl	bdl	bdl	**bdl**	43.5	bdl	2.6	1.4	**4.0**
BCA(SDS)1x	**bdl**	0.7	2.3	1.3	**4.2**	41.2	4.8	bdl	4.2	**4.2**
BCA(SDS)2x	**0.5**	0.9	2.2	2.2	**5.3**	39.6	5.3	bdl	3.4	**3.4**
BCA(HCl)	**0.9**	0.4	1.6	3.1	**5.1**	41.5	8.4	bdl	1.9	**1.9**
BCA(NO)	**bdl**	0.1	0.8	2.5	**3.4**	44.1	6.7	bdl	4.0	**4.0**
NO	**bdl**	bdl	bdl	bdl	**bdl**	43.3	bdl	2.5	1.6	**4.2**

	C					Cl
	O=C-O	C=O, O-C-O	C-(O,N)	C-(C,H)	C tot.	Cl 2p3/2
15layers	2.5	11.1	32.0	6.8	**52.4**	**bdl**
BCA(SDS)1x	2.1	7.1	19.6	16.1	**44.9**	**0.64**
BCA(SDS)2x	1.7	7.3	16.4	19.7	**45.1**	**0.86**
BCA(HCl)	2.9	3.5	9.4	25.7	**41.5**	**0.63**
BCA(NO)	1.3	5.5	18.0	16.5	**41.3**	**0.53**
NO	2.4	10.4	31.3	8.6	**52.6**	**bdl**

Building and quantification of a bioactive coating containing LL37-Alginate complexes

Antoine Matheys

The healing of infected or chronic wounds is a current challenge in the healthcare field, requiring the development of new therapeutic approaches. In this context, a bioactive coating can be adsorbed on the surface of a dressing to improve its performances. Such coating may contain the LL37 peptide which possesses interesting wound healing and antibacterial properties. To immobilize LL37 in this coating, a layer-by-layer assembly method was developed by successive adsorption of oppositely-charged polyelectrolytes on the surface. LL37 was first complexed with negatively-charged alginate (ALG) into protein-polyelectrolytes complexes (PPCs) before being integrated into the assembly with positively-charged chitosan (CHI). The development of this coating construction method triggers the need to develop a robust quantification method to be able to determine the amount of LL37 immobilized in the coating.

The aims of this work were to validate the good construction of the coating using the LbL assembly and to develop a quantification method to assess the amount of LL37 present in the coating. A combination of two quantification tests was used: the bicinchoninic acid (BCA) assay and the NanoOrange (NO) assay. Surface characterization methods such as quartz crystal microbalance and X-ray photoelectron spectroscopy were also used to support this development. Fluorescent LL37 was finally used to enhance the performances of the quantification approach.

As BCA and NO tests are sensitive to both LL37 and CHI, a system of two equations can be computed to evaluate the LL37 and CHI masses. However, the NO test was shown not to quantify the multilayer entirely. This observation triggered the need to identify other options or accurate quantification. Nonetheless, by using the BCA test alone, it is possible to approximate the LL37 mass with an error range of about 10%. This LL37 mass reaches 3 $\mu g/cm^2$ after the deposition of 25 bilayers of [CHI-PPCs(LL37-ALG)]. The use of fluorescent LL37 was finally explored to increase the accuracy of the quantification method.

The present work led to promising developments towards a robust quantification of the components of multilayer films featuring anti-bacterial and wound healing properties. It constitutes a useful step towards the development and application of innovative dressings.

UNIVERSITÉ CATHOLIQUE DE LOUVAIN
Faculté des bioingénieurs
Croix du Sud, 2 bte L7.05.01, 1348 Louvain-la-Neuve, Belgique | **www.uclouvain.be/agro**